E.O. Paton Electric Welding Institute of the National Academy of Sciences of Ukraine

International Scientific-Technical and Production Journal

The Paton WELDING JOURNAL

December 2013
No.12

Published since 2000

English translation of the monthly «Avtomaticheskaya Svarka» (Automatic Welding) journal published in Russian since 1948

Founders
E.O. Paton Electric Welding Institute
of the NAS of Ukraine,
International Association «Welding»

Publisher
International Association «Welding»

Translators
A.A. Fomin, O.S. Kurochko,
I.N. Kutianova
Editor
N.A. Dmitrieva
Electron galley
D.I. Sereda, T.Yu. Snegiryova

Address
E.O. Paton Electric Welding Institute,
International Association «Welding»
11, Bozhenko Str., 03680, Kyiv, Ukraine
Tel.: (38044) 200 60 16, 200 82 77
Fax: (38044) 200 82 77, 200 81 45
E-mail: journal@paton.kiev.ua
www.patonpublishinghouse.com

State Registration Certificate
KV 4790 of 09.01.2001
ISSN 0957-798X

Subscriptions
$348, 12 issues per year,
air postage and packaging included.
Back issues available.

CONTENTS

«The Paton Welding Journal» abstracted and indexed in Ukrainian refereed journal «Source», RJ VINITI «Welding» (Russia), INSPEC, «Welding Abstracts», ProQuest (UK), EBSCO Research Database, CSA Materials Research Database with METADEX (USA), Questel Orbit Inc. Weldasearch Select (France); presented in Russian Science Citation Index & «Google Scholar»; abstracted in «Welding Institute Bulletin» (Poland) & «Rivista Italiana della Saldatura» (Italy); covered in the review of the Japanese journals «Journal of Light Metal Welding», «Journal of the Japan Welding Society», «Quarterly Journal of the Japan Welding Society», «Journal of Japan Institute of Metals», «Welding Technology».

LASER SURFACE ALLOYING OF STEEL ITEMS (Review)

A.V. BERNATSKY
E.O. Paton Electric Welding Institute, NASU
11 Bozhenko Str., 03680, Kiev, Ukraine. E-mail: office@paton.kiev.ua

Analysis of publications devoted to laser surface alloying of steel items has been performed. Processes occurring at formation of the structure of surface layers at laser alloying of steels have been studied. Examples of practical application of laser surface alloying of steels by various materials and mixtures are given. It is shown that laser alloying enables formation of surface of steel items having a high level of hardness, heat-, wear- and corrosion resistance and other physico-mechanical characteristics. It is found that the work performed in this direction was not of a systematic nature, and quite often was aimed at solving a localized task of improvement of performance of a particular material or parts made from it. Therefore, results obtained by various authors cannot be systematized, because of significant differences in the schematics and conditions of research performance. 50 Ref., 2 Figures.

Keywords: *laser alloying, schematic, process, alloyed zone, steel, alloying materials, commercial application*

With increase of requirements to working layer quality [1, 2], process cost effectiveness indices [3], selection of materials, depending on surface properties and cross-section of the parts, as well as increase of volume fraction of complex-alloyed steels in manufacture of parts and tools, the tasks of application of resources-saving technologies for extension of service life of loaded steel items, for instance, by surface alloying, are becoming urgent [4].

Alloying (from Latin ligo — bind, join) means introducing additives (metals, nonmetals and their compounds) into metals, alloys and semiconductors to give them certain physical, chemical and mechanical properties [5]. Alloying of metals and alloys may lead to formation of solid solutions, mixtures of two and more phases, intermetallics, carbides, nitrides, oxides, sulphides, borides and other compounds of alloying elements with the alloy base or of these alloying elements with each other [4, 5].

Alloying results in an essential change of physico-chemical characteristics of the initial metal or alloy and, primarily, of its electronic structure [5]. Alloying elements influence the melting temperature, nature of crystalline lattice defects, formation of grains and fine crystalline structure, region of existence of allotropic modifications and kinetics of phase transformations, dislocation structure, heat- and corrosion resistance, electrical, magnetic, mechanical, diffusion and many other properties of the alloys [3–8].

Alloying is subdivided into bulk and surface [5] alloying. In bulk alloying the alloying element is on average statistically distributed in the metal bulk. As a result of surface alloying, the alloying element is concentrated on the metal surface. Alloying by several elements simultaneously, a certain of content and ratio of which yields the required set of properties, is called complex alloying and the alloys are called complex-alloyed, respectively. For instance, alloying of austenitic chrome-nickel steel by tungsten results in its heat resistance rising by 2–3 times, and at simultaneous application of tungsten, titanium and other elements — by 10 times [5].

Most of the traditional processes of surface alloying of steels (in combination with heat treatment) are based on diffusion saturation by elements from the gaseous or liquid phase and chemical deposition from the gas phase [9]. Common name of these processes is chemicothermal treatment (CTT). Such processes include aluminizing (alloying element is aluminium), carbonization (alloying element is carbon), carbonitriding (alloying elements are carbon and nitrogen), nitriding (alloying element is nitrogen), boriding (alloying element is boron), etc. [5, 9].

However, the above-mentioned CTT methods have a number of common essential drawbacks, both as to the process technology and as to alloyed layer properties. The main disadvantages, limiting the application of these processes as surface-strengthening treatment methods, include [10]:

- long duration of the operation (for instance, carbon saturation rate is about $2.8 \cdot 10^{-5}$ mm/s and it will take 50–70 h to obtain a nitrided layer of 0.5 mm thickness in structural steels at 773–793 K), resulting in a low efficiency of the process;
- deformation and distortion under stresses induced by conditions of heating during the tech-

nological process and subsequent cooling and, as a result, need for additional mechanical treatment operations;

• brittleness and spallation of outer part of the treated layer.

Other disadvantages of the above CTT methods are small thickness of the alloyed layer and its weak adhesion to base metal structure. At forced operation modes the alloyed layer is quickly torn off the part surface.

In view of the growing service requirements to heavy-duty parts of various components and mechanisms, the tasks of improvement of heat- and crack resistance become urgent. However, regular CTT with quenching and tempering, even though it affects the item properties, is clearly insufficient in many cases. It is the most suitable for improvement of wear- and corrosion resistance, and to a smaller degree, for increase of heat resistance as well as resistance to crack initiation and propagation [5].

Application of the above surface alloying methods is largely related to the history of development of mechanical engineering in developed countries. The evolution of these methods proper was caused by the desire to improve the performance of surface layers of loaded steel items. At the current stage of development of equipment and technology, special attention is given to new methods of surface alloying, allowing elimination of the listed disadvantages of the above methods [10]. These new methods are based on application of local heat sources. For metal surface modification preference is given to such methods, which use high energy density flows as heat sources, such as laser, ion, ultrasonic, etc.

Laser technologies provide successful solutions of the problem of development of materials with a specified set of properties by means of purpose-oriented formation of the structure [10–50]. Laser alloying enables forming such surface layers, which have a high level of hardness [10–12], heat resistance [10, 13, 14], wear resistance [10, 15–17], corrosion resistance [10, 18], and of other characteristics [10–20]. Processes of local alloying are realized using both pulsed [6, 10–13, 17] and continuous [6, 8, 10, 12–20] laser radiation. Here various treatment schematics can be applied both «with overlapping» [10, 12, 13, 15–17, 19, 20] and without it [6, 10–13, 17]. Process results also depend on the method of feeding the alloying material into the joint zone [10, 12, 13, 17], kind of alloying element(s) [6, 8, 10–20], properties of matrix material [10–13, 15, 17] and many other factors.

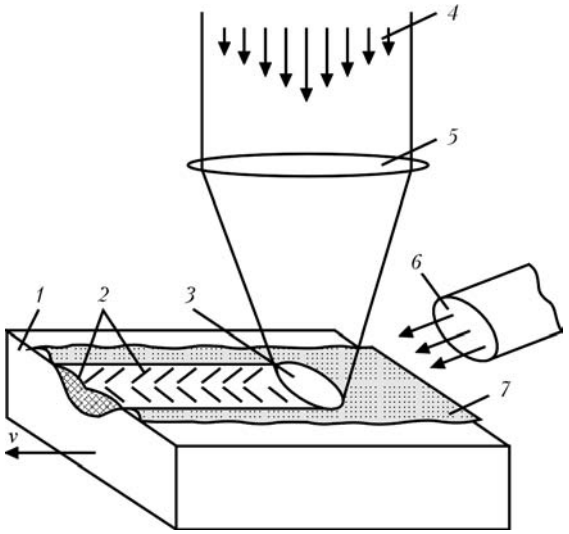

Figure 1. Schematic of laser alloying process [12]: *1* — sample moving at speed v; *2* — alloyed path; *3* — melt pool; *4* — laser beam; *5* — focusing system; *6* — shielding gas; *7* — alloying coating

Surface laser alloying consists in producing alloyed layers with forced feeding of filler materials directly into the zone of impact of focused laser radiation. Schematic of laser alloying process is shown in Figure 1 [12]. A sample with a thin layer of alloying coating is locally surface melted when moving under the laser beam, alloying components go into the volume of liquid metal pool, which then solidifies.

Investigations of the process of laser surface alloying [6, 8, 10–20] show that laser radiation, directed at the treated surface, is partially absorbed by filler and base materials, and partially reflected. As a result of absorption, an intensive heat source becomes active in the laser irradiation zone [10]. At radiation power densities of 10^5–10^6 W/cm^2 active local heating of filler materials occurs, at which a vapour-gas phase forms on the melt pool (liquid phase) surface [12]. At laser alloying interrelated heat mass transfer processes and micrometallurgical processes take place. At laser beam movement the molten metal is driven to the pool tail part as a result of mass transfer phenomenon (integral action of vapour pressure, difference of surface tension forces in the melt pool central and tail parts, and melt turbulent flows) [10]. At the moment of liquid metal existence, mixing of molten alloying composition with metal matrix occurs due to Marangoni thermocapillary convection [21]. Here, steel surface saturation by alloying elements from the compositions, formation of chemical compounds, and partial homogenizing in the liquid metal zone take place [8, 10, 13]. At pool metal solidification an alloyed layer forms. At increase of radiation power density above 10^6 W/cm^2 a transition into

the keyhole penetration mode is observed, which is characterized by formation of a vapour-gas channel in the melt pool [10].

Let us consider in greater detail the processes occurring at formation of the structure of surface layers at laser alloying of steels. Depending on thermophysical characteristics of the base material, namely, on heat conductance, the metal surface is heated up to different temperatures [10, 13, 17, 22]. In the case, when the base material has a low coefficient of heat conductivity, metal in the melt pool is heated up to very high temperatures, while the melt pool depth is small. Alloying element concentration rises abruptly. At the impact of laser radiation on the surface of steels with a high coefficient of heat conductivity, the melt pool depth increases, and alloying element content in the pool decreases, respectively [10]. Here, the temperature in the surface melting zone turns out to be lower than in the first case.

In connection with the fact that laser systems with Gaussian energy distribution in the laser beam have become the most widely accepted, energy maximum is found in the beam center, and beam energy decreases towards its periphery [10, 23]. Thus, the heat source provides greater heating in the center than on the periphery. Therefore, the metal turns out to be also heated nonuniformly [12, 13, 24]. This promotes development of a circular mode of liquid movement, directed from the metal surface to the periphery and in-depth of the melt pool [10–13, 21, 23, 24]. Liquid flows as though twist symmetrically in the opposite directions, i.e. two symmetrical macrovortices are created [12, 13, 21]. They form in the case, when the physicochemical and mechanical properties of liquid metal are the same over the entire melt pool. At further movement of the heat source, several vortices form within the melt pool, as metal properties in the laser irradiation zone differ significantly [12]. On the one side, where cold, unheated by the laser beam metal is adjacent to the melt pool, heat removal is more intensive than from the side of the metal, already exposed to laser irradiation. Thus, temperature gradient turns out to be greater from one side of the melt pool than from the other side [11]. Metal movement occurs from the higher temperature regions to less heated regions [12]. Vortex mode of liquid movement leads to its intensive stirring that promotes formation of a homogeneous structure [10]. Here, the high temperatures combined with the short time, allow preserving the high concentration of alloying components [10–20].

All the experimental data show a sufficiently uniform distribution of alloying additives across liquid pool section [10–20]. This unambiguously points to the principal role of convective mass transfer compared to diffusion transfer [10]. Metal evaporation (and vapour recoil pressure, respectively) at alloying is neglected [12], as the alloying process practically always proceeds below the material boiling temperature.

Zone of treatment after laser alloying has a structure similar to that of the zone after laser quenching with surface melting. The difference lies in that alloying elements are added to molten pool metal. Element diffusion from the surface melting zone into the HAZ usually occurs to not more than 10 μm depth [10, 11]. In some cases, however, redistribution of alloying elements in the solid phase under the surface melting zone at the depth of 200–300 μm was found experimentally [10, 12, 13, 17]. This can be due to formation of thin liquid phase channels along the grain boundaries and blocks in the solid metal and mass transfer along these channels [12, 13, 17]. Processes of mass transfer in the solid phase can be also due to dislocation displacement of atoms as a result of fast local deformation [10, 12].

Difference in the structure of laser alloyed zones from that of diffusion coatings, consists in absence of lamination [10]. Convective mixing of the melt with greater distance from the surface, transition from phases with greater concentration of alloying element to those with its lower concentration does not take place [10, 12, 13, 17]. All the phases in the alloyed zone are approximately uniformly mixed by depth [10].

There exist the following methods of alloying element feeding into the laser irradiation zone [10, 12, 13]:

- application of alloying composition in powder form on the treated surface;
- surface coating with special alloying composition;
- alloying in liquid (liquid alloying medium);
- rolling of alloying material foil over the surface being treated;
- alloying in gaseous alloying medium;
- containing ferromagnetic alloying elements on the matrix surface by the magnetic flux;
- deposition of alloying composition by thermal methods (for instance, gas-flame, plasma, detonation spraying, etc.);
- electrolytic deposition of alloying coating;
- alloying composition feeding into the treatment zone in synchronism with laser radiation.

Each of these processes has its advantages and disadvantages [10–13], which determine the ra-

tionality of its application in a specific case, and the results obtained at slight changes in technological modes and method of material feeding, can make considerable corrections in the derived result. So, in [25, 26] the influence of surfactant concentration on melt convection and laser alloying results was studied experimentally. It is shown [25] that addition of selenium or sulphur as surfactants to alloying coating allowed controlling the surface profile and shape of alloyed path cross-section.

Proceeding from the objectives of laser alloying (improvement of wear resistance, corrosion resistance, back-to-back endurance and other service properties) [10], it is necessary to take into account the known results of work on CTT [1, 4, 5, 9]. On the other hand, it is not possible to perform direct comparison of the processes of formation of alloyed surface layer at laser surface melting [10–25] with CTT processes, at which alloying proceeds as solid-phase diffusion. At laser alloying, as a result of «stringent» thermal cycle with high heating and cooling rates, formation of oversaturated meta-stable highly dispersed structures is characteristic that cannot be achieved at regular CTT [10].

Dimensions of alloyed zone depend, mainly on radiation energy parameters [12], and thickness of coating from alloying material. As a rule, alloying by pulsed radiation provides smaller dimensions of alloyed zone than at treatment by continuous radiation [10–17]. In particular, if at pulsed treatment zone depth is equal to 0.3–0.7 mm, then application of continuous radiation of powerful CO_2-lasers and Nd:YAG lasers allows zone depth to be increased down to 3 mm [10].

A large number of scientific publications devoted to application of the method of laser alloying of a broad range of metals and alloys have appeared recently, owing to the efforts of many research teams. Three groups of materials are traditionally applied as alloying additives: nonmetals, metals and their compounds (for instance, carbides) [10–22].

Alloying by nonmetallic components (for instance, carbon, nitrogen, boron, silicon) is an alternative to traditional methods of carbonization, nitriding, boriding, and siliconizing [10, 12, 13, 17].

Low-carbon steel alloying by carbon naturally leads to formation of a fine-grained structure of martensite and residual austenite, with microhardness reaching 9000 MPa [10, 14, 17].

Steel structure after laser nitriding is nitrous martensite, residual austenite and iron nitrides [6, 10, 12, 27].

Structure of laser borided zones at a small boron content contains α-Fe and boride eutectic [10, 12, 13, 28]. Here, microhardness is equal to $(6–12)\cdot10^8$ MPa [10, 12, 13]. At increase of boron concentration, a small amount of borides (FeB, Fe_2B, Fe_3B) appear in the structure, residual austenite is absent, and microhardness abruptly rises up to $(14–21)\cdot10^8$ MPa [10, 13, 28]. Alloyed surface with increased content of FeB phase performs well at abrasive wear, whereas at shock impact it is recommended to obtain Fe_2B and Fe_3B borides in the structure [12, 28].

At increase of silicon concentration at laser siliconizing, Fe_3Si, Fe_2Si_3, FeSi, $FeSi_3$ silicides form in the structure of laser irradiation zone in addition to α-Fe, and steel microhardness rises from $8\cdot10^3$ up to $(14–15)\cdot10^3$ MPa, heat-, wear- and corrosion resistance are also significantly increased [10, 12, 13, 19, 20].

Alloying by pure metals (aluminium [6, 10, 12, 13, 29], cobalt [10, 12, 13, 30], chromium [6, 10–13, 30, 31], nickel [6, 10–13, 30, 32] etc.), as well as alloys on their base, leads to formation of oversaturated solid solutions and intermetallics. This promotes a significant growth of microhardness and wear resistance of alloyed layers, improves corrosion resistance and other physico-mechanical characteristics of the items. So, for instance, laser treatment promotes 1.5 to 3 times increase of wear resistance at surface hardening with further nitriding; the greatest microhardness and wear resistance of low-carbon steels are achieved by nitriding of aluminium-alloyed surface [33]. However, presence of an increased intermetallic content lowers the ductility and embrittles the alloyed layer that may lead to its premature fracture [6, 10, 17].

Presence of carbides, borides, silicides, nitrides and their combinations in the material structure allows an essential increase of its hardness and wear-, heat- and corrosion resistance [6, 10–21, 34–36]. In particular, improvement of wear resistance of friction surfaces of mill-and-boring machine parts with programmed numerical control is provided by laser alloying with coating (%: 15 Fe + 30 Ni + 20 B + 10 Si + 25 of liquid glass) in nitrogen atmosphere in the following mode: $q = 0.31\cdot10^5$ W/cm^2, v = = 33 mm/s [36]. Here rod and bushing wear are reduced 3.44 and 3.21 times, respectively.

Given below are examples of practical application of laser alloying of steel items by various materials and mixtures. Laser alloying technology has been mastered at CJSC «SiburKhimProm» (Perm, Russia) for strengthening of surfaces of parts operating at various kinds of wear

[11]. In [11, 22, 37] it is shown that at laser alloying by (B_4C + Cr) composition, layers of down to 0.15–0.25 mm depth form on the surfaces of plungers of pump-compressor equipment made from steels 10, 20, 15Kh, 12KhN3A and 12Kh2G2NMFT. X-ray microprobe analysis showed [37] that laser treatment results in intensive saturation of surface layers by alloying elements, for instance, chromium content in the layers rises 9 to 13 times. Phase composition of the layers contains highly oversaturated solid solutions based on alpha and gamma modifications of iron, as well as borides and carbides of chromium and iron. It is established that corrosion rate of alloyed layers decreases by 3 to 8 times (for 573 and 1173 K, respectively), compared to corrosion rate of untreated layers [11]. Wear testing under sliding friction demonstrated that wear resistance of alloyed layers increased 1.5 to 7 times, compared to surface untreated by laser radiation [11, 22]. Thus, it was established that application of laser alloying allows extension of service life of equipment parts 2 to 4 times due to improvement of their performance [11, 22, 37].

The authors of [38] conducted investigations on laser alloying of steel surface by molybdenum to lower the extent of wear of diverse tool equipment. During investigations molybdenum was first applied on steel surfaces by plasma spraying, and then surface-melted by continuous radiation of Nd:YAG laser. A video camera, equipment for sound analysis and a pyrometer group were used to monitor the process. Process monitoring system used the respective environment for determination of beam/material interaction. For instance, sound analysis of spikes allowed qualitative assessment of intensity drops at alloying. Measurement of melt surface temperature using a pyrometer allowed introducing a correlation by molybdenum content into the alloyed zones that has an important role and is associated with the achieved crack resistance and wear intensity [38].

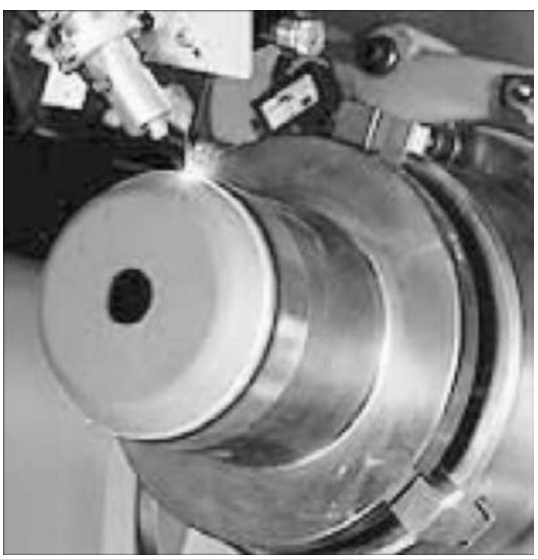

Figure 2. Laser alloying of die tooling elements for hot stamping made from 1.2365 steel (X32CrMoV3-3) [42]

Among the diversity of tools, shearing dies feature special operating conditions, where the matrices and punches are subjected to shock loads, high contact pressures reaching 1500 MPa at high-speed deformation of 0.1–5.0 m/s. Investigations were performed [39, 40] of the regularities of impact wear of working surfaces of matrices and punches of shearing dies, made from U8 and X12M steels, which were alloyed by mixtures based on boron, silicon and carbon compounds. Introduction of developed recommendations on laser boro-carbo-siliconizing in production at «Elektrodetal» plant and Bryansk Works of Process Equipment (Russia) was implemented that resulted in 1.5 to 3 times improvement of tool wear resistance [39].

Laser alloying of hot stamping die tooling parts (Figure 2) was performed [41–44] at Fraunhofer Institut fur Produktions technologies IPT, Aachen. The authors of [41] found that adding molybdenum and vanadium carbide as alloying element at laser alloying significantly increases the hardness of die tooling and improves heat resistance, but does not significantly affect the wear resistance. It is shown [41] that additional alloying by manganese allows improvement of wear resistance of surface layers of parts, which are exposed to high loads. Laser alloying [42–44] of 1.2365 steel (X32CrMoV3-3) was performed by titanium carbide, tungsten carbide and cobalt. Conducted full-scale testing showed that wear resistance of die tooling, which has passed laser alloying, increased by 67 % compared to untreated tooling [42–44]. In addition, important is the fact that the tooling operating time after laser alloying was also increased, that also allowed reducing the cost and increasing production volumes [42–44].

In Russian enterprises «Gidrotermal» Ltd. and OJSC «Inzhenerny Tsentr» (Nizhny Novgorod), laser alloying by mixtures of powders of chromium, molybdenum, aluminium and $(NH_2)_2CO$, as well as aluminium and $(NH_2)_2CO$, is used in manufacture and treatment of elements of power system structure of the type of nozzle, flange, bushing, rotary valve and others made from 38Kh2MYuA steel [45, 46]. It is established [45] that alloyed zones have a thin layer of dendritic structure. This layer is enriched in aluminium and, probably, aluminium nitride. During testing it was found that not the upper layers, but those located at a certain depth, have the highest wear

resistance. The authors of [45, 46] assume that this is related to nitrogen diffusion into the inner layers of the treated zone and formation of aluminium nitrides. Wear resistance of 38Kh2MYuA steel after laser alloying by a powder mixture increases, Cr–Mo–Al–$(NH_2)_2CO$ mixture ensuring an increase of surface wear resistance by 6.5 to 9.5 times, and Al–$(NH_2)_2CO$ mixture increasing subsurface layer wear resistance by 2.86 to 3.58 times [45, 46].

Deep drawing presses which are used to form a standard metal sheet in the automotive industry should stand extreme loads, and even after a large number of operations they should preserve their accuracy and dimensions. Cost of repair and product losses make these items more expensive, so that industrial users are interested in extension of tool service life. Depending on strengthening purpose, during laser alloying of forging tool surface by tungsten carbide, metal tool protection from wear is provided in individual local zones due to high accuracy of laser alloying technology [47]. At Fraunhofer Institute in close cooperation with HB Seissenchmidt AG Company, such technologies allowed achieving up to 500 % extension of tool service life, compared to traditional treatment methods [47].

Investigation of the structure and properties of a wide range of parts from steels 45, U8A and 6KhS at laser alloying by nickel, molybdenum, chromium, boron and tungsten boride at continuous laser impact was performed [48–50]. Influence of the composition and thickness of alloying coating on alloyed zone depth formation was found [48]. Optimum parameters were established [48–50], technology of laser alloying has been developed and introduced in various Russian enterprises of the industry (OJSCs «Zavod «Krasnoe Sormovo», «Pavlovsky Avtobus» «Gorkovsky Metallurgichesky Zavod», «Vyksunsky Metallurgichesky Zavod», «Nizhegorodsky Aviastroitelny Zavod «Sokol»). Application of laser alloying technology provided 1.5 to 2 times increase of wear resistance of surface layer of items (cutters, plungers, axles, bushings, etc.) at simultaneous reduction of used material cost [48].

Conclusions

1. Good prospects for application of the results of laser surface alloying in various industries are noted by many authors. However, despite the indubitable scientific and practical interest laser technologies of surface treatment have not become adequately developed and introduced at present. This is due to insufficient knowledge of general regularities of variation of treated steel properties, depending on phase and structural state at alloying by various materials under the conditions of superhigh heating and deposition rates that restrains development of specific working technologies and recommendations of applied nature.

2. Work performed in the field of laser alloying of steel items, was often aimed at solution of a localized task of improvement of service properties of a particular material or parts from it. Therefore, the results obtained by various authors cannot be systematized, because of significant differences in the schematics and conditions of research performance. This is largely due to absence of principles of controlling structure formation when producing in the steel surface layer a structure ensuring a high level of structural strength characteristics, which form the basis of development of such technologies.

1. Petrenko, K.P. (2013) Structural model of design of strengthening technological processes providing preset quality of surface layer. *Uprochn. Tekhnologii i Pokrytiya*, **1**, 7–9.
2. Pavlov, M.D., Tarasova, T.V., Nazarov, A.P. et al. (2012) Effect of preliminary preparation of product surface on quality of laser clad coatings. *Ibid*., **12**, 31–34.
3. Nazarov, Yu.F., Ivanajskykh, A.V., Tochilin, P.V. et al. (2010) Economic efficiency of high technologies by the example of laser production. *Svarochn. Proizvodstvo*, **3**, 48–50.
4. Saraev, Yu.N., Bezborodov, V.P., Durakov, V.G. et al. (2012) Modification of structure of compositions with protective coatings by alloying and high-energy impact. *Ibid*., **12**, 10–13.
5. Gulyaev, A.P. (1986) *Metals science*. 6th ed. Moscow: Metallurgiya.
6. Chudina, O.V. (2003) *Combined technologies of surface strengthening of structural steels*: Syn. of Thesis for Dr. of Techn. Sci. Degree. Moscow: MGADI.
7. Stadler, F., Antrekowitsch, H., Fragneretal, W. (2013) The effect of main alloying elements on the physical properties of Al–Si foundry alloys. *Materials Sci. and Eng*., **560**, 481–491.
8. Anandan, S., Pityana, L., Majumdar, J.D. (2012) Structure property correlation in laser surface alloyed AISI 304 stainless steel with WC + Ni + NiCr. *Ibid*., **536**, 159–169.
9. Lakhtin, Yu.M., Leontieva, V.P. (1990) *Materials science*. 3rd ed. Moscow: Mashinostroenie.
10. Grigoriants, A.G., Shiganov, I.N., Misyurov, A.I. (2006) *Technological processes of laser treatment*. Moscow: N.E. Bauman MGTU.
11. Kalashnikova, M.S. (2003) *Improvement of service properties of low-carbon steel surface by laser alloying method*: Syn. of Thesis for Cand. of Techn. Sci. Degree. Ekaterinburg: PGTU.
12. Abilsiitov, G.A., Golubev, V.S., Gontar, V.G. et al. (1991) *Technological lasers*: Refer. Book. Vol. 1: Calculation, design and service. Moscow: Mashinostroenie.
13. Kovalenko, V.S., Golovko, L.F., Chernenko, V.S. (1990) *Strengthening and alloying of machine parts by laser beam*. Kiev: Tekhnika.
14. Burakov, V.A., Brover, G.I., Burakova, N.M. (1985) Improvement of heat resistance of high-speed steels by laser alloying. *Metallovedenie i Term. Obrab. Metallov*, **11**, 2–6.

15. Likhoshva, V.P., Shatrava, A.P., Bondar, L.A. (2007) Laser alloying of friction assembly. *Protsessy Litia*, **3**, 35–37.
16. Dobrzanski, L.A., Bonek, M., Hajduczek, A. et. al. (2004) Application of high power diode laser (HPDL) for alloying of X40CrMoV5-1 steel surface layer by tungsten carbides. *J. Mater. Proc. Technol.*, **155/156**, 1956–1963.
17. (2009) *Laser technologies and computer modeling*. Ed. by L.F. Golovko and S.O. Lukianenko. Kyiv: Vistka.
18. Zhong, M., Liu, W., Zhang, H. (2006) Corrosion and wear resistance characteristics of NiCr coating by laser alloying with powder feeding on grey iron liner. *Wear*, **260**, Issues 11/12, 1349–1355.
19. Isshiki, Y., Shi, J., Nakai, H. et al. (2000) Microstructure, microhardness, composition and corrosive properties of stainless steel 304 L. Laser surface alloying with silicon by beam-oscillating method. *Appl. Physics A*, **70**, Issue 4, 395–402.
20. Majumdar, J.D. (2008) Development of wear resistant composite surface of mild steel by laser surface alloying with silicon and reactive melting. *Mater. Lett.*, **62**, 4257–4259.
21. Kruth, J.-P., Levy, G., Klocke, F. et al. (2007) Consolidation phenomena in laser and powder-bed based layered manufacturing. *CIRP Annals — Manufact. Technology*, **56**, Issue 2, 730–759.
22. Ignatov, M.N., Kalashnikova, M.S., Belova, S.A. (2002) Influence of temperature-time parameters on structure and properties of surface layer of structural steels after laser alloying. *Vestnik PGTU*. Series Mechanics and Technology of Materials and Structures, **5**, 154–159.
23. Garashchuk, V.P. (2005) *Principles of physics of lasers. Lasers for thermal technologies*. Kiev: PWI.
24. Biryukov, V.P. (2008) Influence of distribution of laser beam power density on increase in wear resistance of friction surfaces. *Vestnik Mashinostroeniya*, **3**, 33–36.
25. Majorov, V.S., Matrosov, M.P. (1989) Influence of surfactants on hydrodynamics of laser alloying of metals. *Kvant. Elektronika*, 16(**4**), 806–810.
26. (2009) *Laser technologies of treatment of materials: Current problems of fundamental research and applied developments*. Ed. B.Ya. Panchenko. Moscow: Fizmatlit.
27. Kindrachuk, M.V., Ishchuk, N.V., Golovko, L.F. et al. (2007) Principles of formation of nitrided layers by combined laser-chemical-heat treatment of steels. *Metaloznavstvo ta Obrobka Metaliv*, **1**, 31–35.
28. Kindrachuk, M.V., Dudka, O.I., Sukhenko, Yu.G. et al. (2001) Influence of thermocycling on tribotechnical properties of boride layers made by laser alloying. *Transact. of UDUKhT*, **10**, 74–75.
29. Emami, M., Shahverdi, H.R., Hayashi, S. et al. (2013) A combined hot dip aluminizing/laser alloying treatment to produce iron-rich aluminides on alloy steel. *Metall. and Mater. Transact. A*, **2**, 1–9.
30. Biryukov, V.P. (2011) Laser strengthening and alloying. *Fotonika*, **3**, 34–37.
31. Leech, P.W., Batchelor, A.W., Stachowiak, G.W. (1992) Laser surface alloying of steel wire with chromium and zirconium. *J. Mater. Sci. Lett.*, **11**, Issue 16, 1121–1123.
32. Tarasova, T.V. (2010) Prospects of application of laser radiation to increase wear resistance of corrosion-resistant steels. *Metallovedenie i Term. Obrab. Metallov*, **6**, 54–58.
33. Kornienko, O.A., Yakhia, M.S., Ishchuk, N.V. et al. (2008) Formation of coating of tribotechnical purpose by combined, laser-chemical-thermal treatment. In: *Problem of friction and wear*: Transact., **2**, Issue 49, 61–65. Kyiv: NAU.
34. Thawari, G., Sundararajan, G., Joshi, S.V. (2003) Laser surface alloying of medium carbon steel with SiC(P). *Thin Solid Films*, **423**, 41–53.
35. Dobrzanski, L.A., Bonek, M., Labisz, K. (2013) Effect of laser surface alloying on structure of a commercial tool steel. *J. Microstructure and Mater. Properties*, **8**, Issue 1/2, 27–37.
36. Lazko, G.V. (2009) *Peculiarities of structure formation and ways to improve properties of barrier layers on corrosion-resistant steels, formed by laser alloying*: Syn. of Thesis for Cand. of Techn. Sci. Degree. Donetsk: DNTU.
37. Kalashnikova, M.S., Belova, S.A., Mazepina, Yu.A. et al. (2003) Corrosion resistance of structural steel surface layers after laser treatment. *Fizika i Khimiya Obrab. Materialov*, **2**, 34–39.
38. Haferkamp, H., Bach, F.-W., Gerken, J. (1995) Laserstrahllegieren plasmagesprittzer Molybdanschichten in Stahloeberflachen zur Erhoehung des Verschleisswiderstandes. *Metall*, **49**, Issue 7/8, 516–522.
39. Zhostik, Yu.V. (1998) *Study of impact wear of shearing dies and increase in their resistance due to laser alloying*: Syn. of Thesis for Cand. of Techn. Sci. Degree. Bryansk: BGITA.
40. Inyutin, V.P., Kolesnikov, Yu.V., Zhostik, Yu.V. (1986) Effect of laser boronizing on contact deformations of steel 45 under impact-cyclic loading. *Elektr. Tekhnika*. Series 6: Materials, **215**, Issue 4, 77–78.
41. Klocke, F., Rozsnoki, L., Celiker, T. et al. (1996) New developments in surface technology: Laser alloying using Mo/VC and Mn. *CIRP Annals — Manufact. Technology*, **45**, Issue 1, 179–182.
42. Klocke, F., Auer, O., Hamers, M. (1998) Verschleissreduzierung bei Schmiedewerkzeugen. *Maschinenmarkt*, **104**, Issue 34, 32–33.
43. Klocke, F., Auer, O., Hamers, M. (2002) Verschleissschutz von Warmumformwerkzeugen. *VDI-Z Integrierte Produktion Special*, **2**, 67–69.
44. Klocke, F., Auer, O., Hamers, M. (2000) Laser scan help protect tools. *Quelle Diecasting World*, **6**, 18–21.
45. Kastro, V.A. (2012) *Development of technology for laser thermal strengthening and alloying of steels for power machine building with the purpose of increase of service life of items*: Syn. of Thesis for Cand. of Techn. Sci. Degree. Nizhny Novgorod: R.E. Alekseev NGTU.
46. Kastro, V.A., Gavrilov, G.N., Brauer, I. et al. (2011) Peculiarities of steel structure formation in laser thermal cycle. *Zagotovit. Proizvod. v Mashinostroenii*, **12**, 38–41.
47. (1997) Werkzeugehaerten senkt die Kosten. *http://www.archiv.fraunhofer.de/archiv/alte %20jahresberichte/pflege.zv.fhg.de/german/publications/jahres-ber/jb1997/f_oberfl.htm1*
48. Gavrilov, G.N. (2000) *Development and mastering of technologies for surface thermal strengthening and surfacing of metallic materials by laser radiation*: Syn. of Thesis for Dr. of Techn. Sci. Degree. Nizhny Novgorod: NGTU.
49. Gavrilov, G.N., Gorshkova, T.A., Fedoseev, V.B. (1997) Influence of thermochemical effect on laser alloying process. *Izvestiya Inzh.-Tekhnolog. Akad. Chuvash. Resp.: Joint Sci. J.*, **3/4**, 118–121.
50. Gavrilov, G.N., Gorshkova, T.A., Dubinsky, V.N. (1998) Study of wear resistance of steel 45 after laser alloying. *Ibid.*, **1/2**, 122–125.

Received 02.09.2013

STUDY OF EFFECT OF ELECTRIC ARC SPRAYING MODES ON STRUCTURE AND PROPERTIES OF PSEUDOALLOY COATINGS

Yu.S. BORISOV, N.V. VIGILYANSKAYA, I.A. DEMIANOV, A.P. GRISHCHENKO and **A.P. MURASHOV**
E.O. Paton Electric Welding Institute, NASU
11 Bozhenko Str., 03680, Kiev, Ukraine. E-mail: office@paton.kiev.ua

A study of effect of electric arc spraying conditions on structure and properties of steel–copper pseudoalloy coating was performed. A method of multifactor experiment planning was used for determination of level of influence of spraying factors on coating characteristics. Analysis of splat specimens showed that the drops of metal are in a liquid state during collision with a basis at all studied modes of spraying. The regression equations were received which combine technological modes of spraying (rate of wire feed, voltage, consumption of compressed air, spraying distance) with hardness, content of steel and copper constituents, oxides and pores in the coating. It was determined that content of copper in total volume of the coating, obtained by spraying of steel and copper wires of similar diameter, depends on a heat input in spray consumable and makes around 35 vol.% at 0.6–1.0 MJ/kg and approximately 22 vol.% at 1.4–2.2 MJ/kg. Possible reasons of reduction of copper content are the burn-out (evaporation) and oxidation of copper in spraying process due to its reheating above melting point. The most efficient method of reduction of copper loss due to its burning out during spraying of pseudoalloy steel–copper coating is decrease of level of heating of spray particles and increase of their speed due to rise of compressed air consumption and reduction of heat input in the spray consumable. The best complex of structure and properties of electric arc pseudoalloy steel–copper coatings based on indexes of preservation of component relation (1:1), porosity (8 vol.%), level of oxidation (21 vol.%) and hardness (2700 MPa) was received in the case of spraying with 1.0 MJ/kg heat input in the wire and 126 m^3/h consumption of compressed air. 22 Ref., 2 Tables, 8 Figures.

Keywords: *electric arc spraying, pseudoalloy coatings, microstructure, porosity, oxidation, microhardness*

A process of electric arc spraying is characterized by large number of factors having effect on service properties of the coatings. Study of effect of these factors on process of coating formation is necessary in order to control the properties of coating being obtained.

Mechanical properties of the coatings, obtained by electric arc spraying, are concerned with their structure and depend on spraying modes which change coating microstructure (content of oxides and pores in the coating).

Oxides in the coating play a dual role. On the one hand, they significantly increase coating wear resistance since having as a rule higher hardness than the initial pure metals. At the same time, there is some critical quantity of oxides, exceeding of which provides stepwise reduction of coating serviceability under effect of external loads due to rise of its embrittlement [1]. Porosity in the coatings reduces the wear resistance at dry friction [2], however, pores have positive role in anti-friction coatings providing favorable conditions for preservation of oil film [3] during the friction process.

Most of the researchers agree in opinion that increase of pressure of spraying gas promotes decrease of coating porosity [4]. Raising of spraying gas pressure increases dispersion of spray consumable (aluminum, steel, copper) [5, 6] and velocity of particle movement [7]. This results in formation of more dense homogeneous structure of the coating. Change of wire feed rate, voltage on the electrodes and spraying distance have insignificant effect on size of spray particles (aluminum, steel–copper) [5]. Reduction arcing voltage results in some displacement of size of spray particles in area of smaller fractions during spraying of steel, copper or aluminum wires [6, 8, 9]. Increase of arc current from 150 up to 200 A leads to 1.5–2.0 % decrease of coating porosity [10].

However, increase of spraying gas pressure raises oxide content in the coating since reduction of size of spray particles promotes their more intensive interaction with oxygen [11]. Rising of particle diameter from 10 up to 237 μm provides

approximately 30 % decrease of level of drops oxidation [12].

Content of oxides in the coating increases from 10 up to 40 % with rise of spraying distance from 25 to 300 mm due increase of time of particles interaction with oxygen in a jet [3].

When electric arc coatings are used as wear resistance materials, hardness which is determined by conditions of layer formation in metal spraying becomes an important property of the coating. Increase of pressure of spraying gas provides rise of hardness due to formation of denser layer [13]. The coatings from wire with low carbon content acquire hardness on account of large number of oxides [2]. When high-carbon wires are used, the hardness of the coating increases with rise of the distance up to 100 mm and then it reduces at further increase of the distance as a result of rise of pores in the coatings. Hardness of coatings increases from *HB* 193 to *HB* 207 using high-carbon wires if pressure of compressed air is risen from 3 to 7 atm. Increase of wire feed rate and current intensity, respectively, promote coating hardness decrease.

The process of melting and detachment of drops from wires of anode and cathode are not similar during the electric arc spraying [5, 14]. Difference in rates of wire melting (due to difference of melting temperatures of these materials) effects the process of asymmetric melting, formation and detachment of drops in spraying of pseudoalloy coatings using dissimilar wires. This results in formation of inhomogeneous microstructure. Study [15] showed inhomogeneity of distribution of the coating components over a deposition spot during spraying of copper and steel wires.

Uniformity of component distribution is an important characteristic in spraying of pseudoalloy coatings.

The aim of present paper is a study of effect of operating parameters of the electric arc spraying on microstructure (porosity, oxidation level, and homogeneity of component distribution) and hardness of pseudoalloy steel–copper coatings.

Experimental procedure. 2 mm diameter copper M1 grade wire and steel Sv08A grade wire were used as consumables during investigation of the process of formation of pseudoalloy coatings obtained by simultaneous spraying of dissimilar wires. The coatings were deposited using electric arc metallizator EM-14M with VDU-506 power source. A method of mathematical planning of experiment [16] was used to determine a nature of interaction between the conditions of wire spraying and structure of pseudoalloy coatings.

The following parameters were taken as variable factors: wire feed rate v_w, m/h; voltage on arc electrodes U, V; consumption compressed air V_g, m^3/h (pressure of compressed air, atm); spraying distance H, m. The choice was based on the fact that these factors have the most significant influence on structure and properties of the coatings [2, 5].

Half-replicate 2^{4-1} was used for a four-factor experiment. The conditions of experiment were brought in a planning matrix (Table 1). The values of arc power P and complexes of parameters characterizing specific consumption of energy for gas IU/V_g and wire IU/G_w heating were introduced (see Table 1) for analysis process of wire spraying. They allow determining the level of heat input in spray consumable and gas jet.

Table 1. Matrix for mathematical modeling of the experiment*

Number of experiment	Spraying parameters				Power P, kW	IU/V_g, MJ/m^3 of gas	Wire consumption G_w, kg/h	IU/G_w, MJ/kg of wire	d_{part}, μm [6]	S, m^2/kg	H/V_g, h/$m^2 \cdot 10^{-6}$
	v_w, m/h	U, V	V_g, m^3/h (pressure, atm)	H, m							
1	300	48	126 (7)	0.20	9.8	0.28	15.8	2.2	37	19.4	15.9
2	300	48	108 (6)	0.06	9.8	0.33	15.8	2.2	42	17.1	5.6
3	300	22	126 (7)	0.06	4.4	0.13	15.8	1.0	40	17.9	4.8
4	300	22	108 (6)	0.20	4.4	0.15	15.8	1.0	52	13.8	18.5
5	180	48	126 (7)	0.06	3.8	0.11	9.5	1.4	46	15.6	4.8
6	180	48	108 (6)	0.20	3.8	0.13	9.5	1.4	52	13.8	18.5
7	180	22	126 (7)	0.20	1.7	0.05	9.5	0.6	45	15.9	15.9
8	180	22	108 (6)	0.06	1.7	0.06	9.5	0.6	54	13.3	5.6

*Quantity of heat necessary for wire melting — 0.49 MJ/kg.

Received numerical values of IU/V_g and IU/G_w indexes refer to the limiting values of application of electric arc energy. It is assumed that in IU/V_g case it is completely used for heating of spraying gas and in case of IU/G_w for heating of spray wire. These factors are designed for qualitative evaluation of conditions of electric arc spraying process. Table 1 also shows a calculation of particle specific reaction surface S and index of time of their staying in jet H/V_g in order to estimate a process of oxidation of spray consumable particles.

Boundary conditions for the factors were chosen from the analysis of previous experiments and experience of electric arc spraying of coatings using wire consumables [17, 18]. The value of current was connected with change of wire feed rate and made 80 A at 180 m/h and 200 A at 300 m/h rate. Such factors as 90° incidence angle and 30° angle between the electrodes remained constant in addition to varying factors.

Investigation of state of the particles in moment of their collision with the basis was performed using splat-test following procedure described in [13]. Spraying of the splat specimens were made on the plates from polished stainless steel of 50 × 30 × 1 mm size by moving metallizator. Velometer of luminous objects ISSO-1 [19] was used for determination of velocity of particles in process of the electric arc spraying of wire consumables.

For microstructure investigation the coatings were sprayed over St3 specimens of 20 × 15 × × 3 mm size. The specimens were subjected to sand-blasting before spraying. Thickness of the coating made 500–700 μm.

All the experiments were carried out on modes corresponding to experiment plan. Microstructure of the coatings and external view of the splats were studied using metallographic microscope «Neophot-32». Image processing program «Atlas» was used for determination of content of components, oxides and pores in the coating. Microhardness was determined on microhardness tester PMT-3. The measurements were taken along the whole coating section.

Results of experiment. Analysis of the results was carried out considering indexes of process of heat input in gas and wire and conditions of particle interaction with gas medium (Table 2).

Study of shape of melt particles after collision with the surface (splat-test). The analysis of splats obtained by simultaneous spraying of copper and steel wires showed that the particles have a star-shaped form in all experiments (Figure 1).

Such type of splats is received from the particles being in a liquid state at a moment of collision with the basis, i.e. the particles do not solidify during in-flight at the spraying distance that is explained by short time of the flight [20]. Measurement of the particle velocity showed that their velocity makes around 100 m/s at the moment of particle collision with the basis. Time of particle staying in a jet equals 0.6–0.2 ms at spraying distance 0.06–0.20 m.

The color of copper constituent on the splats received during experiments 1 and 2 indicates its overheating that, apparently, being caused by combination of maximum heat inputs in the jet and wire (Table 2, experiments 1 and 2), resulting in heating of the metal to higher temperature. Spattering of the particles observed on splats 1, 2, 5 and 6 indicates their overheating related with the same problems.

Study of microstructure of pseudoalloy steel-cooper coatings. The analysis of coating structures obtained by simultaneous spraying of copper and steel wires showed that all the coatings are dense with obvious lamellar structure at given range of spraying modes (Figure 2). Such type

Table 2. Indexes of process of heat input in gas and wire and conditions of interaction of particles with gas medium

Number of experiment	Heat input in jet IU/V_g, MJ/m^3			Heat input in wire IU/G_w, MJ/kg				Size of specific reaction surface of the particles S, m^2/kg			Index of time of particle staying in jet H/V_g, h/m^2·10^{-6}	
	0.28–0.33	0.11–0.13	0.05–0.06	2.2	1.4	1.0	0.6	17–19	15–16	13–14	16–19	5–6
1	×			×				×			×	
2	×			×				×				×
3		×				×		×				×
4		×				×				×	×	
5		×			×				×			×
6		×			×					×	×	
7			×				×		×		×	
8			×				×			×		×

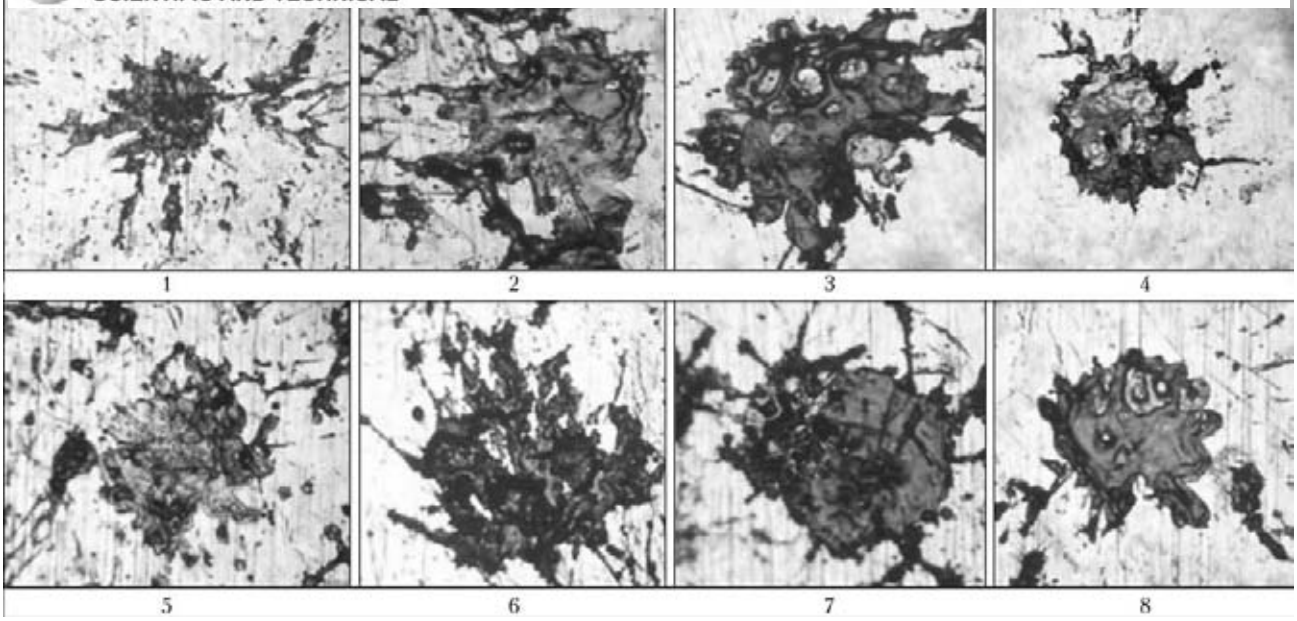

Figure 1. Splats of particles obtained by simultaneous spraying of copper and steel wires using spraying conditions according to the matrix of Table 1 (here and below 1–8 — numbers of experiments)

of structures is typical for the coating formed from the particles being in a liquid state at the collision moment and having sufficiently high velocity that corresponds to results of splats' investigation.

Table 3 shows content of components in the coating, level of oxidation and porosity.

The analysis of component content in the coatings showed a change of relative content in the coatings of copper and steel as a result of spraying. Copper content in the spray consumable using equal diameters of wires (2 mm) makes 50 vol.%. Thus, such a high values of wire heat input (Table 2, experiments 1, 2, 5 and 6) that correspond to 2.2 and 1.4 MJ/kg values provide, respectively, 36, 33, 30 and 29 vol.% content of copper in total content of copper and steel constituents. Reduction of this heat input to 1.0 MJ/kg (experiments 3 and 4) and 0.6 MJ/kg (experiments 7 and 8) increases the content of copper in total content of copper and steel constituents to 51, 48, 47 and 48 vol.%, respectively.

This phenomenon is obviously related with the fact that temperature of the molten particles during spraying can significantly exceed the temperature of copper melting [5] and achieve boiling temperature 2800 K. Since the temperatures of boiling and pressure of vapors of copper and iron are different (pressure of copper vapor (113 MPa) is higher in comparison with that of iron (13.3 MPa) [21]), increase of energy con-

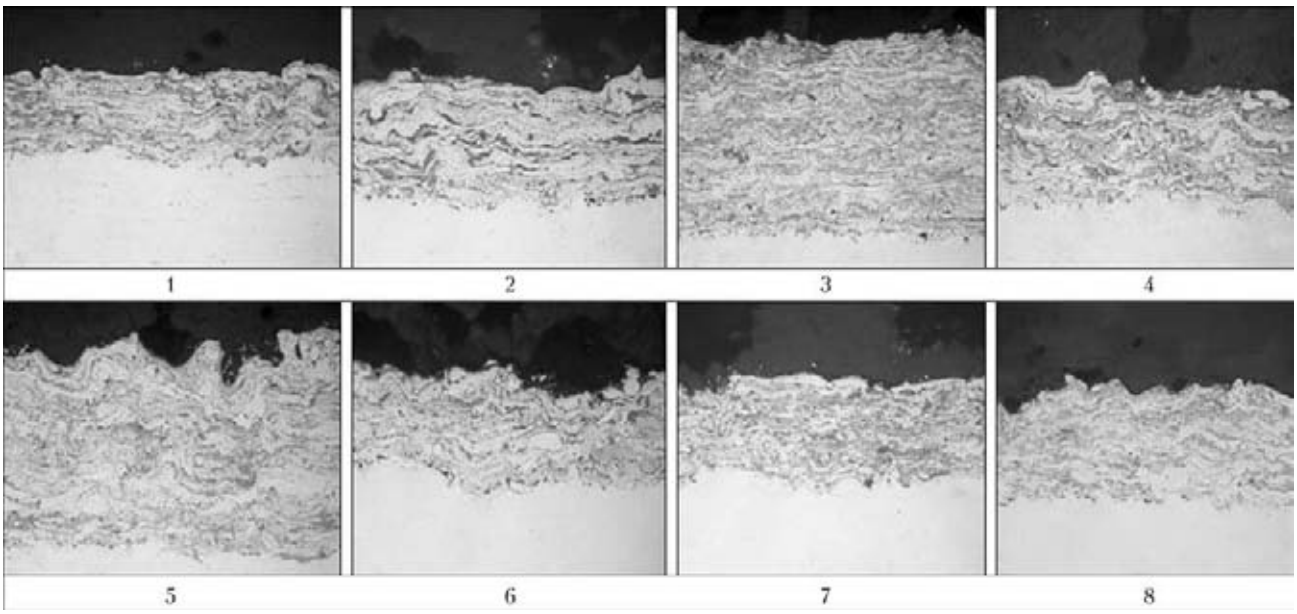

Figure 2. Microstructure (×200) of steel–copper coatings

Table 3. Content of components, level of oxidation and porosity of pseudoalloy steel–cooper coating

Number of experiment	Content of copper in coating, vol.%	Content of steel in coating, vol.%	Content of oxides, vol.%	Porosity, vol.%	Content of copper in total content of metal constituents, vol.%
1	24	42	27	7	36
2	23	47	20	10	33
3	37	36	21	8	51
4	33	36	25	6	48
5	21	49	25	5	30
6	19	46	22	13	29
7	31	35	26	8	47
8	35	38	21	6	48

sumption for wire heating (see Table 2, experiments 1, 2, 5 and 6) results in more intensive heating of copper wire during melting and, obviously, to its partial evaporation in spraying. The conditions, caused by properties of electric arc (electrodynamic forces acting in area of arc discharge) also promote transfer of copper particles in gas phase [21, 22]. Another possible reason for reduction of content of copper constituent can be the more intensive oxidation of copper in process of spraying in comparison with that of iron.

Increase of consumption of compressed air and wire feed rate lead to preservation of copper content in the coating. This can be explained by the fact that increase of compressed air consumption and, as a result, rise of speed of jet increases velocity of particles and reduces their temperature that decreases the intensity of process of copper evaporation. Regression equation, reflecting effect of process parameters on copper content in the coatings, indicates also that the most efficient method for preservation of relationship of content of components in the coating relative to the initial one is increase of the compressed air consumption and reduction of voltage for decrease of copper constituent burn out. The level

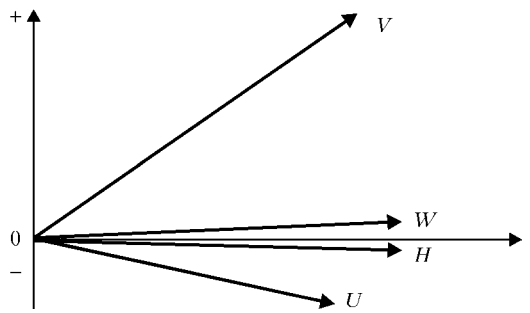

Figure 3. Level of effect of spraying factors on content of copper in coatings

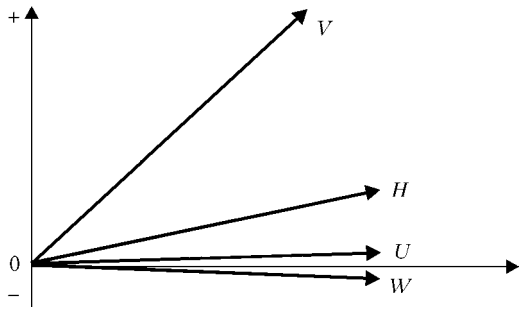

Figure 4. Level of effect of spraying factors on oxidation of coatings

of influence of spraying parameters on copper content in the coating (Figure 3) is shown by the next equation: %Cu = 49.09 + 0.03W – 0.6U + 1.5V + 0.004H. Change of spraying distance in 0.06–0.20 m range does not provide significant effect on content of components in the coating.

The maximum content of oxides was found in the coatings sprayed using the modes with the maximum consumption of compressed air and maximum spraying distance (see Table 3, experiments 1 and 7). It is related with the fact that a rise of consumption of the compressed air results in reduction of diameter of the spray particles at wire dispersion [6]. This leads in enlargement of area of development of oxidation process. Increase of spraying distance promotes in turn the rise of time of particle staying in the jet and development of process of particle interaction with the oxygen. The level of effect of spraying factors on oxide content in the coatings (Figure 4) is represented by equation %MeO = = 2.44 – 0.002W + 0.01U + 2.75V + 0.02H.

Figure 5 shows a dependence of oxide content in the coating on index of particle staying in the jet (H/V_g).

The results of examination of coating porosity showed that it does not exceed 13 %. As can be seen from the regression equation, the value of porosity is first of all effected by the compressed air consumption, increase of which leads to rise

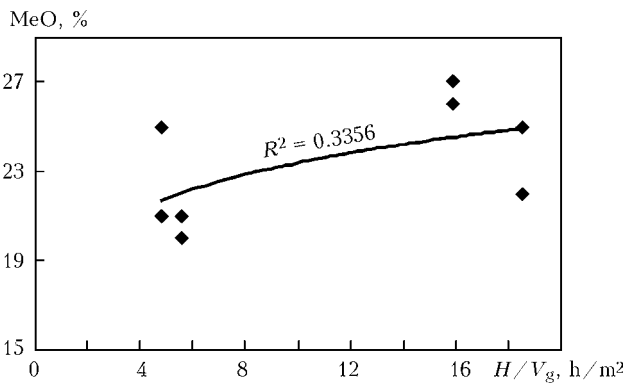

Figure 5. Dependence of coating oxidation level on index of time of particle staying in jet

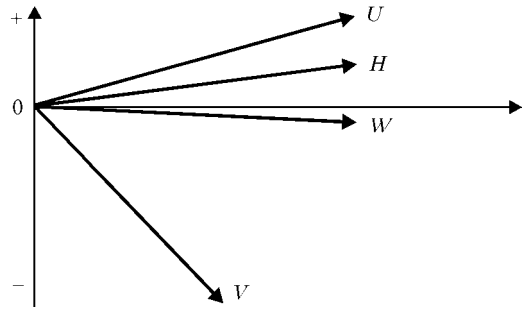

Figure 6. Level of effect of spraying factors on porosity of coatings

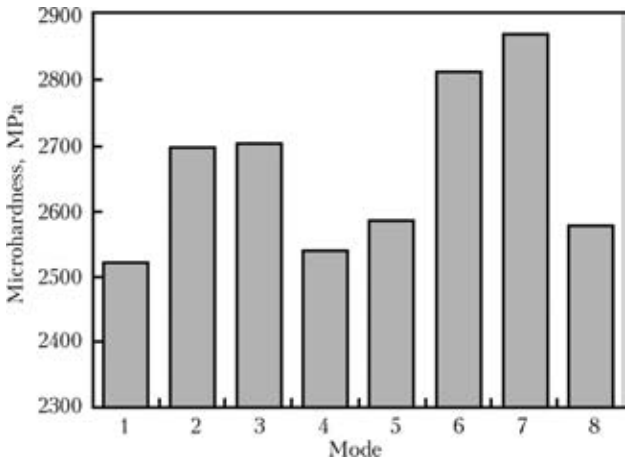

Figure 7. Dependence of microhardness of steel–copper coating on spraying mode

of particle in-flight velocity, decrease of size of spray drops, and formation of more dense coating, respectively. The level of influence of spraying factors on value of coating porosity (Figure 6) is described by equation, $\%P = 16.03 - 0.002W + 0.07U - 1.75V + 0.01H$.

Relationship of density of solid material to density of melt ($\rho_s/\rho_l = 8.93/8.03 = 1.11$ for copper and $\rho_s/\rho_l = 7.87/7.02 = 1.12$ for iron) also effects the coating porosity. Since density of melt of the coating material is less than its density in solid state, the volume of molten particles in solidification reduces that result in pore formation.

Figure 7 represents a histogram of dependence of microhardness of pseudoalloy steel–copper coating on spraying mode.

Gauging of hardness in quantity of 50 measurements was carried out along the whole cross section. The dependence of microhardness on position of measurement points was not observed. The microhardness of coatings received with different modes of spraying lies in 2500–2900 MPa range.

Received regression equations, binding spraying parameters with coating hardness show that the coating hardness increases with the rise of compressed air consumption and spraying distance. It is caused by growth of level of oxidation

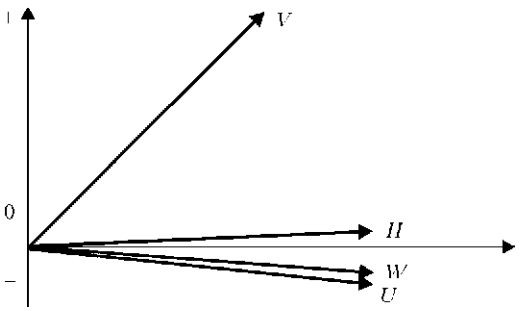

Figure 8. Level of effect of spraying factors on microhardness of steel–copper coatings

of the coating constituents at increase of these parameters and strengthening of coating material by oxide inclusions. Rising of the wire feed rate and voltage equally result in decrease of the coating hardness due to increase of heat input into the spray consumambes that can lead to their softening. The level of influence of spraying factors on microhardness of steel–copper coatings (Figure 8) is represented by regression equation $HV = 2680 - 0.8W - 0.77U + 12V + 0.324H$.

The best complex of structure and properties of electric arc pseudoalloy steel–copper coatings based on indexes of preservation of component relationship (37 vol.% Cu, 36 vol.% Fe), porosity (8 vol.%), level of oxidation (21 vol.%) and hardness (2700 MPa) was obtained in the case of spraying using wire heat input 1.0 MJ/kg and 126 m^3/h compressed air consumption (see Table 1, experiment 3). In other words, obtaining of the coating with low porosity is provided by combination of average level of input of arc energy into heating of spraying gas (air), limited intensity of heating of wire melt and increased rate of high dispersion spraying products.

Conclusions

1. Study of the process of pseudoalloy coating spraying was performed on the example of steel–copper pseudoalloy using the method of mathematical modelling of experiment. Analysis of the splats, received with applied range of spraying modes, showed that the particles in moment of collision with the basis are in the molten state and being characterized by high velocity (approximately 100 m/s). Coating structure is lamellar and consists of copper and steel components with oxide inclusions.

2. It was determined that change of heat input into the spray consumable during electric arc spraying of pseudoalloy coatings from copper and steel wires leads to variation of relationship of copper and steel constituents in the coating. Specific content of copper in relation to steel makes around 30 vol.% in spraying with 1.4–2.2 MJ/kg wire heat input and that makes

around 50 vol.% at 0.6–1.0 MJ/kg. Possible reasons for reduction of copper content are the burn out (evaporation) and oxidation of copper in process of spraying due to its overheating above the melting point. The most efficient method of reduction of copper loss resulting in obtaining of uniform component content in the pseudoalloy steel–copper coating is increase of the compressed air consumption up to 126 m^3/h and reduction of heat input in the spray consumable to 0.6–1.0 MJ/kg for decreasing of copper constituent burn out.

3. The maximum 26–27 % content of oxides was found in the coatings during spraying with 126 m^3/h compressed air consumption and 0.2 m spraying distance. It is related with the increase of dispersion of the spray consumables and rise of time of the particle interaction with oxygen. The value of porosity, first of all, is effected by compressed air consumption, rising of which from 108 to 126 m^3/h results in decrease of size of spray drops and consequently in formation of more dense coating.

4. Microhardness of received coatings lies in 2500–2900 MPa range. Received regression equations, binding spraying parameters with coating hardness, show that hardness of coating increases with the rise of compressed air consumption from 108 to 126 m^3/ h and spraying distance from 0.06 to 0.20 m. This is caused by growth of level of oxidation of coating constituents.

5. The main factor of spraying affecting the characteristics of pseudoalloy steel–copper coating is the compressed air consumption, rising of which leads to preservation of component content in the coating relatively to the initial one, reduction of porosity and increase of hardness.

1. Korobov, Yu.S. (2006) *Improvement of arc spraying technology on the base of modeling of interaction between metal and gases and study of coating properties*: Syn. of Thesis for Dr. of Techn. Sci. Degree. UralGTU.
2. Vadivasov, D.G. (1956) *Repair of parts by metal spraying*. Saratov.
3. Krasnichenko, L.V. (1958) *Modern technology of metal spraying*. Moscow: Trudrezervizdat.
4. Brusilo, Yu.V. (2009) Specifics of coatings produced by electric metal spraying with posterior electrocontact sintering-up. In: *Visnyk Nats. Transport. Univers*. Pt 1. Kiev: NTU, 75–82. Issue 19.
5. Pourmousa, A., Mostaghimi, J., Abedini, A. et al. (2005) Particle size distribution in a wire-arc spraying system. *J. Thermal Spray Technology*, **14**, 502–510.
6. Borisov, Yu.S., Vigilanskaya, N.V., Demianov, I.A. et al. (2013) Investigation of dispersion of dissimilar wire materials during electric arc spraying. *The Paton Welding J.*, **2**, 24–30.
7. Newbery, A.P., Grant, P.S., Neiser, R.A. (2005) The velocity and temperature of steel droplets during electric arc spraying. *Surface and Coatings Technology*, **195**, Issue 1, 91–101.
8. Ageev, V.A., Belashchenko, V.E., Feldman, I.E. et al. (1989) Analysis of methods for control of spraying particle parameters in electric arc spraying. *Svarochn. Proizvodstvo*, **12**, 30–32.
9. Newbery, A.P., Grant, P.S. (2003) Large arc voltage fluctuations and droplet formation in electric arc spraying. *Powder Met.*, 46(**3**), 229–235.
10. Liao, H.L., Zhu, Y.L., Bolo, R. et al. (2005) Size distribution of particles from individual wires and the effects of nozzle geometry in twin wire arc spraying. *Surface and Coatings Technology*, **200**, Issue 7, 2133–2130.
11. Boronenkov, V.N., Korobov, Yu.S. (2012) *Fundumantals of arc spraying. Physical-chemical principles*. Ekaterinburg: UralGU.
12. Korobov, Yu.S., Boronenkov, V.N. (2003) Kinetics of interaction of spray metal with oxygen in electric arc metal spraying. *Svarochn. Proizvodstvo*, **7**, 30–36.
13. Planche, M.P., Liao, H., Coddet, C. (2004) Relationships between in-flight particle characteristics and coating microstructure with a twin wire arc spray process and different working conditions. *Surface and Coatings Technology*, **182**, Issues 2/3, 215–226.
14. Hussary, N.A., Heberlein, J.V.R. (2001) Atomization and particle–jet interactions in the wire-arc spraying process. *J. Thermal Spray Technology*, **10**, Issue 4, 604–610.
15. Zhu, Y.L., Liao, H.L., Coddet, C. et al. (2003) Characterization via image analysis of cross-over trajectories and inhomogeneity in twin wire arc spraying. *Surface and Coatings Technology*, **162**, Issues 2/3, 301–308.
16. Novik, F.S., Arsov, Ya.B. (1980) *Optimization of processes of technology of metals by methods of experiment planning*. Moscow: Mashinostroenie; Sofia: Tekhnika.
17. Kats, N.V., Antoshin, E.V., Vadivasov, D.G. (1966) *Metal spraying*. Moscow: Mashinostroenie.
18. Troitsky, A.F. (1960) *Principles of metal spraying*. Tashkent: Gosizdat UzSSR.
19. (1979) *Development of velocimeter of luminous objects USSO-1*: Report on R&D activity. Minsk: IF AN BSSR.
20. Kuznetsov, V.D., Pashchenko, V.D. (1999) *Physical-chemical bases of coating formation*: Manual. Kiev: NMTs VO.
21. *http://*www.masters.donntu.edu.ua/2006/fizmet/yeresko/dis/dis(ru).htm. Analysis of technology of copper elimination by evaporation from molten metal under electric arc action
22. Zigalo, I.N., Baptizmansky, V.I., Vyatkin, Yu.F. et al. (1991) Copper in steel and problems of its elimination. *Stal*, **7**, 18–22.

Received 19.06.2013

INFLUENCE OF STRUCTURAL PARAMETERS ON MECHANICAL PROPERTIES OF R6M5 STEEL UNDER THE CONDITIONS OF STRENGTHENING SURFACE TREATMENT

L.I. MARKASHOVA, Yu.N. TYURIN, O.V. KOLISNICHENKO, M.L. VALEVICH and **D.G. BOGACHEV**
E.O. Paton Electric Welding Institute, NASU
11 Bozhenko Str., 03680, Kiev, Ukraine. E-mail: office@paton.kiev.ua

The work is devoted to investigation of structural-phase changes in surface layers of high-speed steel R6M5 after strengthening pulsed-plasma surface treatment in various modes and influence of forming structure parameters on tool performance. As a result of comprehensive investigations and calculation-analytical prediction of strength properties, fracture toughness coefficient and crack resistance of surfaces, strengthened in various technological modes, it was established that optimum properties of subsurface layers are ensured at recommended modes of pulsed-plasma surface treatment, increasing the total strength level by 25 %, compared with base metal due to refinement of grain structure (by 1.5 to 2 times), increase of the contribution of substructural, grain, dislocation and dispersion strengthening mechanism. Here, the level of local inner stresses in the treated layer is equal to ~0.018 to 0.44 of the theoretical strength of material that is not dangerous in terms of crack formation, because of the absence of abrupt gradients as to inner stresses and uniformly increased dislocation density (10^{11}–2.10^{11} cm^{-2}) compared to base metal. It is shown that at a significant strengthening of treated layers of high-speed steel, the value of fracture toughness coefficient is by 15 % higher compared to base metal. Thus, application of recommended modes of pulsed-plasma surface treatment leads to modifying the structural-phase state of the surface layer and improvement of its mechanical properties. 31 Ref., 9 Figures.

Keywords: *pulsed-plasma treatment, surface, high-speed steel R6M5, light microscopy, electronic microscopy, analytical assessment, strength, fracture toughness, crack resistance*

Tool steel R6M5 is designed for operation under the conditions of high contact loads and temperatures, and this, as a rule, are metal-working tools, where the item working layer is exposed to the most intensive wear. Considering the complicated service conditions, improvement of the set of physico-mechanical properties of this layer by recrystallization and structure modification is of interest. Preliminary studies showed [1–4] that the most significant changes in the surface layer structure are observed at application of concentrated heat sources: laser, electron beam, plasma, etc. Technology of pulsed-plasma treatment (PPT) developed at PWI is also used with the same purpose [5–7].

Technology of steel PPT is based on the impact of concentrated plasma flows in the pulsed mode on material surface, leading to increase of hardness, grain refinement, structure fragmentation and elimination of clusters of coarse carbide particles, as well as formation of martensite with excess carbon content (because of partial dissolution of carbides) and alloying elements in the treated layer [7–18]. At present, however, the information on the influence of various technological parameters of PPT on structural-phase transformations, and of structural parameters — on service characteristics (properties of strength, ductility and crack resistance) of treated items is limited.

The objective of this work is experimental study of the structure and calculation-analytical prediction of properties in surface layers of samples from R6M5 steel after PPT in various modes.

Materials and investigation procedure. Samples from R6M5 steel (GOST 19265–73) were first subjected to standard heat treatment — quenching (T_q = 1200–1230 °C) and tempering (T_t = 540–560 °C). PPT (impact duration t_p ~ ~ 0.5 s) was conducted in the following modes: I — direct impact of pulsed electric discharge (distance H = 60 mm, heat flow q ~ ~ $0.7 \cdot 10^5$ W/cm^2), and II — indirect action of electric discharge (H = 30 mm, q ~ ~ $0.5 \cdot 10^5$ W/cm^2).

Investigations of structural-phase state of surface of samples, treated by PPT, were conducted using a comprehensive procedural approach, in-

cluding optical metallography (the Union Versamet-2, Japan), scanning electron microscopy (Philips SEM-515, Holland) and JEOL transmission microdiffraction electron microscopy JEM-200 CX (Japan) with accelerating voltage of 200 kV. Obtained experimental data allowed performance of calculation-analytical assessment of a concrete (differentiated) contribution of individual structural parameters (phase composition, size of grains, subgrains, dislocation density, etc.) into the change of total (integral) values of mechanical characteristics of strength σ_y, fracture toughness coefficient (stress intensity factor K_{1c}) and crack resistance ($\tau_{l.in}/\tau_{theor}$).

Integral values of yield limit $\Sigma\sigma_y$ of R6M5 steel after PPT in various modes were calculated using Hall–Petch, Zeger, Orowan and other dependencies [19–28], allowing assessment of differentiated contribution $\Delta\sigma$ of specific structural-phase parameters into $\Sigma\sigma_y$.

Fracture toughness of treated layer material was determined from dependence $K_{1c} = (2E\sigma_y\delta_{cr})^{1/2}$ [29], where E is the Young's modulus; σ_y is the calculated strengthening, MPa; δ_{cr} is the crack opening displacement, equal to average size of subgrains, μm.

Level of local internal stress $\tau_{l.in}$, i.e potential sources of crack initiation and propagation in the strengthened layer, was calculated using dependence $\tau_{l.in} = Gbh\rho/[\pi(1 - \nu)$ [30, 31], where G is the shear modulus, MPa; b is the Burgers vector; h is the foil thickness, equal to $2\cdot10^{-5}$ cm; ν is the Poisson's ratio; ρ is the dislocation density, cm^{-2}.

Investigation results. It is experimentally established that base metal structure (grain size number D_{gr}, μm; volume fraction of structural components V_{fr}, %) at depth $\delta > 100$ μm from treated surfaces (Figure 1, layers 4 and 7) consists of fine-needled martensite (D_{gr} ~ 2.5–10 μm, $V_{fr} = 70$ %), residual austenite (D_{gr} ~ 2.5–10 μm, $V_{fr} = 20$ %) and carbides ($D_{gr} = 0.5$–20 μm, $V_{fr} = 10$ %) (Figure 2). Integral microhardness of steel was $HV0.05$ ~ 7010 MPa (Figure 3). Volume fraction of strengthening carbide particles located in grain volumes $V_{fr} = 8$ %. Total fraction of carbides in the material is 18 %.

After PPT (mode I) a surface-melted layer 1 ($\delta \le 5$ μm) forms on sample surface (Figure 1, *a*). Below is layer 2 ($\delta \le 40$ μm), where coarsening of austenitic-martensitic structural components by 2–2.5 times (D_{gr} ~ 5–25 μm) and overall lowering by 20 % of total microhardness ($HV0.05 \le 6200$ MPa) take place (see Figures 2 and 3). This is exactly why zones of microcrack initiation were found in surface-melted layer 1 ($\delta \le 5$ μm) along the boundaries of residual austenite and carbides, using optical and transmission microscopy.

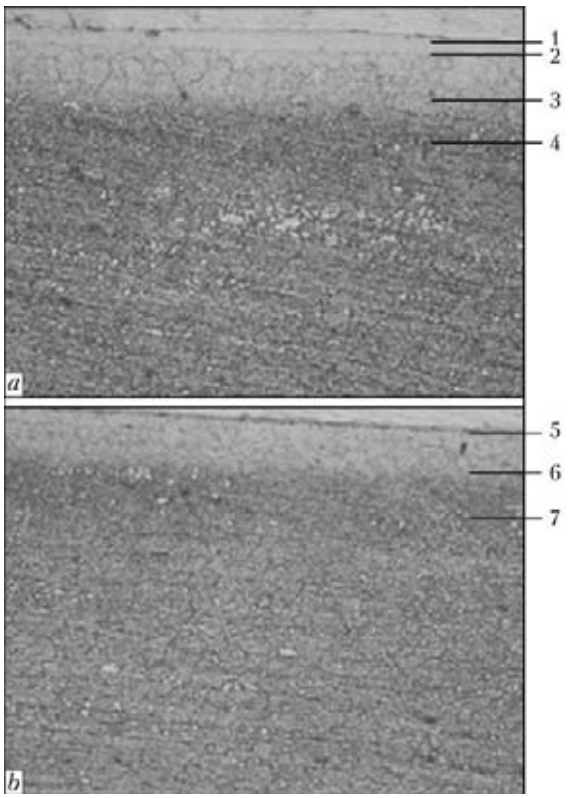

Figure 1. Microstructure (×500) of samples from R6M5 steel after PPT in modes I (*a*) and II (*b*) (changes by depth of treated surface down to base metal): 1 — surface-melted; 2, 5 — structured; 3, 6 — transition layer; 4, 7 — base metal

PPT of samples in mode II leads to 1.5 to 2 times refinement of austenitic-martensitic structural components (D_{gr} ~ 1.5–5 μm) in modified layer 5 ($\delta = 0$–40 μm) (Figure 2). 20 % increase of total microhardness ($HV0.05 \le 9200$ MPa) was also found (Figure 3). No cracking in surface layer 5 after PPT in mode II was noted. The observed refinement of granular structure in the layer of high-speed steel R6M5 at PPT in mode II is due to austenite alloying at dissolution of secondary carbides. Primary carbides do not dissolve and inhibit austenite grain growth, thus

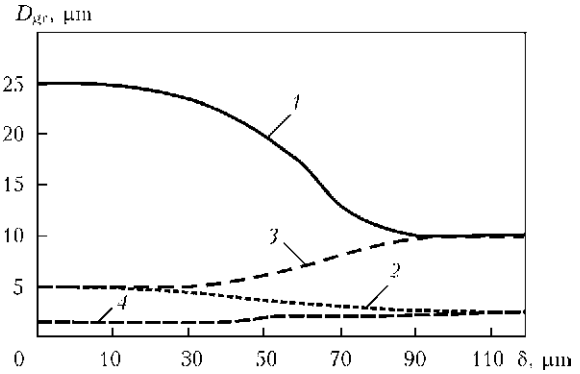

Figure 2. Change of structure dimensions D_{gr} (austenite and martensite) by depth δ of treated layers of samples from R6M5 steel after PPT: *1*, *2* — mode I; *3*, *4* — mode II

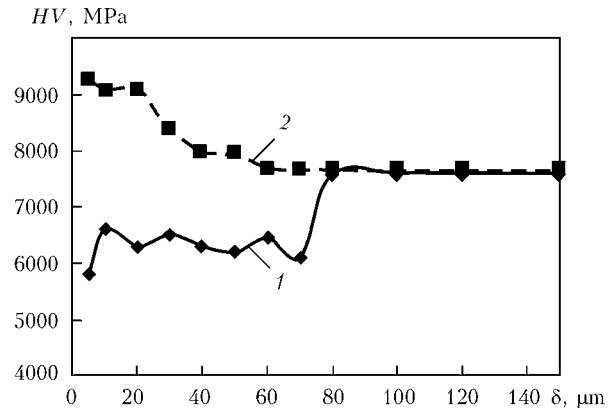

Figure 3. Change of microhardness HV by depth δ of treated layers of samples from steel R6M5 after PPT: *1* — mode I; *2* — mode II

leading to preservation of disperse structure of R6M5 steel at heating close to melting temperature.

Investigations of the change of chemical element concentration (iron, chromium, tungsten, vanadium, molybdenum) by the depth of the layer of samples from R6M5 steel, treated by PPT in modes I and II, showed their uniform distribution that is indicative of the absence of additional alloying of the subsurface layers due to electrode material. Carbides of a complex composition of Me_6C type of a globular shape $(FeCr)_3(W, Mo)_3C$ with prevalence of tungsten and particle sizes d_p ~ 0.21–2 μm were found in the strengthened layer.

Transmission electron microscopy studies showed that base metal structure (δ > 100 μm) is represented by tempering martensite with $\rho \leq 10^{11}$ cm^{-2}, residual austenite with $\rho \leq 10^8$–10^9 cm^{-2} and carbides (Figure 4).

In the layer of austenite grains (δ ≤ 40 μm) treated in mode I a coarsening of the substructure with formation of slightly disoriented block structure at overall non-uniformity of dislocation density ($\rho \sim 10^8$–10^9 cm^{-2}) is observed. In martensite of this zone an abrupt lowering of dislocation density ($\rho \sim 10^9$–10^{10} cm^{-2}) is noted compared to base metal martensite (Figure 5, *a*) that accounts for microhardness lowering (see Figure 3). The most dense ($\rho \sim (2–4)\cdot 10^{10}$ cm^{-2}) and extended (l ~ 0.2–0.3 μm) dislocation clusters form along contact boundaries of carbide phases and inner volumes of austenite grains, where $\rho \sim 10^9$ cm^{-2}.

In surface-melted layer 1 (δ ≤ 5 μm) increase of dimensions of substructural elements (blocks, cells) at their slight disorientation is observed, as well as non-uniform lowering of dislocation density at formation of abrupt gradients ($10^8 \leq \rho \leq 10^{10}$ cm^{-2}) of dislocation density, i.e. stress raisers — zones of crack initiation and propagation (Figure 6, *a*). In the transition layer (δ ~ ~ 40–100 μm) with greater distance from sample surface, the tendency to lowering of dislocation density is preserved, but this lowering is not so significant compared to redistribution in PPT treated layer. Moreover, increase of microvolumes with tempering structure (substructure, blocks) is observed that is in sharp contrast with base metal structure, which is characterized by finer-grain structure with dense and non-uniformly distributed dislocations.

Investigations of fine (dislocation) structure showed that PPT in mode II leads to higher dislocation density in the treated layer (δ ≤ 40 μm)

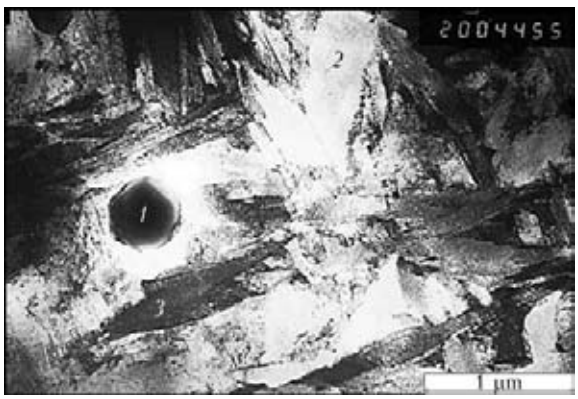

Figure 4. TEM-microstructure (×20000) of base metal of sample from R6M5 steel: *1* — carbides; *2* — residual austenite; *3* — tempering martensite

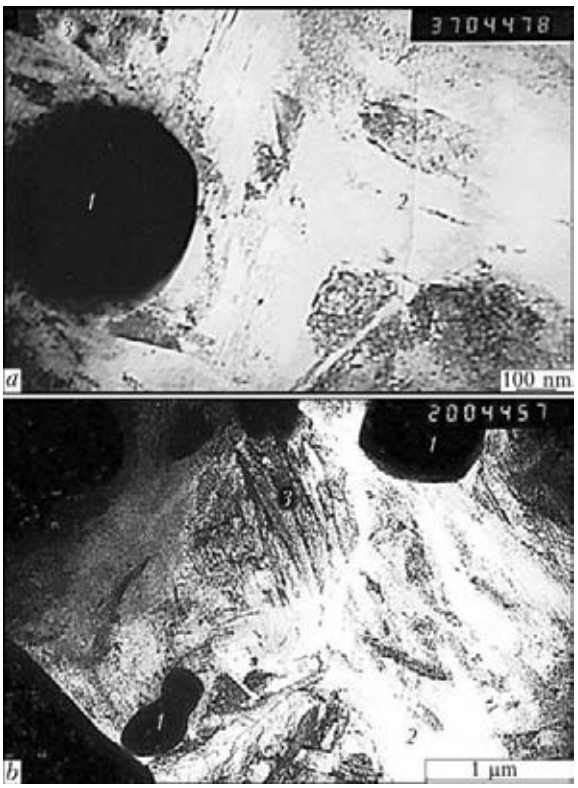

Figure 5. TEM-microstructure of surface layers of samples from steel R6M5 (δ = 5–40 μm) after PPT in modes I (*a* — ×3700) and II (*b* — ×20000): *1* — carbides; *2* — residual austenite; *3* — martensite

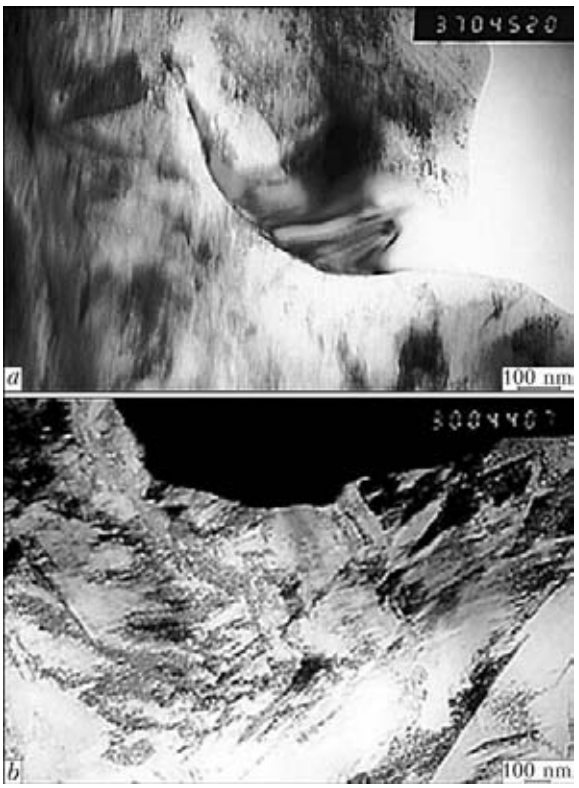

Figure 6. TEM-microstructure of surface layers of samples from steel R6M5 ($\delta \le 5$ μm) after PPT in modes I (*a* — ×37000) and II (*b* — ×3000)

up to $\rho \le 2 \cdot 10^{11}$ cm^{-2} compared to $\rho \le 10^{11}$ cm^{-2} in the base metal (see Figures 4 and 5, *b*) that is in agreement with microhardness measurement results. For residual austenite grains a refinement of the substructure, formation of disoriented block structure are observed at overall uniformity of dislocation density ($\rho \sim 4 \cdot 10^9$ cm^{-2}). It is shown that martensite grains are also characterized by substructure refinement (lath width is 2 times smaller compared to base metal). With increase of the distance from the surface, a tendency to lowering of dislocation density and increase of microvolumes with tempering structure (substructure, blocks) is preserved.

Thus, it is established that in subsurface layers of R6M5 alloy structure refinement, increase of dislocation density and absence of extended dislocation clusters — sites of microcrack initiation and propagation — are found after PPT in mode II.

In order to assess the influence of PPT (various modes) on the most important service properties of working surfaces of tools from R6M5 steel, calculation-analytical evaluation of the properties of strength σ_y, fracture toughness K_{1c} and crack resistance $\tau_{l.in}/\tau_{theor}$ of modified steel layer was performed. It is established that after PPT in mode I leading to surface melting of the alloy surface layer, total $\Sigma\sigma_y$ level in the treated surface ($\delta \le 40$ μm) decreases compared to the base metal by 50 % (640–940 MPa against 1330–1800 MPa

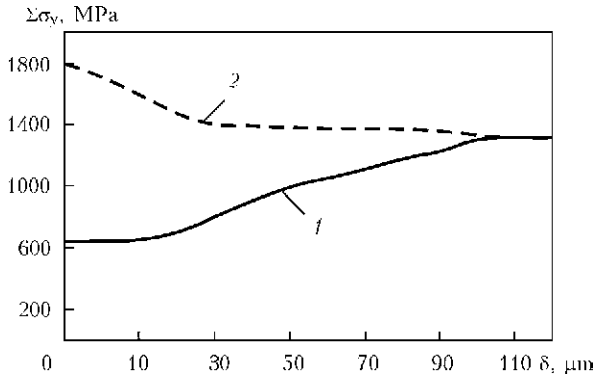

Figure 7. Change of average values of yield point $\Sigma\sigma_y$ by depth δ of treated layers of samples from steel R6M5 after PPT in modes I (*1*) and II (*2*)

in base metal) (Figure 7). The observed lowering of alloy strength in the surface layer is due to reduction of the contribution of substructural strengthening $\Delta\sigma_s$ ~ 190–300 MPa compared to $\Delta\sigma_s$ ~ 590–780 MPa in the base metal, grain strengthening $\Delta\sigma_{gr}$ ~ 200–330 MPa compared to $\Delta\sigma_{gr}$ ~ 280–480 MPa in the base metal, dislocation strengthening $\Delta\sigma_d$ ~ 20–50 MPa compared to 200 MPa in the base metal. Therefore, softening in the alloy surface-melted layer (mode I, ρ ~ 40 μm) is due, predominantly, to the influence of coarsening of structure, and substructure, lowering of dislocations density and their nonuniform distribution.

At application of PPT mode II by treated layer depth (δ ~ 0–40 μm) total strength level increases by 25 % (1400–2160 MPa at 1300–1800 MPa in the base metal). This is due to increased contribution of substructural ($\Delta\sigma_s$ ~ 490–870 MPa), grain ($\Delta\sigma_{gr}$ ~ 440–640 MPa), dislocation ($\Delta\sigma_d$ ~ ~ 200–283 MPa) strengthening, as well as strengthening due to dispersed particles ($\Delta\sigma_p$ ~

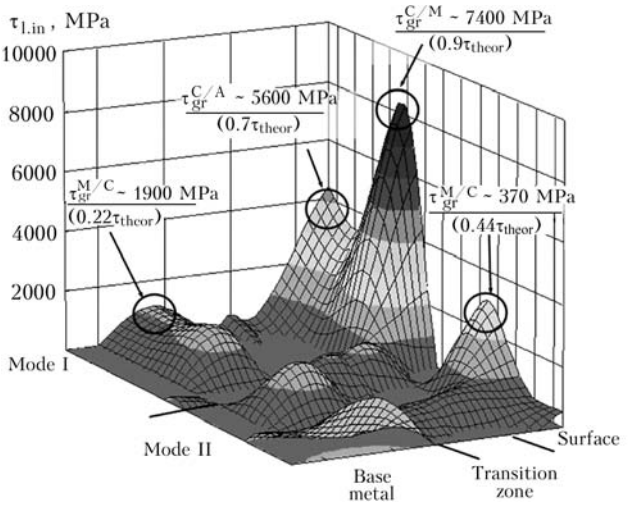

Figure 8. Level of local internal stresses $\tau_{l.in}$ in comparison with theoretical strength τ_{theor} in subsurface layers and in base metal of samples from R6M5 steel depending on PPT modes: C/M, C/A — interfaces of carbide–martensite and carbide–austenite structures, respectively

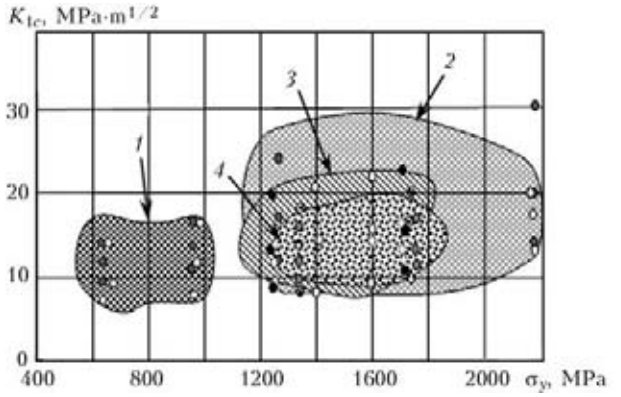

Figure 9. Change of strength σ_y and toughness K_{1c} of R6M5 steel by treated layer depth (δ ~ 0–100 μm) after PPT in modes I and II compared to base metal: *1* — mode I; *2* — mode II; *3* — transition zone; *4* — base metal

~ 60–150 MPa). This is also due to structure refinement, increase of total dislocation density, as well as realization of dispersion strengthening mechanism in the alloy subsurface layers.

Assessment of local inner stresses $\tau_{l.in}$ and their gradients $\Delta\tau_{in}$ along the structural component boundaries, the relationship of these values and theoretical strength of material by depth in the layer from PPT treated surface to base alloy R6M5 are given in Figure 8.

It is shown that after PPT of R6M5 alloy in mode I the highest $\tau_{l.in}$ values are found in the subsurface layers (δ ~ 0–40 μm from outer surface) at the overall lowering of dislocations density and softening. These values form on interfaces of martensite/carbide (M/C) structures, being equal to 5600–7400 MPa or (0.67–0.90)τ_{theor}. Gradients of local internal stresses $\Delta\tau_{in}$ along the boundaries of these structural elements are equal to 5200–7000 MPa and are potential crack initiation sources. After PPT in mode II, ρ increase (from 10^{11} up to $2\cdot10^{11}$ cm^{-2}) is observed compared to untreated alloy at comparatively uniform distribution of dislocation clusters that does not lead to formation of abrupt gradients of internal stresses $\Delta\tau_{l.in}$. This type of dislocation clusters correspond to value $\tau_{l.in}$ ~ 1480–3700 MPa that is equal to ~ 0.018–0.440 of theoretical strength τ_{theor}. Here maximum $\tau_{l.in}$ values (~ 3700 MPa) are characteristic for M/C structure interfaces and do not create a risk of crack initiation.

Role of structural factors is manifested also in the change of strength of subsurface layers of tools from R6M5 alloys, namely properties of strength σ_y in combination with toughness characteristic K_{1c}, that is illustrated by the appropriate diagrams (Figure 9). It is found that K_{1c} value in the modified layer in mode I (with surface melting) is by 35 % lower than in mode II (without surface melting). Here, strength properties also decrease 1.8 times. After PPT in mode II, value K_{1c} in the modified layer of the alloy is by 15 % higher than in the base metal at a considerable strengthening of the entire layer.

Thus, proceeding from the conducted investigations and performed calculations it is established that application of mode II can be recommended for PPT of high-speed steel R6M5 as it leads to such structural-phase changes, which ensure a significant increase of the most important service properties, namely strength, ductility and crack resistance.

Conclusions

1. Pulsed-plasma treatment of samples from steel R6M5 using the mode of direct impact of pulsed electric discharge (mode I) leads to surface layer softening.

2. It is shown that in mode II total strength level increases up to 1400–2160 MPa at 1300–1800 MPa in the base metal across treated surface layer depth (δ ~ 0–40 μm) that is due to the contribution of substructural ($\Delta\sigma_s$ ~ 490–~ 870 MPa), grain ($\Delta\sigma_{gr}$ ~ 440–640 MPa), dislocation ($\Delta\sigma_d$ ~ 200–283 MPa) strengthening mechanisms, as well as strengthening due to dispersed particles ($\Delta\sigma_p$ ~ 60–150 MPa).

3. It is established that high level of strength and crack resistance (up to ~ 26 MPa·m$^{1/2}$) of surface layer of R6M5 steel after PPT in mode II is achieved at refinement (D_{gr} ~ 1–5 μm) of steel grain structure.

4. Pulsed-plasma treatment of samples with application of an indirect electric discharge (mode II) improves structural-phase state of modified layer and the set of its physico-mechanical properties, that is why mode II is the recommended mode for treatment of high-speed steel R6M5.

1. Mironov, V.M., Mazanko, V.F., Gertsriken, D.S. et al. (2001) *Mass transfer and phase formation under pulse effects*. Samara: Samara GU.
2. Burakov, V.V., Fedoseenko, S.S. (1983) Formation of structures of higher wear resistance in laser hardening of metal-working tools. *Metallovedenie i Term. Obrab. Metallov*, **5**, 16–17.
3. Volkhin, S.A. (1990) Influence of structure of tool steels after hardening and tempering on parameters of laser-hardened layers. *Sudostroit. Promyshlennost*, **23**, 44–48.
4. Sobusyak, T., Sokolov, K.N. (1991) Effect of laser heat treatment on structure and properties of high-speed steel. *Problemy Mashinostr. i Avtomatiz.*, **5**, 45–53.
5. Kikin, P.Yu., Pchelintsev, A.I., Rusin, E.E. (2003) Increase in heat- and wear resistance of high-speed steels by shock-wave action. *Fizika i Khimiya Obrab. Materialov*, **5**, 15–17.
6. Gureev, D.M., Lamtin, A.P., Chulkin, V.N. (1990) Influence of pulsed laser radiation on state of cobalt interlayer of hard alloys. *Ibid.*, **1**, 51–54.

7. Babushkin, V.B. (1990) Peculiarities of structure formation in high-speed and high-chromium die steels in laser heating. *Izvestiya Vuzov. Chyorn. Metallurgiya*, **4**, 68–70.
8. Markashova, L.I., Kolisnichenko, O.V., Valevich, M.L. et al. (2012) Structure and mechanical properties of tools from high-speed steel in pulse-plasma surface treatment. In: *Building, materials science, machine-building*: Transact. Issue 64, 211–220. Dnepropetrovsk: GVUZ PGASA.
9. Markashova, L.I., Tyurin, Yu.N., Kolisnichenko, O.V. et al. (2012) Analytical estimation of structural parameter contribution into change of mechanical properties of high-speed steel after pulse-plasma surface treatment. In: *Proc. of 6th Int. Conf. on Mathematical Modelling and Information Technologies in Welding and Related Processes*. Kiev: PWI, 49–53.
10. Cordier-Robert, C., Crampon, J., Foct, J. (1998) Surface alloying of iron by laser melting: Microstructure and mechanical properties. *Surface Eng.*, 14(**5**), 381–385.
11. Chudina, O.V., Borovskaya, T.M. (1994) Strengthening of steel surface by chemical-heat post treatment. *Metallovedenie i Term. Obrab. Metallov*, **12**, 2–7.
12. Chudina, O.V. (1997) Surface alloying of iron-carbon alloys with application of laser heating. *Ibid.*, **7**, 11–14.
13. Ritter, U., Kahrmann, W., Kurpfer, R. et al. (1992) Laser coating proven in practice. *Surface Eng.*, 8(**4**), 381–385.
14. Lugscheider, E., Boplender, H., Krappitz, H. (1992) Laser cladding of paste bound hardfacing alloys. *Ibid.*, 7(**4**), 341–344.
15. Navara, E., Bengsston, B., Li, W.B. et al. (1984) Surface treatment of steel by laser transformation hardening. In: *Proc. of 3rd Int. Congr. on Heat Treatment of Materials* (Shanghai, 7–11 Nov. 1983). Shangri: Metal Society, 40–44.
16. Tverdokhlebov, T.N., Diachenko, V.S. (1980) Influence of laser treatment conditions on resistance of high-speed steel tools. In: *Cutting equipment and tools*. Moscow: Mashinostroenie.
17. Hancock, I.M. et al. (1988) Laser modification of high-speed steel. In: *Proc. of Int. Conf. on Heat Treatment* (London, 11–15 May 1987). London: Metal Society, 189–195.
18. Tyurin, Yu.N., Zhadkevich, M.L. (2008) *Plasma hardening technologies*. Kiev: Naukova Dumka.
19. Suzuki, H. (1967) About yield strength of polycrystalline metals and alloys. In: *Structure and mechanical properties of metals*. Moscow: Metallurgiya.
20. Eshby, M.F. (1972) On Orowan stress. In: *Physics of strength and plasticity*. Moscow: Metallurgiya.
21. Goldshtejn, M.I., Litvinov, V.S., Bronfin, B.M. (1986) *Metallophysics of high-strength alloys*. Moscow: Metallurgiya.
22. Conrad, H. (1973) Model of strain hardening for explanation of size grain effect on flow metal stress. In: *Ultrafine grains in metals*. Ed. by L.K. Gordienko. Moscow: Metallurgiya.
23. Armstrong, R.V. (1973) Strength properties of metals with ultrafine grains. *Ibid*. Moscow: Metallurgiya.
24. Petch, N.J. (1953) The cleavage strength of polycrystalline. *J. Iron and Steel Inst.*, 173(**1**), 25–28.
25. Orowan, E. (1954) *Dislocation in metals*. New York: AIME.
26. Ashby, M.F. (1983) Mechanisms of deformation and fracture. *Adv. Appl. Mech.*, **23**, 118–177.
27. Kelly, A., Nickolson, R. (1966) *Dispersion hardening*. Moscow: Metallurgiya.
28. Ebelling, R., Ashby, M.F. (1966) Yielding and flow of two phase copper alloys. *Phil. Mag.*, 13(**7**), 805–809.
29. Romaniv, O.N. (1979) *Fracture toughness of structural steels*. Moscow: Metallurgiya.
30. Koneva, N.A., Lychagin, D.V., Teplyakova, L.A. et al. (1986) Dislocation-disclination substructures and hardening. In: *Theoretical and experimental study of disclinations*. Leningrad: LFTI.
31. Conrad, H. (1963) Effect of grain size on the lower yield and flow stress of iron and steel. *Acta Met.*, **11**, 75–77.

Received 06.06.2013

OPTIMISATION OF CHEMICAL COMPOSITION AND STRUCTURE OF METAL OF REPAIR WELDS DURING ELIMINATION OF DEFECTS IN PIPE WELDED JOINTS USING MULTILAYER WELDING

A.A. RYBAKOV, T.N. FILIPCHUK and **Yu.V. DEMCHENKO**
E.O. Paton Electric Welding Institute, NASU
11 Bozhenko Str., 03680, Kiev, Ukraine. E-mail: office@paton.kiev.ua

The structure and properties of metal of repair welds, produced using multipass welding during elimination of defects in welds of gas and oil pipelines, were investigated. The changes of chemical composition and impact toughness at negative temperatures and also peculiarities of structure characteristics of metal of separate passes of repair welds were determined. It was shown that in manual arc and mechanized submerged arc welding and welding in shielding gases applying consumables, conventional for manufacture of pipes, the metal of the last passes of repair weld is excessively enriched by different alloying elements (manganese, silicon, chromium, molybdenum, etc.) present in such materials. This leads to the formation of unfavorable structure: areas of upper bainite, developed grid of polygonization boundaries, boundary precipitates of carbon second phase, which in its turn provokes formation of cold cracks in welds. Considering the results of investigations the requirements were developed to the chemical composition of welding wire for repair of defects in pipe welds using multipass welding, providing restriction in the content of alloying elements. In multipass submerged arc welding it was also offered to use aluminate flux. The wire of recommended composition was tested during repair of defects in pipe welds using welding in shielding gas and provided high impact toughness of metal of repair welds in combination with a sufficient resistance against cracks formation. The results of investigations can be used for repair of defects in welds during manufacture of pipes and also in multipass welding of other metal structures. 5 Ref., 4 Tables, 7 Figures.

Keywords: *pipe, weld, repair, defects, multipass welding, welding consumables, impact toughness, structure, cracks*

It is known that during manufacture of large-diameter pipes, welded using multipass submerged arc welding, the elimination of separate inner defects in welds (pores, slag inclusions, lacks of penetrations or lacks of fusion) by their preliminary removal and further filling of formed groove by multilayer welding is admitted in a restricted amount (for example, not more than for 5 % of pipes) [1–3, etc.]. In accordance with the valid standard documents the length of such «repair» area should be restricted by 50–500 mm. It is assumed that qualitative characteristics of such areas, including the level of mechanical properties of metal, should meet the requirements specified to the main welded joints of pipes.

The repair of defects in pipe welds is performed by manual arc welding, mechanized submerged arc welding or welding in shielding gases. The number of necessary passes of repair weld is determined by depth of a groove, formed during removal of defect, which in its turn depends on the site of its location in weld section and thickness of a pipe wall. In typical cases, for example, up to six-ten passes of repair weld are performed for pipes with the wall thickness of 15–20 mm. In CIS countries in mechanized submerged arc welding the fused manganese high-silicon flux AN-60 and wire of the Sv-10G2 type are mainly applied. Such combination of welding consumables provides comparatively low values of tough characteristics of metal of repair weld (at the level of 30 kJ/cm^2 at 0 °C).

At the same time the requirements to tough properties of weld metal of pipes themselves, including the sites of defects repair, grew sufficiently. According to the valid standard documents the mean values of impact toughness of metal of welded joints of pipes for main pipelines should be more often of not less than 49 J/cm^2 at –20 °C and for the pipelines being laid down under water the same requirements are valid at –30 and even –40 °C.

To provide these values it is necessary to optimize the chemical composition of metal of repair welds including that of welding consumables providing higher alloying.

As is shown in the work [4], during repair of defects in welds of pipes using multilayer welding there is one more problem connected with cold cracks formation in repair areas of welds. It is noted that their formation is predetermined by

increase of mass fraction of alloying elements in the last layers of repair welds. Thus, in case of using flux AN-60 and wire Sv-10G2 during repair of defects in longitudinal weld of a pipe with the wall thickness of 15.7 mm the content of manganese in the latter (in our case in the fifth one) pass of repair weld was growing up to 2.4 %, and silicon — up to 1.0 %. To compare, let us note that in the metal of longitudinal weld of pipe, the amount of these elements did not exceed 1.73 and 0.45 %, respectively. As a result, in the metal of closing passes of repair weld the areas with unfavorable structure were formed, which during cooling of metal under the conditions of relatively rigid contour provoked formation of mentioned cold cracks. It should be assumed that in case of application of welding consumables providing higher alloying and larger thickness of a wall of welded pipes, and as a consequence, a small number of passes, the danger of deterioration of metal structure and initiation of cracks in the repair areas will grow.

At the present article the results of investigations, carried out by the authors during solution of task of optimization of chemical composition and structure of weld metal in the sites of defects repair using arc welding, were considered to provide the increased requirements to tough characteristics of weld metal and prevention of cold cracks formation.

The repair (simulation of repair operation of defects located at the depth of about 10–12 mm) was carried out on the specimens of steel X70 1420 × 18.7 mm pipes with longitudinal welds produced under flux AN-60 using wire Sv-08G1NMA. On the specimens, cut out of pipes at the centre of longitudinal weld using specialized electrodes ANR-2, the groove of 15 mm depth was made, which simulated the defect removal. In some cases during use of specimens of pipes with wall thickness of 15.7 mm the depth of groove before welding was 10 mm. The content of main elements in metal of longitudinal weld was in the following ranges, wt.%: 0.05–0.06 C; 1.62–1.79 Mn; 0.429–0.470 Si; 0.008–0.009 Nb; 0.15–0.19 Mo; 0.180–0.236 Ni; 0.015–0.018 Ti. Some variations of separate elements in metal of longitudinal weld are connected with application of steel X70 pipes of different thickness (different chemical composition) in the experiments.

The grooves were filled mainly using mechanized CO_2 welding, mixture Ar + 20 % CO_2 and under flux, and on the separate specimens — using manual arc welding. The grooves of 15 mm depth were welded up in eight passes, and that of 10 mm depth — in five passes. The typical welding consumables were applied used in manufacture of pipes: for submerged arc welding — wire Sv-08GA, Sv-10G2, Sv-08KhM, Sv-08GM, Sv-08G1NMA, S2Mo and flux AN-60, AN-67B, OR 107, OR 132, OK 10.71, OK 10.74; for welding in shielding gas — wire Sv-08G2S, GMoSi; for manual arc welding — electrodes Schwarz 3K. The chemical composition of welding wires is given in Table 1.

Table 1. Content of main alloying elements in welding wire, wt.%

Wire grade	C	Mn	Si	Ni	Mo	Cr
Sv-08GA	0.09	0.95	0.05	0.14	–	–
Sv-10G2	0.10	1.70	0.05	0.12	–	–
Sv-08G2S	0.09	2.01	0.85	0.11	–	–
Sv-08KhM	0.08	0.50	0.20	0.14	0.50	1.02
Sv-08GM	0.08	1.19	0.35	0.11	0.59	–
Sv-08G1NMA	0.09	1.20	0.31	0.49	0.52	–
S2Mo	0.07	1.15	0.21	0.11	0.50	–
GMoSi	0.10	1.11	0.60	–	0.50	–

The submerged arc welding was performed using wire of 2.5 mm diameter (I_w = 320–350 A, U_a = 28–30 V, v_w = 17–20 m/h), in shielding gas — using wire of 1.2 mm diameter (I_w = 160–180 A, U_a = 26–28 V), and manual arc welding — using electrodes of 3.2 mm diameter (I_w = = 130–150 A, U_a = 25–26 V).

From the produced joints the specimens were selected to determine the chemical composition of weld metal, its impact toughness and metallographic examinations. The analysis of chemical composition of metal of single passes was performed by spectral method using «Spektrovak 1000» device of Baird Company and diffraction spectrometer DFS-36.

The areas of determination of chemical composition, represented in Figure 1, were located in the metal of longitudinal weld being repaired (area 1), in metal of the first pass of repair weld (area 2), in metal of intermediate passes (areas 3 and 4) and in the metal of closing pass of this weld (area 5).

The tests on impact toughness were carried out at the temperature from –10 to –40 °C on the specimens with a sharp notch marked at the centre of deposit according to GOST 6996.

The microstructure of metal was studied applying optical and scanning electron microscopy at the magnification of 50–500 on the sections after etching in nital (4 % alcohol solution of nitrogen acid), in hot solution of sodium picrate and saturated water solution of picric acid.

It was established that for all the investigated variants of combinations of welding consumables that with increase in number of passes of repair weld, the level of metal alloying was growing naturally. As is seen from Figure 2, the amount of manganese and silicon in metal of the second

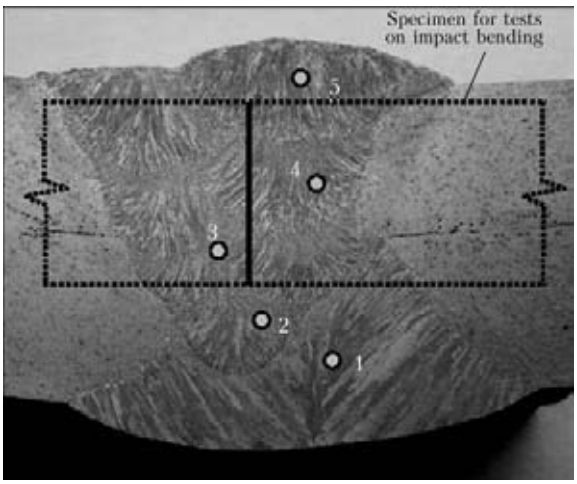

Figure 1. Characteristic macrosection of the investigated repair welds and zones of determination of chemical composition 1–5

pass grows to 2.35 and 0.62 %, respectively, and continues growing further in next passes up to the maximal values in the closing pass: 2.85 and 0.99 % respectively. Similarly the content of chromium and molybdenum is changed, which is shown on the example of use of wire Sv-08KhM in the process of defects repairing (Figure 3).

The intensity of growing of mass fraction of any alloying element is determined in the first turn by the applied welding consumables. As is seen from Figure 4, the highest amount of silicon, as was supposed, is present in the last pass of the weld produced using acid high-silicon flux AN-60, moreover, its content in metal of this pass is growing from 0.76 to 0.99 % with increase in mass fraction of manganese in welding wire (to remind, in the longitudinal weld of a pipe the amount of silicon did not exceed 0.45 %). The transition of silicon from flux into the metal of repair weld is considerably decreased with the decrease of SiO_2 amount in flux. The minimum growth of amount of silicon is observed during application for the considered purpose of molten neutral flux AN-67B or ceramic aluminate-basic flux of the type OR 132 for the considered purpose.

The content of manganese in the metal of multipass repair welds depends greatly on its amount in welding wire. Thus, using wire Sv-10G2 with 1.7 % Mn the mass fraction of this element in the metal of a last pass amounted to 2.85 %. At a lower amount of manganese, for example, in wire Sv-08G1NMA (1.2 % Mn) or Sv-08KhM (0.5 % Mn), its maximum amount in repair weld was decreased to 1.97 and 1.77 % respectively. The rate of increment of other alloying elements in the investigated multipass welds was also determined by their content in welding wire.

The generalized data of chemical composition of the last passes of repair welds being produced in eight or five passes for different methods of welding and welding consumables are given in Table 2. It is seen that use of almost any of the combinations of welding consumables, usually applied in manufacture of pipes, leads to considerable growth of mass fraction of any alloying elements in the closing passes of investigated welds. Thus, in submerged arc welding the excessive amount of manganese is present in case of using wire Sv-10G2, silicon — flux AN-60, OK 10.71, OK 10.74, chromium — wire Sv-08KhM, molybdenum — wire Sv-08G1NMA, Sv-08GM, Sv-08KhM, S2Mo. The same data were also obtained during application of other welding methods. For example, in the metal of repair

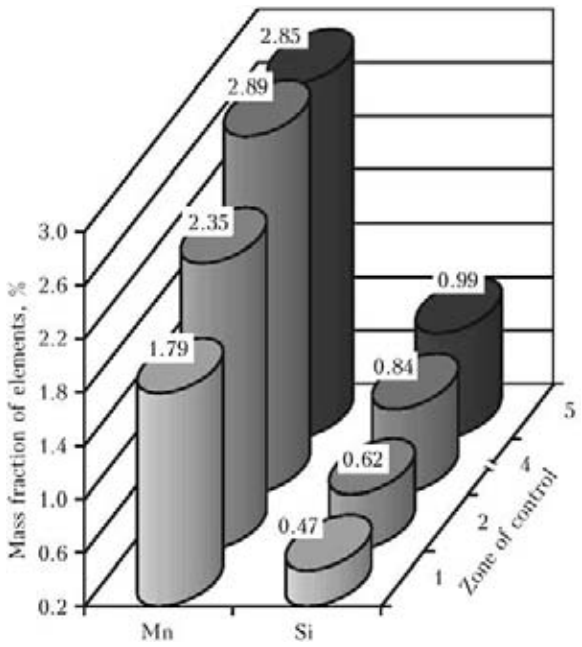

Figure 2. Mass fraction of manganese and silicon in metal of different passes of repair weld produced using wire Sv-10G2 and flux AN-60

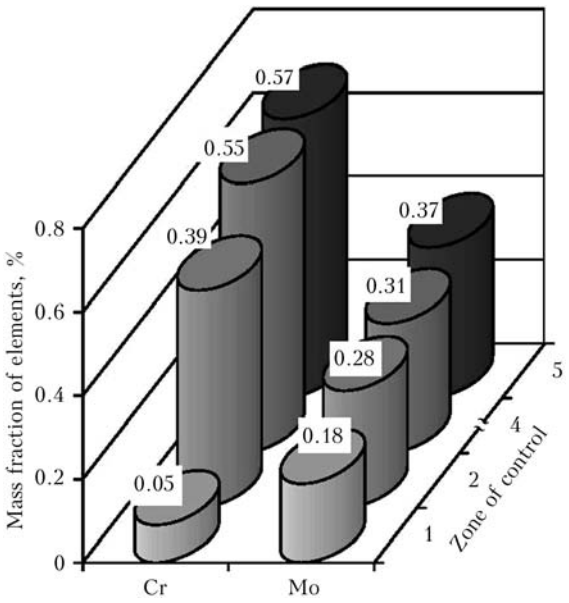

Figure 3. Mass fraction of chromium and molybdenum in metal of different passes of repair weld produced using wire Sv-08KhM and flux AN-67B

Table 2. Chemical composition of metal of last passes of repair welds (wt.%) produced using different methods of welding and different welding consumables

Variant number	Welding consumables		C	Si	Mn	S	P	Cr	Mo
Manual arc welding									
1	Schwarz 3K		0.055	0.268	1.22	0.011	0.015	0.05	0.422
Mechanized welding in shielding gas									
2	Sv-08G2S	CO_2	0.081	0.569	1.48	0.013	0.016	0.06	0.021
3	Sv-08G2S	Ar + 20 % CO_2	0.089	0.810	1.40	0.014	0.016	0.06	0.022
4	GMoSi	Ar + 20 % CO_2	0.093	0.408	0.88	0.009	0.017	0.07	0.461
Mechanized submerged arc welding									
5*	Sv-10G2	AN-60	0.073	0.990	2.854	0.016	0.021	0.05	0.003
6*		AN-67B	0.080	0.320	2.390	0.016	0.024	0.05	0.022
7		OR 107	0.065	0.460	2.376	0.016	0.023	0.06	0.028
8		OK 10.71	0.088	0.723	2.368	0.015	0.022	0.06	0.027
9	Sv-08G1NMA	AN-60	0.044	0.974	1.967	0.017	0.026	0.03	0.534
10		AN-67B	0.056	0.281	2.348	0.015	0.022	0.03	0.515
11		OR 107	0.059	0.442	2.117	0.017	0.023	0.04	0.404
12		OK 10.71	0.071	0.670	2.156	0.015	0.024	0.05	0.431
13*	Sv-08KhM	AN-60	0.072	0.761	1.770	0.017	0.025	0.67	0.368
14*		AN-67B	0.073	0.254	1.748	0.017	0.027	0.57	0.356
15		OR 107	0.049	0.431	1.701	0.016	0.023	0.58	0.411
16*	S2Mo	OK 10.74	0.059	0.613	1.740	0.016	0.028	0.07	0.461
17*	Sv-08GM	OK 10.74	0.060	0.618	1.600	0.017	0.029	0.06	0.470

The variant numbers of repair welds produced in eight passes are marked with asterisk.

welds being welded in shielding gas, the content of silicon increases (wire Sv-08GA, in particular during welding in the mixture Ar + 20 % CO_2) or molybdenum (wire GMoSi). In the metal of last passes of repair welds produced using manual arc welding using electrodes Schwarz 3K with the mass content of molybdenum 0.5 % the increased amount of this element was observed.

The increased content of alloying components in metal of repair welds is accompanied, as was noted, by corresponding change of its structure. Thus, in making the multilayer deposits by manganese wire Sv-08GA or Sv-10G2, when the content of manganese in metal of last passes increases up to 2.4–2.8 %, in the structure of metal, except of acicular forms of ferrite, considerable amount of lamellar ferrite with ordered carbide phase, Widmanstatten ferrite and also separate areas of polygonal pre-eutectoid ferrite and pearlite is observed. For metal with such structure very low characteristics of toughness are typical. The enrichment of such metal with silicon from flux or wire results in additional embrittlement of ferrite matrix.

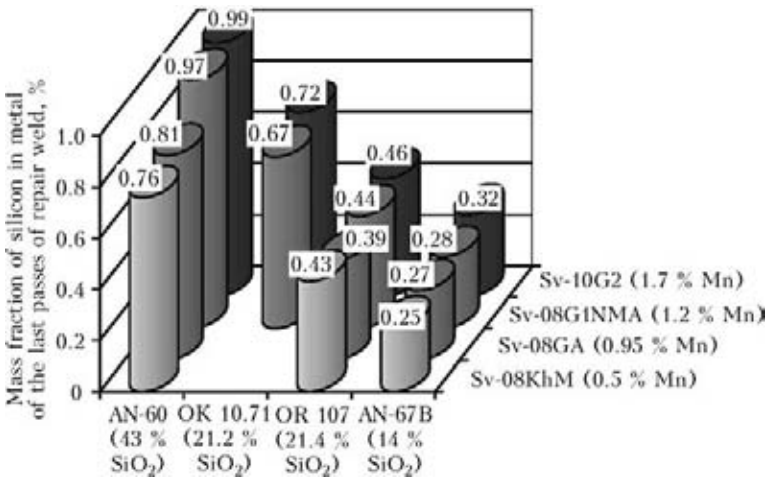

Figure 4. Dependence of silicon content in metal of the last passes of repair weld on the applied welding consumables (in brackets the content of manganese in the wire and SiO_2 in flux is given)

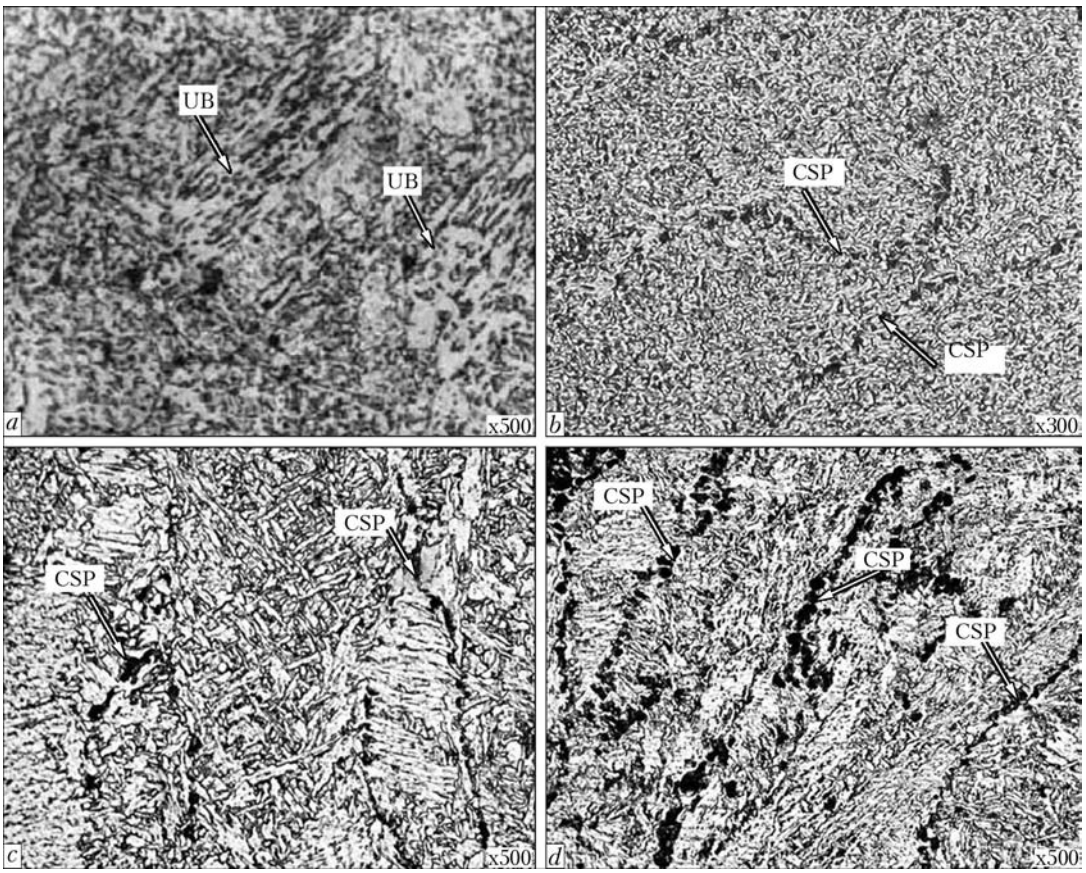

Figure 5. Characteristic microstrucutre of metal of the last (*a*) and intermediate (*b–d*) passes of repair welds with increased content of alloying elements (etching in 4 % solution of nitrogen acid): *a*, *b* — mechanized submerged arc welding with wire S2Mo, flux OK 10.74 (Table 2, variant 16*); *c* — manual welding, electrodes Schwarz 3K (Table 2, variant 1); *d* — mechanized welding in shielding gas, wire GMoSi, Ar + 20 % CO_2 (Table 2, variant 4); UB — areas with the structure of upper bainite; CSP — carbon second phase (carbides, MAC-phase)

When producing multilayer repair welds using alloyed wires (Sv-08G1NMA, Sv-08KhM, Sv-08GM, S2Mo, GMoSi) with mass fraction of molybdenum of more than 0.5 %, due to increased content of manganese, molybdenum and chromium, decreasing the temperature of austenite transformation, alongside with acicular ferrite in the metal of last passes the areas of upper bainite (Figure 5, *a*) are formed, the amount of MAC-phase is increased, the developed grid of polygonization boundaries is formed. The formation of single polygonization boundaries in metal of repaired weld, produced using mentioned wires, begins during welding of the second pass and in the third and the following passes these boundaries are located in the form of closed contours. Besides, in the metal of intermediate passes subjected to repeated heating, where the content of molybdenum is already significant, the boundary formations of the second carbon phase are formed: MAC-phase and carbides (Figure 5, *b*). The similar clusters of carbon phase along the boundaries of crystallites and polygonization boundaries are present also in the metal of intermediate passes during manual arc welding (Figure 5, *c*; Table 2, variant 1) and welding in shielding gas (Figure 5, *d*; Table 2, variant 4) using electrodes or wire alloyed with molybdenum. The mentioned structural peculiarities predetermine the decreased resistance of metal of such repair welds against cracks formation, which is proved by the presence of these defects in the investigated specimens in the form of large cracks escaping to the surface of a weld and net of microcracks, localized mainly along the grain-boundary formations of carbon second phase: MAC-phase and carbides (Figure 6).

It is known that to provide tough characteristics of weld metal on microalloyed steel, including pipe steel, molybdenum (or molybdenum in combination with nickel) is actively used as alloying elements. For example, during manufacture of pipes for longitudinal or spiral welds the wire of the type S2Mo and S3NiMo is applied [5]. The results of our tests on impact bending prove also the efficiency of alloying of metal of multipass repair welds using mentioned elements to enhance its tough properties (Table 3). Thus, the application of wire with molybdenum in welding of repair welds in the mixture Ar + 20 % CO_2 (wire GMoSi) and under agglomerated aluminate-basic flux of the type OK 10.74 (wires S2Mo and Sv-08GM), as was already expected, allowed obtaining relatively high *KCV*

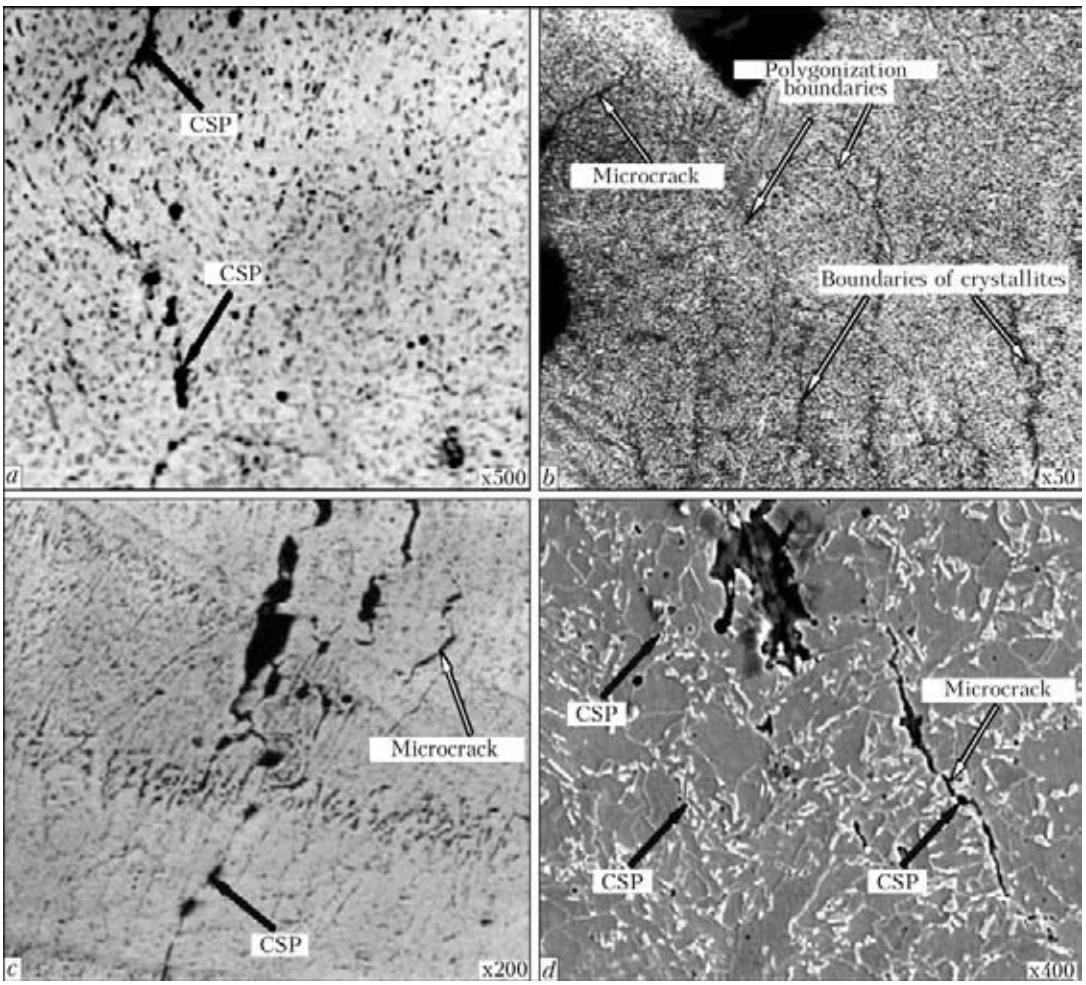

Figure 6. Cracks in the metal of repair welds: *a* — etching in the hot solution of sodium picrate; *b*, *c* — etching in the saturated water solution of picric acid; *d* — etching in 4 % spirit solution of nitrogen acid; *a–c* — optic; *d* — scanning electron metallography

Table 3. Impact toughness of metal of multipass repair weld in use of different welding consumables

Welding method	Variant number	Welding consumables	*KCV*, J/cm^2, at *T*, °C	
			−20	−40
Manual arc	1	Schwarz 3K	65.5–107.0 / 81.0	40.3–61.2 / 48.8
Mechanized in shielding gas	2	Sv-08G2S, CO_2	27.6–34.3 / 30.8	–
	3	Sv-08G2S, Ar + 20 % CO_2	34.9–48.6 / 42.9	–
	4	GMoSi, Ar + 20 % CO_2	74.5–124.4 / 93.2	31.8–63.8 / 53.1
Mechanized submerged arc	5*	Sv-10G2, AN-60	21.2–29.6 / 25.0	–
	13*	Sv-08KhM, AN-60	29.8–35.4 / 32.2	–
	16*	S2Mo, OK 10.74	65.9–75.8 / 70.3	37.7–42.4 / 40.8
	17*	Sv-08GM, OK 10.74	77.8–109.8 / 90.7	–

Note. The variant numbers of welding consumables are given according to Table 2.

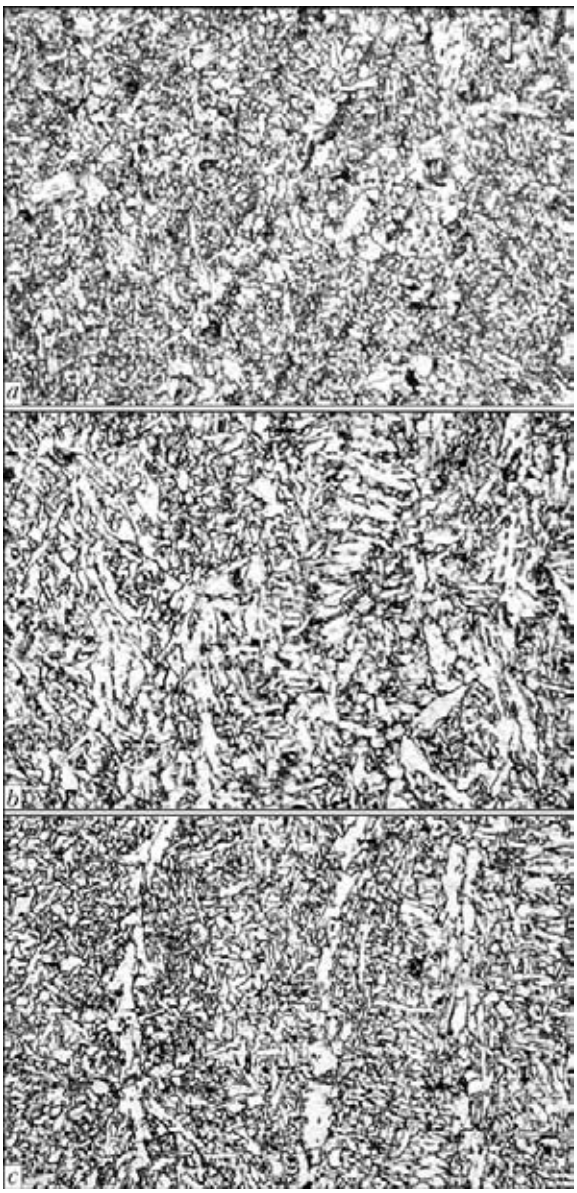

Figure 7. Microstructure (×500) of metal of different passes of repair weld produced using mechanized welding in the mixture Ar + 20 % CO_2 using wire NiMo1-1G with limited molybdenum content: *a*, *b* — intermediate 2–3 and 5–6 passes, respectively; *c* — last passes

values at the temperature of –20 (on average more than 70 J/cm^2) and –40 °C (on average more than 40 J/cm^2). However the structure of metal of the last passes of such repair welds, from the point of view of elimination of danger of cold cracks formation, remain unacceptable.

The results of carried out tests allowed formulating the requirements to the chemical composition of welding wire to repair the defects in welds of pipes using multipass welding. Such a wire should contain the limited amount of manganese, silicon and the additional alloying with molybdenum should provide its presence in the metal of the last passes of multilayer repair weld in the amount of not more than 0.3 %. In submerged arc welding the recommended wire

Table 4. Chemical composition of metal of repair welds in welding in the mixture Ar + 20 % CO_2 using wire NiMo1-1G, wt.%

Control zone	C	Mn	Si	Ni	Mo	Ti	V
First passes	0.08	1.35	0.37	0.87	0.24	0.025	0.05
Closing passes	0.08	1.36	0.40	0.87	0.26	0.022	0.04

should be applied in combination with the flux, for example, aluminate one, excluding the excessive enrichment of metal of multipass weld with manganese and silicon. The wire NiMo1-1G, the chemical composition of which is the following, wt.%: 0.081 C, 1.7 Mn, 0.57 Si, 0.88 Ni, 0.04 V, 0.29 Mo, 0.056 Ti, 0.014 S, 0.017 P, was tested in multipass (a number of passes was eight) welding in the mixture Ar + 20 % CO_2 simulating the repair of defect with its preliminary removal in the longitudinal weld of steel X70 pipe of 18.7 mm wall thickness. The applied wire was additionally alloyed with a low amount of nickel. The data of spectral analysis given in Table 4 proved the sufficient stability of chemical composition of repair welds. The content of main alloying elements (manganese, silicon, nickel, molybdenum, titanium) in metal of the first and closing passes practically was not changed, moreover it did not exceed the recommended values.

During the test on impact bending of specimens with a sharp notch the metal of repair welds, produced using the mentioned wire, was characterized by high values of impact toughness at the temperature of –10 (170.4–199.8), –20 (140.9–170.2) and –40 °C (67.8–136.2 J/cm^2). At the same time, in the metal of such weld, including its last passes, the sufficiently dispersed structure of acicular ferrite at the absence of polygonization boundaries and areas with coarse grain boundaries formations of phases with the increased carbon content: MAC-phase, carbides (Figure 7), is formed.

The results of investigations can be used also in multilayer welding of other metal structures.

1. *DSTU ISO 3183-2:2006*: Petroleum and natural gas industries. Steel pipes for pipelines. Technical delivery conditions. Pt 2: Pipes of class B requirements.
2. *ANSI/API Specification 5L-2007*. Specification for line pipes, ISO 3183:2007. Petroleum and natural gas industries. Steel pipes for pipelines. Technical delivery conditions.
3. *DNV offshore standard OS-F101* (2007) Submarine pipeline systems. Det Norske Veritas.
4. Rybakov, A.A., Filipchuk, T.N., Goncharenko, L.V. (2013) Cracks in welded joints of large diameter pipes and measures for their prevention. *The Paton Welding J.*, **4**, 15–20.
5. Mandelberg, S.L., Bogachek, Yu.L., Kovalevsky, V.A. et al. (1986) Increase in impact toughness of weld metal of large-diameter pipes from microalloyed steels. *Avtomatich. Svarka*, **1**, 36–40.

Received 11.07.2013

INFLUENCE OF RESIDUAL STRESSES IN WELDED JOINTS OF TWO-LAYER STEELS ON SERVICE RELIABILITY OF METAL STRUCTURES

V.V. CHIGARYOV[1] and **I.V. KOVALENKO**[2]
[1]Priazovsky State Technical University
7 Universitetsky Lane, 87500, Mariupol, Ukraine. E-mail: chigarew@pstu.edu
[2]Company «Iliich Mariupol Metallurgical Works»
20 Levchenko Str., 87504, Mariupol, Ukraine. E-mail: oksikov19@mail.ru

The main purpose of the present investigations is determination of influence of residual stresses in the near-weld zone of cladding layer of two-layer steel VSt3 + 10Kh13 on its operation properties. The task put before the authors was to compare theoretical and experimental values of residual stresses in welded specimens of two-layer steels VSt3 + 08Kh13, VSt3 + 10Kh13, VSt3 + 10Kh17N13M2T and to determine the material which is the most suitable for the further service. To define the level of residual stresses of cladding layer the low-cycle uniaxial loading of specimens and mathematical calculations were used. The results of measurements of residual stresses carried out using strain gauges and comparison of their values with theoretical ones allow making the confirmation that preset values of residual stresses in the near-weld zone of the joint VSt3 + 08Kh13 equal to 100 MPa evidences of the presence of reserve of operation reliability of the joints. On this reason the bimetal steels, described in the given work, are suitable for manufacture of large metallurgical units. 6 Ref., 1 Table, 5 Figures.

Keywords: *arc welding of bimetals, residual stresses, cladding layer, near-weld zone, elasticity modulus, strain gauge, layer deformation, service properties*

The continuous growth of requirements to the quality of manufacture of metallurgical units, performance of their repair applying the technology of welding of two-layer steel predetermine the appearance of new methods for calculation and determination of service properties. The prediction of life of metal structures plays here the special role. In this connection the developments in the mentioned direction are very challenging.

Two-layer steels VSt3 + 10Kh13 are widely applied both as corrosion- and heat-resistant materials during manufacture of parts operating in water, salt solutions, aggressive thermal environments, petroleum industry [1]. Thus, the values of rate of general corrosion on the side of cladding layer amount to 0.1–0.3 mm/year.

The investigations directed to determination of working efficiency of welded joints of two-layer steels have a significant importance, as far as these materials are applied both during manufacture as well as during repair of industrial units.

According to the data of work [2] due to increase in the level of residual stresses and formation of heterogeneities in the structure of joints during welding of two-layer steels the values of impact toughness are decreased by 20–25 % as compared to the initial state. Moreover, near the welded joints the defects can arise caused by plastic shortening deformation [3]. The tendency of welded joints to formation of such defects is higher the lower is the deformation capacity.

The purpose of this work is determination of residual stresses of near-weld zone of two-layer steel VSt3sp (killed) + 10Kh13, study and analysis of regularities of distribution of stresses in the welded joint.

To carry out the investigations the plates of 20 × 100 × 600 mm size of two-layer steel VSt3sp + 10Kh13, supplied according to the standard TU 14-1-1670–86, were used.

Welding of plates, intended for tests, was carried out according to the technology developed by the contractor company «Promtekhmontazh Ltd» using welding machine ADF-1002 of the type 2TS-17S. The welding was performed in two passes: the first pass — the main layer (steel VSt3sp) at I_w = 520–570 A, U_a = 38–40 V, v_w = = 22 m/h, with flux AN-348A and wire Sv-08A. The preparation of edges of plates both for the main layer as well as for secondary one was V-shape.

The welding of separating (transition) layer was performed in one pass, after welding of the main layer under the following conditions: I_w = = 280–300 A; U_a = 23–25 V; v_w = 18–20 m/h, with flux AN-45 and wire Sv-10Kh16N25M6.

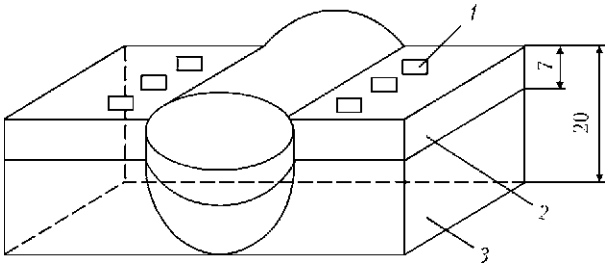

Figure 1. Section of welded specimen of two-layer steel for investigations: *1* — strain gauge; *2* — cladding layer; *3* — base metal

For welding of cladding layer 10Kh13 the following conditions were applied: I_w = 330–350 A; U_a = 24–28 V; v_w = 18–20 m/h, flux AN-18, wire Sv-10Kh16N25M6.

The measurements of residual stresses were carried out on welded specimens after one loading cycle of $20 \cdot 10^3$ oscillations [3]. The welded joints of the following compositions were investigated: VSt3sp + 08Kh13, VSt3sp + 10Kh13, VSt3sp + 10Kh17N13M2T. The working pressure at the loading of specimen amounted to 1210 MPa, and the value of deformation at the surface of the specimen was ε_{av} = 0.0031. The main purpose of these tests was the measurement of real values of residual stresses of welded specimens (Figure 1).

As one of the criteria for evaluation of the service reliability of welded joint of two-layer steel the level of residual stresses was determined. The state of specimens and averaging of value of yield strength of base and cladding layers are given in the Table.

The stress σ_a in the specimen at the distance Q from the surface was determined according to the following formula:

$$\sigma_a = \frac{1}{2} E (h - a) \frac{d\varepsilon}{d\varepsilon}(a) - 3E(h - a) \int_0^a \frac{\varepsilon(\delta)}{(h - a)^2} d\delta, \quad (1)$$

where a is the thickness of all removed layers; h is the total thickness of specimen; E is the elasticity modulus; δ is the thickness of removed layer; $\varepsilon(a)$, $\varepsilon(\delta)$ is the deformation at the lower surface of the specimen during removal of layer of thickness a and δ.

In the carried out investigations the thickness of removed layer Δi (mm), total thickness of all the removed layers α_i (mm), deformation $\varepsilon(\alpha_i) = \varepsilon_i$, measured using gauge of resistance, were considered. To calculate the derivatives the parabolic approximation was used:

$$\frac{d\varepsilon}{d\alpha}(0) = \varepsilon_1 \left(\frac{\Delta_1 + \Delta_2}{\Delta_1 \Delta_2} \right) + \varepsilon_2 \left[\frac{-\Delta_1}{\Delta_2(\Delta_1 + \Delta_2)} \right] =$$

$$= \varepsilon_1 K_0^{(2)} + \varepsilon_2 K_0^{(3)},$$

$$\frac{d\varepsilon}{d\alpha}(\alpha_1) = \varepsilon_{i-1} \left[\frac{-\Delta_{i+1}}{\Delta_1(\Delta_i + \Delta_{i+1})} \right] + \varepsilon_i \left(\frac{\Delta_{i+1} - \Delta_i}{\Delta_i \Delta_{i+1}} \right) + \quad (2)$$

$$+ \varepsilon_{i+1} \left[\frac{\Delta_i}{\Delta_{i+1}(\Delta_i + \Delta_{i+1})} \right] =$$

$$= \varepsilon_{i-1} K_i^{(1)} + \varepsilon_i K_i^{(2)} + \varepsilon_{i+1} K_i^{(3)}.$$

The values of coefficients $K^{(1)}$, $K^{(2)}$, $K^{(3)}$ are given in Table 3.7 of work [4]. A half of the sum and integral values in the under-integral position are also indicated there. The value of residual stress $\sigma(\alpha_i)$ (the sum of values in the last three columns) is also given in work [4]. According to the calculation results the diagrams of distribution of residual stresses across the section of cladding layer were plotted (Figure 2).

In the presented material the emphasis is made on the fact that residual stresses arising at different stages of technological process of manufacture of structure metallurgical assemblies and elements have often a great influence on static and fatigue strength of structures. Therefore, the accurate calculation and analysis of real distribution of residual stresses can open the new possibilities of safe operation of metallurgical assemblies and units.

As is seen from Figure 2 of the diagrams of distribution of residual stresses of the specimens, not subjected to loading, in all the investigated compositions there are tensile residual stresses in the cladding layer. The nature of distribution of stresses across the section of cladding layer is approximately the same [2] for all the specimens: gradual increase from the fusion line of layers up to the maximum value at the depth of 0.2–0.8 mm from the free surface of cladding layer. While approaching the surface of cladding layer the value of stresses is decreased.

The maximum values of residual stresses for the composition VSt3sp + 12Kh13 amount to about 200 MPa, whereas those for the composition VSt3sp + 10Kh13 are about 140 MPa. One should pay attention to the fact that the presence of residual tensile stresses in the cladding layer

Averaged values of properties of investigated steels

Number of specimen	Composition	$G_{0.2}^{BM}$, MPa	$G_{0.2}^{CL}$, MPa
12-9	VSt3sp + 08Kh13	260	450
16-9	VSt3sp + 10Kh17N13M2T	260	490
2C-3	VSt3sp + 10Kh13	260	460

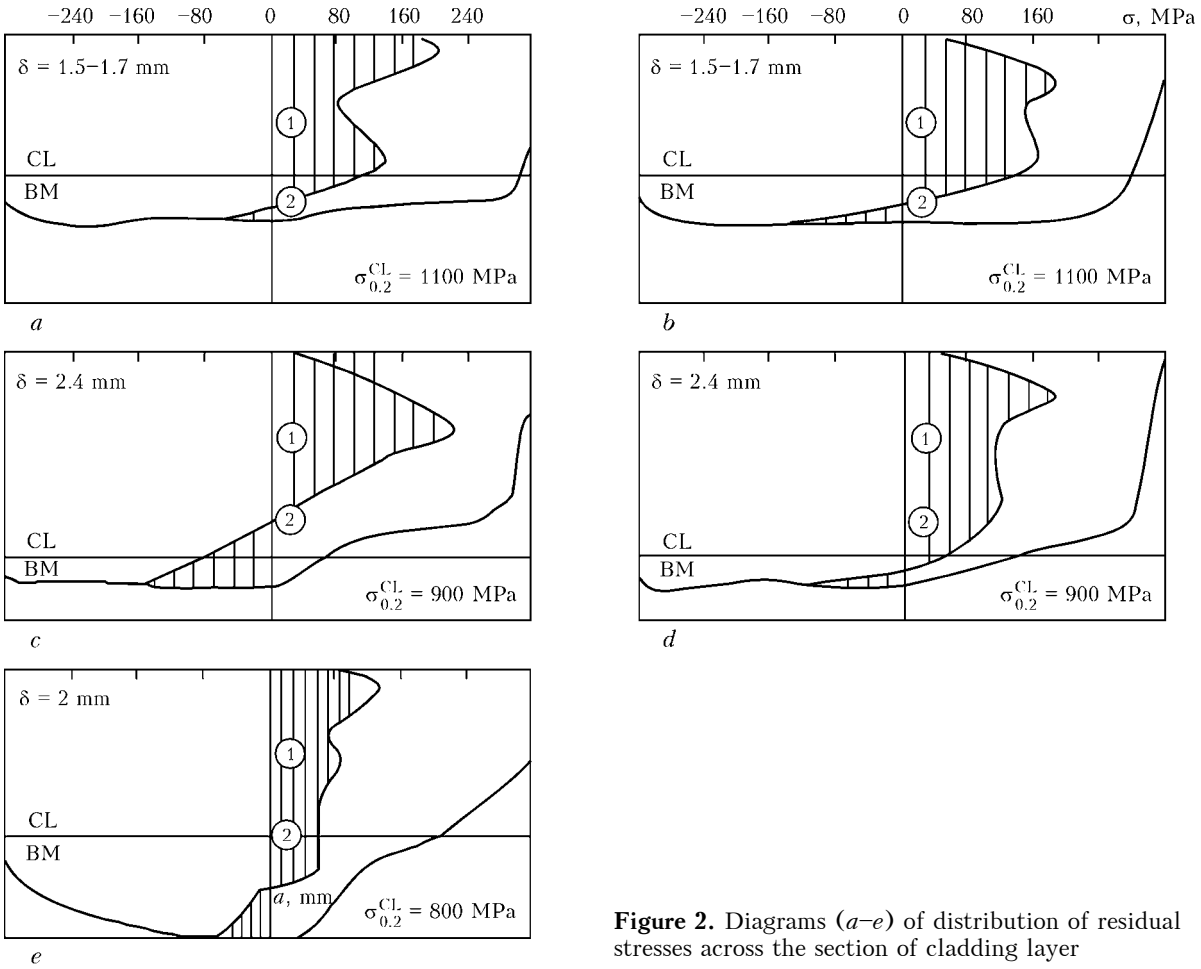

Figure 2. Diagrams (*a–e*) of distribution of residual stresses across the section of cladding layer

can influence the life period of specimen and future metal structure as a whole, especially, when both layers of composition are subjected to loading within the limits of elastic area. These arguments are decisive during selection of material of cladding layer (Figure 3).

Experimental and calculative data of residual stresses in the cladding layer after loading of the specimen, when $\varepsilon_{0.2}^{CL} < \varepsilon_{av} < 2\varepsilon_0^{BM}$, prove the presence of residual compression stresses, their maximum value is different and depends on the level of load and yield strength of material of cladding layer. Thus, in the specimen 14-10 (VSt3sp + 08Kh13), preliminary loaded up to σ_{av} = = 900 MPa, the maximum value of residual compression stresses is 100 MPa, and in the specimen 12-19 (VSt3sp + 08Kh13), loaded at σ_{av} = 1050–200 MPa. Study of diagram of the specimen 13-1 (VSt3sp + 10Kh17N13M2T), having yield strength of material of cladding layer of 270 MPa, is of particular interest. As is seen, the stresses are distributed with a uniform decrease from the maximum on the surface to the fusion line, after the intersection of which their sign is changed. The attention should be paid to the fact that in this specimen the maximum value of residual stresses is highest as compared to the simi-

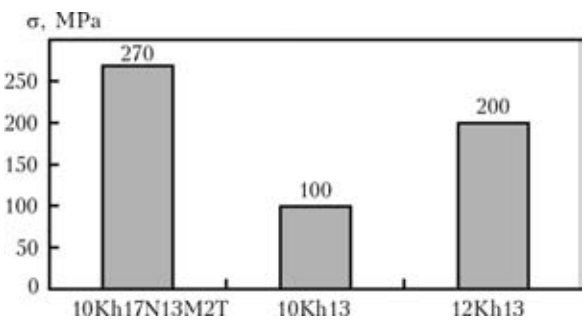

Figure 3. Dependence of residual stresses in the near-weld zone on material of cladding layer

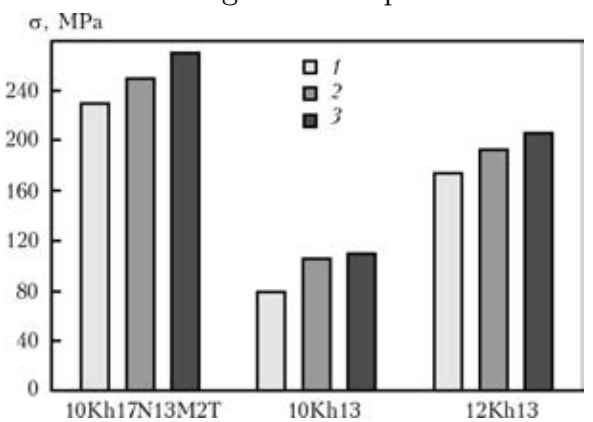

Figure 4. Influence of thickness of cladding layer on residual stresses in the near-weld zone: *1* — δ = 5; *2* — 7; *3* — 10 mm

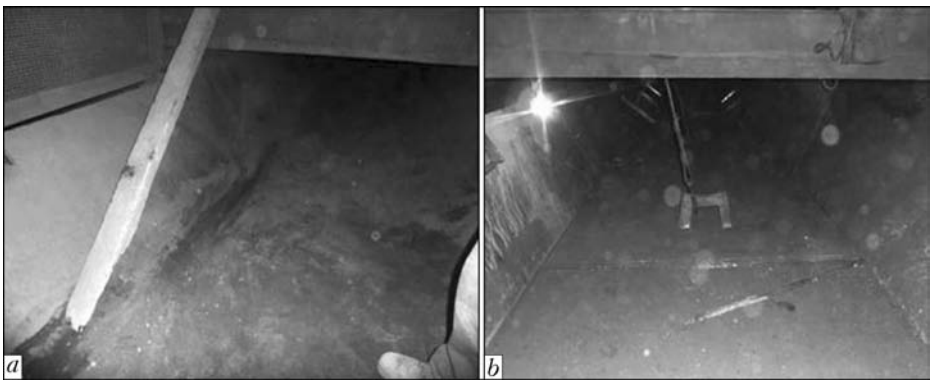

Figure 5. Chute of scrapper mechanism before (*a*) and after (*b*) restoration

lar values for other specimens and corresponds to the stress values of yield strength of material of cladding layer [5].

It is obviously connected with the fact that working deformations of the specimen considerably exceed the deformations of yield strength of material of cladding layer, i.e. the condition is observed, when $\varepsilon_{av} > \varepsilon_{0.2}^{CL}$. In this case residual compression stresses can be equal to the stresses of yield strength of material of cladding layer, as far as the last one is subjected to elastic-plastic deformation both during loading as well as during reset of working loading.

In the course of carried out investigations the value of longitudinal residual stresses, as a rule tensile ones, was considered, which is the result of selection of thickness of cladding layer (Figure 4). It should be also noted that the dependence given in this Figure is influenced by different levels of plastic deformation in welding, heating and cooling [6]. Basing on the analysis of diagrams of residual stresses σ_{av} in specimens during welding using automatic machine ADF-1002 of type 2TS-17S the following peculiarities can be pointed out: the zone of compressive stresses predetermines the nature and properties of metal so that the thickness of cladding layer is directly proportional to the value of residual stresses in the cladding layer of all the investigated specimens.

As a result of introduction of developed technology of welding the chute of scrapper mechanism of traveling-grate sintering machine, designed by the contractor organization, the design of the metallurgical unit was produced capable to withstand the high preset loads and long operation period, as well as to prove the rationality of application of bimetal VSt3sp + 10Kh13 as a base material.

Thus, the results of carried out works evidence of the fact that to provide the guaranteed quality joint of the considered bimetals the application of the technology described above is possible. In this case the operation period can be increased to 80 %.

Conclusions

1. The established value of residual stresses in the near-weld zone of the joint VSt3sp + 08Kh13, equal to 100 MPa, is the best value among the investigated steels with the presence of residual compressive stresses, their maximum value is different and depends on the level of load and yield strength of material of cladding layer.

2. As a result of application of bimetal VSt3sp + 08Kh13 as the base material during manufacture of a chute of scrapper mechanism instead of the metal VSt3sp, the increase of operation period up to 80 % is guaranteed.

1. Medovar, B.I. (1958) *Welding of chrome-nickel austenitic steels*. Moscow: Mashgiz.
2. Glikman, L.A., Babaev, A.N., Kostrov, E.N. (1962) Fatigue strength and intensity of welded samples with deposited layer 10Kh13. In: *Properties of materials applied in turbine construction and methods of their tests*. Moscow-Leningrad: Mashgiz.
3. Nedoseka, A.Ya. (1988) *Principles of design of welded structures*. Kiev: Vyshcha Shkola.
4. Kovalenko, I.V. (2013) *Improvement of technology of arc welding of two-layer steels in manufacturing of industrial metal structures*: Syn. of Thesis for Cand. of Techn. Sci. Degree. Mariupol.
5. Nikolaev, G.A., Kurkin, S.A., Vinokurov, V.A. (1982) *Welded structures. Strength of welded joints and deformations of structures*. Moscow: Vysshaya Shkola.
6. Stafakov, Yu.P., Pobal, I.L., Knyazeva, A.G. (2002) Growth of cracks near interface of dissimilar materials under conditions of compression. *Fizich. Mezomekhanika*, **1**, 81–88.

Received 25.01.2013

THE E.O. PATON ALL-WELDED BRIDGE IS SIXTY YEARS OLD

L.M. LOBANOV and **V.I. KYRIAN**
E.O. Paton Electric Welding Institute, NASU
11 Bozhenko Str., 03680, Kiev, Ukraine. E-mail: office@paton.kiev.ua

The question of construction of motor-road bridge across the Dnieper river was raised before the Great Patriotic War. By that time the technical project of the bridge with driving atop and split through main truss girders, manufactured using riveting, was drawn up and approved. In that period at the Electric Welding Institute of the Academy of Sciences of the UkrSSR the method of automatic submerged arc welding was developed allowing producing high-quality welds and Evgeny O. Paton proposed to manufacture spans of the bridge using welding. In spite of the opinion of opponents, the initiative of Evgeny Paton was supported by the Government of the USSR, and the decision was taken to construct the Kiev bridge applying welding with riveted site joints. To fulfill the project, the supports were manufactured in 1940–1941, and at the plant of metal structures in Dnepropetrovsk the production of assembly elements of spans using automatic submerged arc welding began. However, the construction of bridge was interrupted because of the war, and it was restored after its termination. As far as equipment and technologies providing high quality of assembly welds were created by that time, Evgeny Paton proposed to construct all-welded bridge in Kiev across the Dnieper river applying automatic welding not only under shop conditions, but also in site. The all-welded Kiev bridge across the Dnieper river was constructed in close cooperation with the Kiev enterprise «Proektstalkonstruktsia», the plant of metal structures in Dnepropetrovsk, Bridge Construction Group of the Ministry of Rail Roads, the E.O. Paton Electric Welding Institute of the Academy of Sciences of the UkrSSR and the Ministry of Municipal Economy of the UkrSSR. 3 Ref., 16 Figures.

Keywords: *automatic submerged arc welding, all-welded bridge, spans, assembly elements, construction, collaboration of organizations*

At the beginning of the 1930s the welding began to be applied widely in ship building, industrial building, transport, handling machine building and other fields of industry instead of riveting. It allowed introducing many innovations and simplifications reducing the volume of consumed metal and labor intensity in manufacture of structures. However, the transition from riveting to welding was considerably difficult, especially during manufacture of large-size metal structures and, in the first turn, spans of bridges operated under the conditions of low climatic temperatures and complex alternating loading.

There was troubled news from the West Europe about the serious problems with welded bridges. One could not but remind the widely known cases of fractures of welded bridges in Germany and Belgium. That was quite enough to form the negative attitude towards application of welding in bridge construction.

In that period at the Laboratory of Electric Welding of the All-Ukrainian Academy of Sciences (Kiev), transformed in 1934 into the Electric Welding Institute of the Academy of Sciences of UkrSSR, the purposeful study of load-carrying capacity of welded joints and structures was started. In that laboratory, organized and headed by the academician Evgeny Paton, during the first period the experimental investigations were carried out by comparing the results of tests of similar welded and riveted joints of specimens, girders and integral structures at static, alternating and impact loadings. The carried out tests allowed obtaining the most visual and convincing proves of strength of welded joints and advantages of welding technology. In those and other comparative investigations the welded joints were fractured due to fatigue not in weld metal, but in base metal in the joint zone. It became obvious that the main cause of their fracture is the concentration of stresses created by the shape of joints and welds or technological defects of welding.

It was also assumed that insufficient strength and toughness of weld metal, its lower homogeneity than that of base metal will decrease the resistance of structures to fatigue fractures. In that period the works on search for rational design and technological solutions were carried out providing preset cyclic life of welded joints and assemblies. The investigations related mainly to bridges, railway cars and cranes. They persuasively showed that welded joints and assemblies can be reasonably applied in critical structures,

undergone the effect of alternating stresses. The full strength of butt joints with removed «weld reinforcement» and base metal at alternating loads was proved.

The question of construction of motor-road bridge in Kiev across the Dnieper river was raised before the Great Patriotic War. By that time the technical project of the bridge with driving atop and split through main truss girders, covering the spans of 58 m length (in the floodplain part) and 87 m (in the navigable one) was drawn up and approved. As in that period at the Electric Welding Institute of the Academy of Sciences of the UkrSSR the method of automatic submerged arc welding was developed allowing the producing of high-quality welds, E.O. Paton proposed to manufacture spans of the bridge using welding. And then, the opponents of application of welding in bridge construction raised their swelled heads over. At the meeting they stood up for the technology of riveting of bridges widely used by that time, and in support of that they presented the pictures from the foreign journals with fractured spans, in building of which the welding was applied.

Evgeny Paton, basing on the results of the first profound research works of welding process, as well as on his intuition, was firmly convinced that the cause of the disasters abroad was not in the main principles of welding process, but in its wrong primitive application. The designers used to leave the design of bridges, accepted during riveting, unchanged, i.e. they did not consider the peculiarities of the process of joining the elements using welding. Besides, the steel applied for riveting turned to be quite unsuitable for welding, and quality of welds in use of manual welding at that time was disastrously low.

After Evgeny Paton had briefly stated the principles of construction of the welded bridge in Kiev across the Dnieper river, including the selection of steel suitable for welding, the application of automatic submerged arc welding and strict control of quality of welded joints, N.S. Khrushchev, the Secretary of the Central Committee, resumed: «We will weld the bridge. I mean weld! Failures of other countries shall not discourage us».

Only due to a high authority and engineering courage Evgeny Paton succeeded to win a favorable decision of the directive bodies. The initiative of Prof. Paton was supported by the Government of the USSR, which resulted in taking the decision on the construction of Kiev bridge with welded and riveted site joints, in accordance with which the necessary changes in the project were made.

To realize the project the supports were manufactured and right on the approach of the Great Patriotic War the plant of metal structures in Dnepropetrovsk started manufacturing of assembly elements of spans using automatic submerged arc welding. The war interrupted construction of the bridge.

In 1946, Evgeny Paton, being recognized as the leader in the field of welding and bridge construction and foreseeing the great challenges in manufacture of bridge spans using welding, appealed to the Government of the USSR with proposal to implement welding in construction of bridges, which supported his initiative and issued special resolution on this matter. To fulfill the resolution of the government Prof. Paton united and organized the mutual work of designers of bridges and colleagues of the Electric Welding Institute. They conducted a great complex of investigations and designing developments to work out the basic principles of designing the welded bridges, stated by E.O. Paton already in 1933 [1]. As a result of this great work the main problems were solved opening the wide possibilities of application of welding in construction of bridges. They are described in work [2] in details and related to modernization of design of the bridge, its assemblies and applied steel. The creation of proper equipment and technology, providing the high quality of both the shop and also site welds [3] was principally important.

The obtained results allowed E.O. Paton to raise the question about construction of all-welded bridge in Kiev across the Dnieper river, applying automatic welding not only under shop conditions but also in site. The proposal of Paton, supported by the Government of the USSR, was accepted, and the technical project, and later the working projects were amended correspondingly, considering the results of the recent investigations of the Electric Welding Institute and also modernized design changes in accordance with the Resolution of the Council of Ministers of the USSR of May 17, 1948 of the project assignment which related to the following points:

- truss girders of the bridge shall be welded with a solid wall of not higher than 3.6 m;
- existing type of supports shall be preserved along the whole length with girth rails on columns;
- in the navigable spans the truss girders shall be applied with the solid haunches.

All these and other developments of the E.O. Paton Electric Welding Institute served as the research background for designing, manufacture

Figure 1. All-welded E.O. Paton bridge across the Dnieper river in Kiev

and construction of the first largest all-welded bridge in Europe (Figure 1). The plant manufacture of metal structures of the bridge of total weight of 10,000 t was performed since December, 1951 till April 1953, and erection works — since April, 1952 to October, 1953. The total length of the bridge is 1543 m. It has 24 spans — 20 by 58 m and 4 navigable by 87 m. In the cross section the span structure has four double-T main girders with the solid wall, placed one against another at the distance of 7.6 m, which are united between one another by transverse braces. The longitudinal braces are present only along the lower girth between the middle main girders along the whole length of the bridge. Over the supports the longitudinal braces were mounted between all the four main girders. The upper girths are joined by transverse rolled beams with the ferroconcrete plate of a roadway included into their operation for bending. The width of the bridge is 27 m (roadway is 21 m, two footways of 3 m each).

The realization of construction of the bridge was entrusted to the Ministry of Municipal Economy of the USSR, which organized the Special management of bridge construction.

The construction of Kiev bridge across the Dnieper river was carried out by the staff colleagues of Kiev department of «Proektstalkonstruktsia», plant of metal structures (Dnepropetrovsk), Bridge Construction group of the Ministry of Rail Roads, the E.O. Paton Electric

Figure 2. General view of the rig cross-arm for assembly and welding of large-size assembly elements in the workshop of plant of metal structures in Dnepropetrovsk

Figure 3. Process of assembly of trusses in the rig

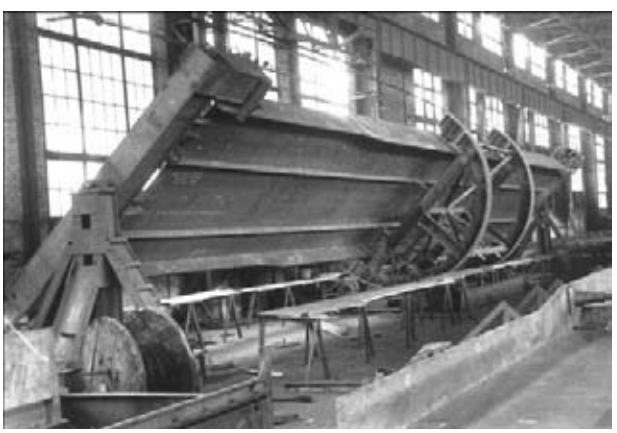

Figure 4. Long beam in the tilter

Figure 5. Welding of wall butt weld using tractor TS-17-M

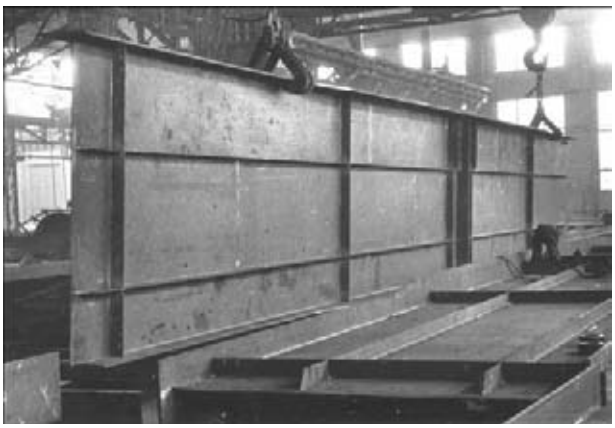

Figure 8. Welding-on of edges of stiffeners

Figure 6. Welding-on of stiffener using semi-automatic machine PSh-5 with holder DSh-27

Figure 9. Welding of girth welds of haunch in the rig

Welding Institute of the Academy of Sciences of the UkrSSR and the Ministry of Municipal Economy of the UkrSSR in close cooperation between each other.

The plant of metal structures in Dnepropetrovsk provided and equipped the special workshops for production of large blocks and put into service the mass production line for assembly elements (Figures 2–4). The workers of the Bridge Construction Group trained and instructed by the specialists of the Electric Welding Institute (Figures 5–9), carried out the welding works all the year round. The inspection, monitoring and acceptance of welding works were performed by the inspection bodies, organized and governed by the Electric Welding Institute (Figure 10).

The delivery of ready assembly elements of the bridge to Kiev was performed by railway transport (Figures 11 and 12). Welding of site

Figure 7. Process of welding of longitudinal butts using tractor TS-17M in the tilter

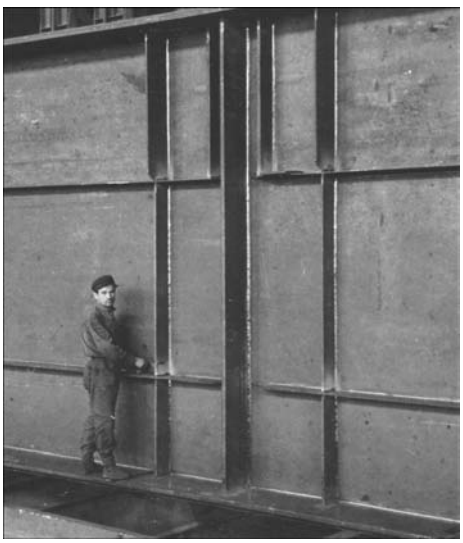

Figure 10. Inspection of welds

Figure 11. Echelon with main beams on the plant rails

Figure 12. Haunch loaded on the platform

joints, as well as shop welding was performed using automatic machines (Figures 13 and 14).

The E.O. Paton Kiev welded road bridge is unique by a number of its characteristic features not only in our country, but also in the whole world. His uniqueness consists in the following:

• all the joints in the bridge spans are manufactured at the plant and in site using welding, i.e. the bridge is all-welded. If to take into account its total length of 1543 m and about 10,000 t of steel used for spans and the total length of welds of 10,668 m, one can confirm that even today it remains the largest all-welded bridge in the world;

• manufacture of assembly elements at the plant and producing of site welds was performed mainly using automatic and semi-automatic welding. Manual welding was applied in producing less critical elements of the bridge (braces, transverse beams, etc.);

• during designing the bridge the principle of blocks enlargement was used, which allowed producing 97 % of all the shop welds of main trusses and 88 % of all the site welds of main trusses using automatic and semi-automatic welding. Moreover, the presence of large single-type blocks allowed mechanizing the assembly-welding operations and organizing line method of

Figure 13. Welding of vertical site butt using automatic machine A-314

Figure 14. General view of welded site butt in the span

manufacture at the plant and in site, which enhanced the quality of welding works and decreased their labor efficiency.

The exclusive role in the construction of this bridge belongs to Evgeny Paton, who persistently worked over the problem of welded construction of bridges during many years and was the initiator of construction of the all-welded bridge in Kiev. Till the last days of his life E.O. Paton steadfastly kept an eye on its construction.

Figure 15. Testing of the bridge

Figure 16. Solemn opening of the bridge in November 5, 1953

The bridge was inspected by the laboratory of the Moscow Road Transport Institute both during the process of construction as well as after its completion. In conclusion the bridge was tested on static and dynamic loading (Figure 15). The tests gave the positive results.

In November 4, 1953 the Governmental Commission carried out the full-scale inspection of the built road-transport bridge across the Dnieper river in Kiev, studied the technical documentation and resolved to accept the bridge into the permanent operation since November 5, 1953 applying all types of loads on it envisaged by the project without the speed limit. The main works on the construction of the bridge were evaluated by the Governmental Commission for «excellent».

In November 5, 1953 the Council of Ministers of the UkrSSR approved the Act of the Governmental Commission of the acceptance of the all-welded road-transport bridge across the Dnieper river in Kiev according to the Resolution № 2348 and appointed to open the traffic along the bridge for November 5, 1953 (Figure 16). That was the end of the responsible and the most difficult stage in formation of the welded construction of bridges.

In December 18, 1953 according to the Resolution of the Council of Ministers of the USSR the newly built bridge was named after Evgeny Paton.

In 1995 the American Welding Society included the all-welded bridge in Kiev across the Dnieper river into the list of outstanding engineering structures.

After 60 years of operation the E.O. Paton bridge is continuing its reliable operation at the design load of N-10 and considerably increased intensiveness of traffic (80,000 vehicles per day at the design value of 10,000).

1. Paton, E.O., Gorbunov, V.I. (1933) Principles of design of welded bridges. *Avtogennoe Delo*, **4**, 2–5.
2. Lobanov, L.M., Kyrian, V.I., Shumitsky, O.I. (2003) Fifty years of the E.O. Paton bridge. *The Paton Welding J.*, **10**/**11**, 12–20.
3. Paton, E.O., Lebed, D.P., Radzevich, E.N. et al. (1954) *Application of automatic welding in construction of large town all-welded bridge*. Kiev: AN UkrSSR.

Received 04.11.2013

SYSTEMS OF PROCESS CONTROL AND MONITORING OF CONDITIONS — THE IMPORTANT FACTORS OF QUALITY ASSURANCE IN ELECTROSLAG WELDING OF THICK METAL

S.N. LITVINENKO[1], **K.P. SHAPOVALOV**[1], **I.S. SAVCHENKO**[1], **S.N. KOSINOV**[1], **K.A. YUSHCHENKO**[2], **I.I. LYCHKO**[2] and **S.M. KOZULIN**[2]

[1]NKMZ — Novo-Kramators Machine-Building Works

4 Ordzhonikidze Str., 84305, Kramatorsk, Donetsk region, Ukraine. E-mail:shapovalov@nkmz.donetsk.ua

[2]E.O. Paton Electric Welding Institute, NASU

11 Bozhenko Str., 03680, Kiev, Ukraine. E-mail: office@paton.kiev.ua

At the NKMZ the installation, unique by its technical capabilities, is successfully used for electroslag welding of large-size parts, allowing manufacture of welded-cast, rolled-welded and welded-forged steel billets of weld section of up to 5000 × 6000 mm and weight of more than 100 t. The required quality of metal of welded joint is provided due to a strict keeping of preset welding condition parameters during the whole period of weld fulfilment without forced interruptions of the welding process. This is attained by a high reliability of operation of electric control circuit and drives of executive units of the installation, as well as by application of method of doubling the feeding of electrode wires into the zone of welding. Setting of selected condition parameters, control and visual inspection of the welding process are realized from two central panels, and also using the automatic system of welding conditions monitoring. The system of control represents a multi-functional complex, in which the control of parameters of the technological process (acquisition and processing of information) is realized by the controller SIMATIC S7-300, and the display of parameters, recording and record-keeping of accumulated information are realized by an industrial computer in a panel-type version PC 670 and text panels of operator OP 7. Software of the control system was developed using the Siemens package of programs WinCC V5.1 and operates under the control of operational system Microsoft Windows. 3 Ref., 6 Figures.

Keywords: *specialized equipment for welding of thick metal, electroslag welding with consumable nozzle, control systems, monitoring of welding conditions, doubling of feeding the electrode wires, reliability in electroslag process fulfilment*

The NKMZ is the leader in production of large-size steel metal structures of heavy machine-building units using electroslag welding with a consumable nozzle (ESW CN).

The new stage in the development of technology and equipment of ESW CN started in 2002 when a new installation, unique by its technical capabilities, for ESW of large-size thick parts was manufactured and put into service in the plant [1], having no analogues in the world practice of the welding production. Using this installation it is possible to produce welded-cast, rolled-welded and welded-forged steel billets of butt section of up to 5000 × 6000 mm and more than 100 t weight. It also makes it possible to perform ESW of two butts of up to 2000 × × 6000 mm section simultaneously.

In welding of products with large-size butts the forced interruptions of the ESW lead, as a rule, to the formation of almost non-repairable defects in the weld, causing high material losses and decreasing the efficiency of the technological welding process. The reliability of the ESW process is guaranteed by a strict keeping of preset parameters over the period of weld making without forced interruptions of the welding process for the time exceeding 1.5–3.0 min [2].

Welding equipment of the installation provides a high reliability of the ESW CN process with producing the guaranteed quality of the electroslag joints, first of all, due to reliability of electric control circuit and drives of executive controls of the installation, and also by applying the method of doubling the feeding of electrode wires into the zone of welding [3]. The doubling is realized by scheme «36 working + 36 spare». Moreover, working and doubling wires are fed from independent drives. The total number of simultaneous wire feeding can reach 72 pieces.

Welding equipment of the installation includes two, independent from each other, blocks (left and right). Each block is completed with twelve three-electrode welding machines ASh-110, assembled on traverses (Figure 1) so that to provide the doubling welding wire feeding in the guiding channels of consumable nozzles (Fi-

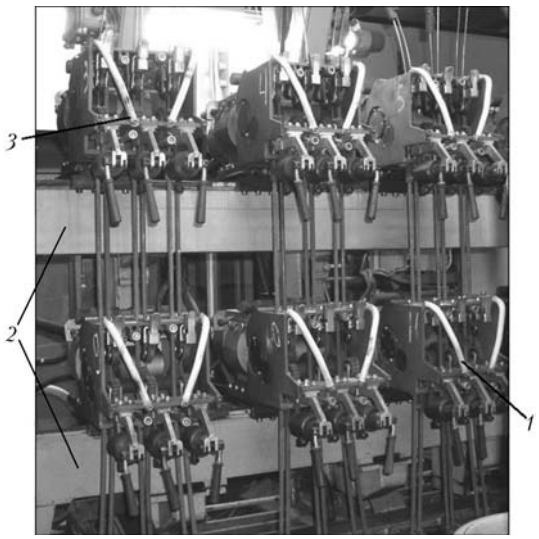

Figure 1. Appearance of welding machines ASh-110 assembled into blocks: *1*, *3* — working and doubling welding machines, respectively; *2* — traverses for fastening the machines

gure 2). The supply is realized from four power sources TShS 3000/3 (A-481 E), connected in parallel (two for each block). Setting of selected condition parameters, control and visual inspection of the welding process are realized by means of two central panels, as well as by automatic system of monitoring the welding conditions, arranged in a central cabin (Figure 3).

To fulfil the preparatory and setting-up works (before and after welding), local control panels are used, located in site of the preparatory operations. Electric systems of control and drives of all the elements of the installation are mounted in control cabinets, arranged on its gantry.

Industrial experience shows that the reliability of ESW process is provided mainly by elimination of forced interruptions of electrode wire feeding into the zone of welding. The ESW process is started (mainly from «liquid start») by feeding the working wires, while the doubling ones are located in the «waiting» mode, which is characterized by the feed speed, equal to zero, or by so-called advancing speed, amounting to 10–20 % of working one. In case of a forced interruption of the working wire the control system is automatically switches on the feeding of proper doubling machine, switches off the ma-

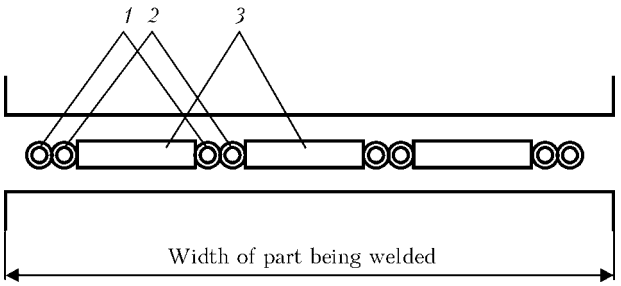

Figure 2. Scheme of consumable nozzles with channels for wire feeding (variant for one phase): *1*, *2* — channels for movement of working and doubling welding wires, respectively; *3* — plates of consumable nozzle

Figure 3. Central cabin of control of installation machines: *1*, *2* — respectively, control panels of right and left blocks; *3* — industrial computer PC 670 of system of welding conditions monitoring; *4* — signal lamps of control of welding wires movement

chine, coming out of order, and sends simultaneously signals to the central cabin about the situation by a light indication and also by a sound. Then the welders-operators detect the cause of interruption and eliminate the occurred trouble. After trouble elimination the manager of works from the central cabin takes a decision about the replacement of the doubling machine by the remedied working one. In this case the remedied machine becomes a doubling one and can be used in interruption of wire movement on the already operating machine.

The automatic computer system provides continuous objective control and monitoring of main condition parameters, as well as thermodeformational cycle of welding. The control system represents a multi-functional complex, in which the control of technological process parameters (acquisition and processing of information) is realized by a controller SIMATIC S7-300, and the display of parameters, recording and record-keeping if accumulated information are realized by an industrial computer in a panel-type version PC 670 and text panels of the operator OP 7. The software of the control system was developed by using the package of programs WinCC V5.1 of «Siemens» and it is governed by the operational system Microsoft Windows. The appear-

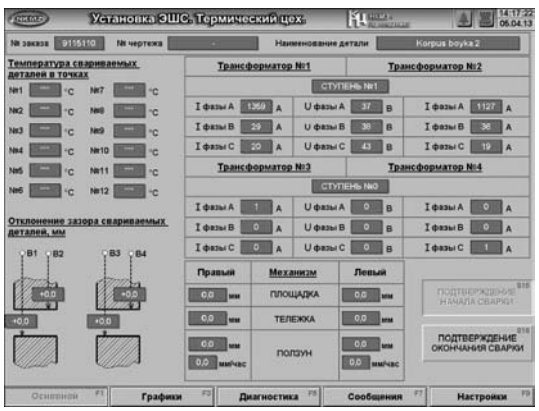

Figure 4. Appearance of main window of control and monitoring system

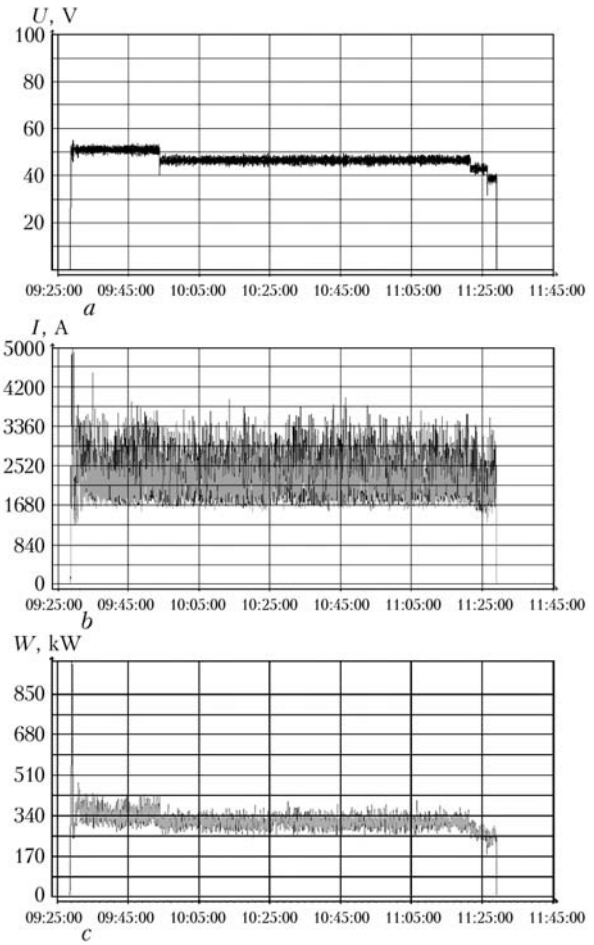

Figure 5. Appearance of general graphic information obtained in the system of monitoring: *a* — welding voltage; *b* — welding current; *c* — electric power of welding

ance of the main window of control and monitoring system is shown in Figure 4.

The system of control and monitoring allows recording on-line such important parameters of the welding process as voltage, current, generated electric power, rate of electrode wire feeding (Figure 5), welding speed, heating temperature of edges being welded, etc.

The required technological information is taken from specialized sensors and other electric equipment directly in site. Signals from sensors are processed by a controller, which transforms the input data by a definite algorithm into appropriate technological parameters of the process.

All the electric parameters of the process (welding voltage, current, electric power, welding wire feed rate) can be observed directly during welding with separation by binding to power welding circuit of the installation. For example, it is possible to display the values of voltage or current separately at each phase for each power source or in binding with other values, while the wire feed rate — at each machine. The obtained values of the mentioned parameters can be corrected by the manager of works in central control panels.

Oscillograms of records of condition parameters are the objective characteristics of the welding process, which confirm the quality of the fulfilled process (its compliance with preset welding conditions) and promote consolidation of technological discipline among the welders. The decoding of records of a definite case (in time coordinates) can help, if necessary, in finding the causes of defect formation in the weld or for evaluating the conditions during the interested time of welding (Figure 6).

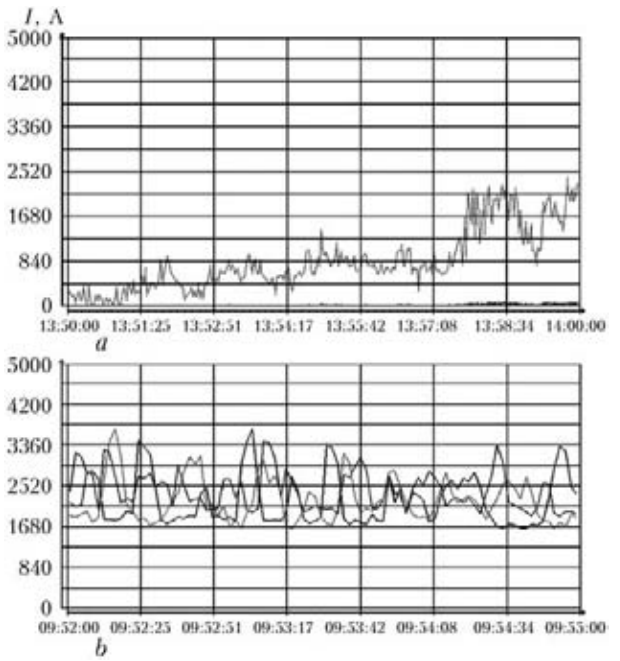

Figure 6. Oscillograms of welding current for single-phase of consumable nozzle at the area of weld after 50 min since the welding beginning ($v_{w.f}$ = 115 m/h) (*a*) and three-phase scheme of consumable nozzles after 32 min since the welding beginning ($v_{w.f}$ = 150 m/h) (*b*)

It is important to note that the analysis of obtained records of oscillograms can be useful also in optimizing the conditions and technique of welding for the new technological processes of ESW CN of thick metal of the new products.

In conclusion, it can be outlined that the high reliability of operation of executive settings of the installation for manufacture of large-sized metal structures by ESW CN in combination with use of method of doubling the electrode wire feeding into the zone of welding, and also the obligatory control and monitoring of welding conditions provide the effective guaranteed producing of welded joints of thick-section metal of the required quality.

1. Nevidomsky, V.A., Krasilnikov, S.G., Panin, A.D. et al. (2002) New machine for electroslag welding of large parts at JSC «NKMBF». *The Paton Welding J.*, **2**, 49–51.
2. Voloshkevich, G.Z., Sushchuk-Slyusarenko, I.I., Lychko, I.I. (1965) Increase in reliability of electroslag process in welding of long welds. *Avtomatich. Svarka*, **6**, 50–53.
3. Kompan, Ya.Yu., Grabin, V.F., Abralov, M.A. et al. (1975) *Electroslag welding of titanium alloys*. Tashkent: Fan.

Received 10.07.2013

METHODS OF GENERATION OF EXTERNAL MAGNETIC FIELDS FOR CONTROL OF ELECTROSLAG WELDING PROCESS

I.V. PROTOKOVILOV[1], **V.B. POROKHONKO**[1], **A.T. NAZARCHUK**[1], **Yu.P. IVOCHKIN**[2] and **D.A. VINOGRADOV**[2]
[1]E.O. Paton Electric Welding Institute, NASU
11 Bozhenko Str., 03680, Kiev, Ukraine. E-mail: office@paton.kiev.ua
[2]Joint Institute for High Temperatures, RAS
13 Izhorskaya Str., Build. 2, 125412, Moscow, Russia. E-mail: vortex@iht.mpei.ac.ru

Efficiency of application of electromagnetic actions for control of joint formation during electroslag welding is determined in many respects by application of external magnetic fields to welding zone and structural peculiarities of corresponding devices. The aim of present work lied in analysis of methods for generation of external magnetic fields during electroslag welding of butt joints and evaluation of their effect on weld pool melt. The main methods of generation of longitudinal and transverse magnetic fields in a welding gap are considered, and principal schemes of corresponding electromagnetic devices are given. It is shown that direction and intensity of electromagnetic force effecting the weld pool melt is determined first of all by spatial orientation of the external magnetic field in relation to object being welded, value of field magnetic induction and its frequency characteristics. Rationality of application of that or another scheme of application of magnetic field in the gap depends on welded joint parameters, and it should be considered separately for each individual case. Appropriateness of application of magnetic fields providing constant (cyclic) rearrangement of hydrodynamic structure of flows in the weld pool or creating melt vibration was indicated. In this case, usage of pulsed magnetic fields generated by discharges of capacitor batteries to electromagnet coil is perspective. Relevance of development of new schemes and devices for generation of magnetic fields and their power sources is shown. 15 Ref., 9 Figures.

Keywords: *electroslag welding, weld pool, magnetic field, hydrodynamics, electromagnetic action, devices for magnetic field application, magnetic induction, electromagnetic force*

Electroslag welding (ESW) is one of the most efficient methods for joining of thick-walled parts and structures from different metals and alloys [1–3]. Scope of application and reasonable areas of ESW utilization could be more significant, if the joints performed by electroslag technology had relatively higher mechanical properties. Their low mechanical properties are caused by coarse, large-grain weld metal structure and unfavorable effect of welding thermal cycle on near-weld metal zone.

Control of weld pool hydrodynamics using external magnetic fields can provide effective improvement of service properties of the joints, performed by ESW. Positive effect of electromagnetic actions on welding process efficiency, refining of weld metal structure and mechanical properties of welded joints is marked in many works [4–12]. However, wide practical application of the obtained results is limited to significant extent by difficulty of receiving of external magnetic fields of necessary induction in the welding zone and inconvenience of corresponding devices.

The aim of present paper lies in the analysis of methods and structural schemes of application of external magnetic fields in the welding zone during ESW of butt joints, evaluation of their effect on weld pool melt considering the possibility of intensification of electromagnetic action.

Physical mechanism of the electromagnetic action during ESW lies in interaction of external magnetic filed with welding current passing in the melts of slag and metal pools [4]. A volume electromagnetic force $\vec{f}_e$ resulting in force action on the melt is formed due to such interaction in the weld pool. Value and direction of specified force is determined by vector product of current density in the melt $\vec{j}$ and induction of external magnetic field $\vec{B}$: $\vec{f}_e = \vec{j} \times \vec{B}$. It is sufficiently difficult to vary the value and direction of welding current in a wide range without deterioration of electroslag process stability and quality of welded joint formation. Therefore, efficiency of application of electromagnetic action is first of all determined by the parameters of external mag-

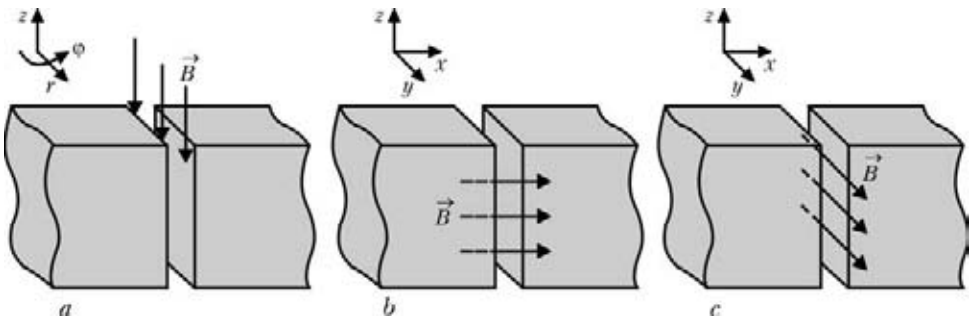

Figure 1. Variants of application of external magnetic fields to welding zone during ESW: *a* — longitudinal magnetic field; *b*, *c* — transverse magnetic fields

netic field, namely its spatial orientation in relation to object being welded, amplitude and frequency characteristics.

It should also be noted that the efficiency of application of magnetic fields in the welding zone is determined to significant extent by magnetic properties of parts being welded. More favorable conditions in most cases are developed during welding of nonmagnetic materials (titanium, aluminum etc.), since then the effect of shunting of magnetic field by surrounding ferromagnetic masses in the welding gap is minimal. An exception are the cases when the parts being welded or elements of fixture simultaneously perform functions of magnetic conductor.

Magnetic fields used in the welding processes are divided on longitudinal (along the electrode axis) and transverse (normal to electrode axis) ones [4, 5, 13, 14] (Figure 1) depending on the direction of induction vector. In turn, the force lines of the latter can be oriented normal to (Figure 1, *b*) or parallel (Figure 1, *c*) to edges being welded.

Longitudinal magnetic field under ESW conditions can be generated using a solenoid located in the welding gap in area of dry electrode extension [4, 6, 9] (Figure 2, *a*). Strictly speaking, the longitudinal magnetic field in this case is realized only in the middle part of the solenoid. The magnetic field having radial constituent in addition to axial one penetrates the weld pool. Thus, welding current will have (j_r, j_z, 0) constituents, external magnetic field (B_z, B_r, 0) and electromagnetic force $\vec{f_e} = \vec{j} \times \vec{B} = (0, 0, j_z B_r - j_r B_z)$ in the cylindrical coordinates (z, r, φ). It can be observed that the electromagnetic force generated by external magnetic field will result in melt movement in horizontal planes.

Studied scheme, providing local application of magnetic field in zone of melting of electrode wire, where the current density is maximum, allows effecting heat-and-mass transfer in given region and control formation and detachment of drops of electrode metal. However, only insignificant leakage field penetrates the metal pool that does not allow effecting the weld metal structure. Besides, present scheme of generation of magnetic field in the welding zone is poorly adaptable to fabrication and complex for practical realization in the most cases since the dimensions of magnetic system are limited by value of welding gap (25–35 mm). A scheme with magnetic conductor introduced in the welding zone and coil located outside (Figure 2, *b*) is considered to be more perspective.

Transverse magnetic field, the force lines of which are directed normal to the edges being welded (see Figure 1, *b*), can be realized with the help of windings covering the parts being welded and simultaneously performing functions of the magnetic conductor (Figure 3). The electromagnetic force will have the $\vec{f_e} = (0, j_z B_x - j_y B_x)$ constituents in Cartesian coordinate system (x, y, z). Since welding current constituent j_z significantly exceeds j_y constituent, then it can be considered that the main effect from action of indicated magnetic field lies in formation of the electromagnetic forces in the melt, oriented along the edges being welded (along y axis, see

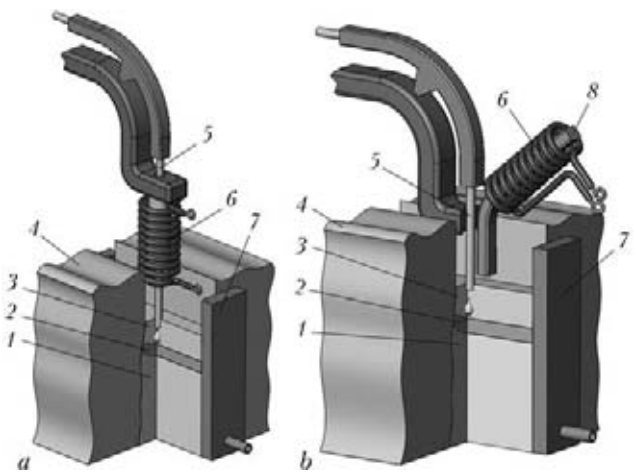

Figure 2. Schemes of application of longitudinal magnetic field by means of solenoid, positioned in welding zone (*a*), and bar magnetic conductor (*b*): *1* — weld; *2* — metal pool; *3* — slag pool; *4* — specimen being welded; *5* — wire; *6* — electromagnetic system; *7* — water-cooled forming strap; *8* — magnetic conductor

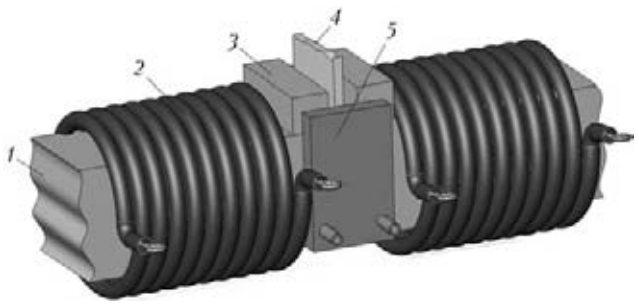

Figure 3. Scheme of application of transverse magnetic field with the help of coils mounted to welded parts: *1* — specimen being welded; *2* — electromagnetic system; *3* — tabs; *4* — electrode; *5* — water-cooled forming strap

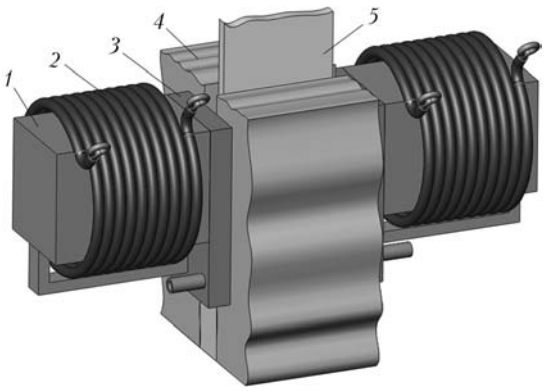

Figure 4. Scheme of application of transverse magnetic field with the help of electromagnets with bar magnetic conductor: *1* — bar magnetic conductor; *2* — coil; *3* — water-cooled forming strap; *4* — specimen being welded; *5* — electrode

Figure 1, *b*). If external magnetic field is constant and welding current is alternating, then reciprocating motion (vibration) of the melt is created along the edges being welded with welding current frequency (50 Hz). Indicated effect can have positive influence on heat-and-mass transfer in the weld pool and refining of weld metal structure.

If welding current and magnetic field are alternating (or both constant), then presence of x and z constituents of electromagnetic force will result in complex volume pattern of the melt flow [4]. At that, z component of the electromagnetic force has opposite direction in two different parts of the pool, that leads to distortion of free surface of the slag pool. The latter is negative from point of view of welded joint formation since it violates process symmetry.

Advantage of given scheme of magnetic field generation lies in sufficiency of minimum gap between the magnets which is equal to welding one, that allows creating uniform magnetic filed with high induction values (up to 0.4 T). Such power magnetic fields allow influencing the macrostructure of weld metal refining and homogenizing it. It is, however, obvious, that given scheme is difficult to be realized in welding of large-size parts and parts with complex geometry. Therefore, it can find application only in welding of compact structures.

The most adaptable to fabrication and mostly applied scheme used in ESW (found in the literature) is the scheme of application of external transverse magnetic field with the help of electric magnets located near side forming devices [4, 5, 8, 12]. Welding of extended butt joints provides for their movement along the edges with welding speed. Electromagnet cores can be of bar as well as П-shaped forms.

Electromagnets with single-bar cores are sufficiently compact (Figure 4) [5]. Such devices mainly generate field, the force lines of which are normal to the edges being welded. In this case the electromagnetic force in Cartesian coordinate system (x, y, z) will have $\vec{f}_e = (-j_z B_y, 0, j_x B_x)$ constituents (see Figure 1, *c*), i.e. the main component of electromagnetic force will be directed across the edges being welded (along x axis) considering that $j_z > j_x$. This leads to vibration of the weld pool melt across edges being

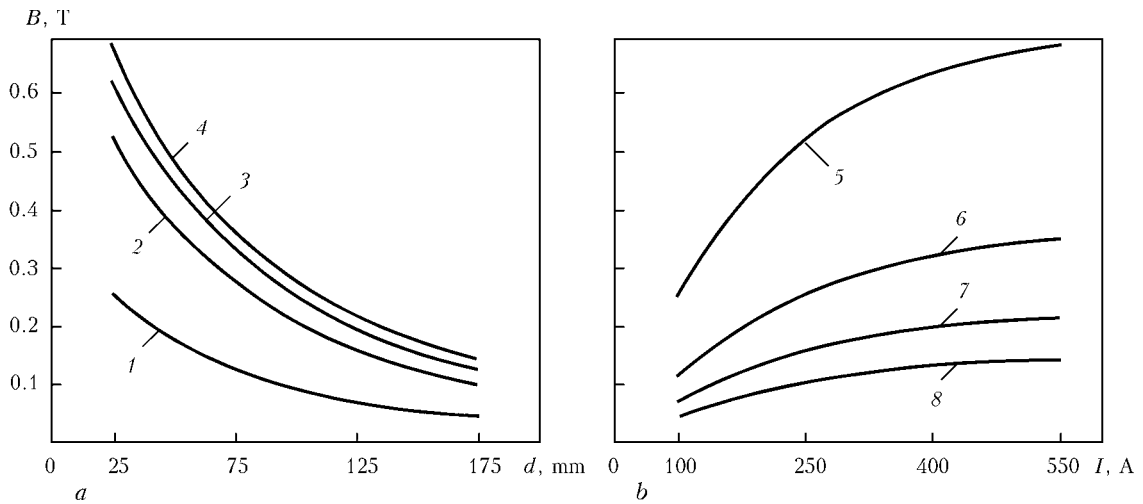

Figure 5. Dependence of magnetic induction on gap d between the magnetic conductors (*a*) and electric current I in electromagnet winding (*b*): *1* — I = 100; *2* — 250; *3* — 400; *4* — 550 A; *5* — d = 25; *6* — 75; *7* — 125; *8* — 175 mm

welded, if constant magnetic field is used (welding current is alternating). Such reciprocating movements of the melt in double-phase area can promote fragmentation of growing crystalline particles and refining of weld metal structure. Transverse vibration in the welding gap also increases penetration of edges being welded that allows reducing rate of welding energy input [4, 10].

Disadvantage of given method of magnetic field application is its leakage due to significant gap between the electromagnet poles, which is determined by thickness of parts being welded and water-cooled forming starps (sliders). Increase of part thickness raises leakage and reduces efficiency of electromagnetic influence.

The results of experimental measurements of induction of magnetic field along the welding axis, generated by electromagnets with 70 cm^2 section of steel magnetic conductor and 160 total number of winds, are given in Figures 5 and 6. They show significant reduction of magnetic field induction at increase of gap between the magnetic conductors (thickness of parts being welded) (Figure 5, *a*) as well as relative inhomogeneity of distribution of magnetic induction in the welding gap (Figure 6).

Combined scheme of magnetic field action to the weld pool can be developed using bar electromagnets. The main principle of scheme lies in application of additional bar electromagnet located in the lower part of butt weld (Figure 7). Combined magnetic field having transverse and longitudinal constituents will effect the weld pool at specified coil connection. Longitudinal and transverse magnetic fields can be alternatively used applying switching of winding connection. Specified scheme expands the possibility of control of weld pool hydrodynamics. It is, however, obvious that it is not applicable during performance of extended welds.

Usage of electromagnets with П-shape core also provides the possibility of application of longitudinal and transverse magnetic fields (Figure 8) in the welding zone.

Magnetic field including mainly axial constituent (Figure 8, *b*) is formed in the gap at orientation of electromagnets along the welding axis and back-to-back connection of winding. Coordinated connection of windings can generate transverse field, the force lines of which have opposite directions in different zones on gap height (Figure 8, *c*). This provides the possibility to influence the melts of slag and metal pools using opposite fields and generating, for example, their vibration in antiphase at corresponding location of the magnets relatively to the weld

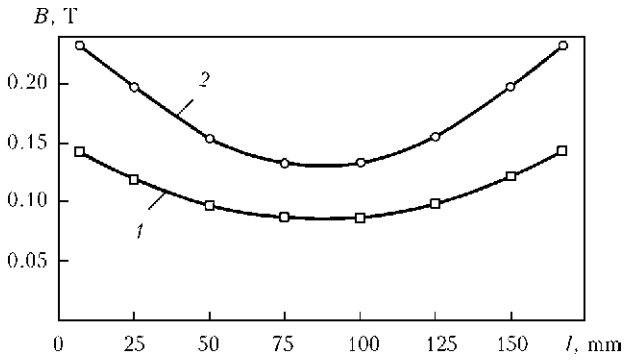

Figure 6. Distribution of magnetic induction in welding gap: *1* — *I* = 200; *2* — 400 A; *l* — distance from edge being welded

pool. Specified effect can be useful for activating the processes of heat-and-mass transfers in the pool and slag–metal interaction.

If electromagnets are located normal to the axis, magnetic field the force lines of which are directed from edge to edge, can be generated (Figure 8, *e*) in the welding zone.

Usage of considered above devices is complicated in series of cases by limited access to the parts being welded. Nonuniformity of magnetic field in the welding gap and necessity of movement of magnets along the edges during welding can be referred to their disadvantages.

Device for application of transverse magnetic field shown in Figure 9 [4] does not have specified disadvantages. The magnetic conductor of this device simultaneously performs the functions of sustaining walls for strap formed welds. Posi-

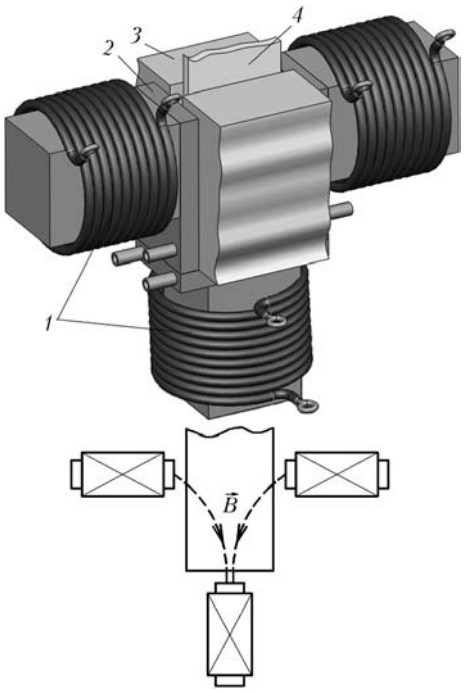

Figure 7. Scheme of application of combined magnetic field with the help of electromagnets with bar magnetic conductor: *1* — electromagnets; *2* — water-cooled forming strap; *3* — specimen being welded; *4* — electrode

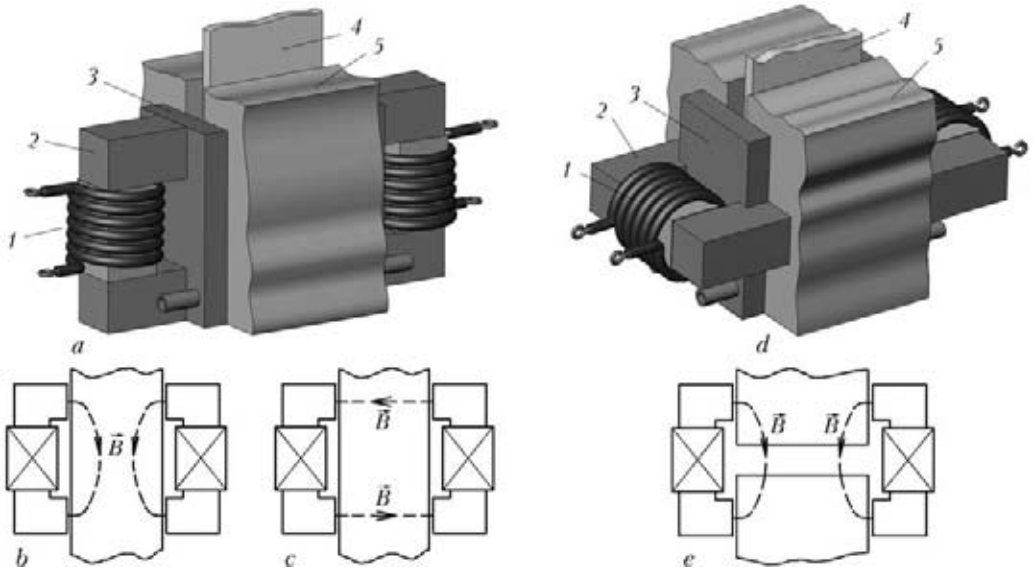

Figure 8. Scheme of application of transverse magnetic field with the help of electromagnets with П-shaped core, oriented along (*a–c*) and normal to (*d*, *e*) welding axis: *1* — coil; *2* — П-shaped core; *3* — water-cooled forming strap; *4* — electrode; *5* — specimen being welded

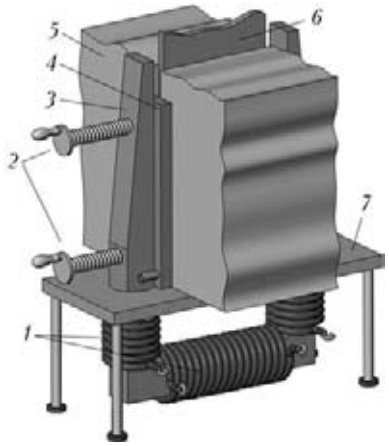

Figure 9. Device for electroslag welding in external magnetic field: *1* — coils; *2* — clamps; *3* — magnetic conductor; *4* — water-cooled forming strap; *5* — specimen being welded; *6* — electrode; *7* — support

tioning of magnet coils under the welding table in many respects facilitates operator work. The device allows generating the magnetic field along the whole weld length. Magnetic induction in the gap was calculated on formulae $\overline{B} = k\mu 0In/(l_{Fe}/\mu_{Fe} + d)$, where k is the coefficient considering leakage of field in the gap (0.75); $\mu_0 = 4\pi \cdot 10^{-7}$; I is the current intensity in windings; n is the quantity of winds; l_{Fe} is the length of magnetic conductor; μ_{Fe} is the magnetic permeability of magnetic conductor material; d is the gap between the poles.

Efficiency of electromagnetic action is determined by its frequency and amplitude characteristics except for spatial orientation of magnetic field.

Data given in the literature show sufficiently wide range of application of magnetic fields 0.01–0.20 T [4–12] used in ESW. Likely, that the relatively small induction values 0.01–0.05 T are enough for control of metal microstructure. However, experience of authors in application of control magnetic fields in electroslag processes shows that application of magnetic fields of higher power 0.1–0.2 T is necessary for influence the metal solidification and its macrostructure, control of weld pool parameters and penetration of base metal.

It should also be noted that action schemes, generating stable electrovortex flows in the pool, can have negative effect on chemical homogeneity and properties of deposited metal. Application of the fields providing constant (cyclic) rearrangement of hydrodynamic structure of flows or creating vibration of the pool melt is more efficient. Usage of pulsed magnetic fields, generated by discharges of capacitor batteries to electromagnet winding [15], is more perspective in this direction. Such scheme of action due to high peak currents in the windings (up to 10 kA) allows generating power magnetic fields in the welding zone when reducing of mass-and-dimension characteristics of corresponding devices.

Conclusion

Each scheme of generation of magnetic fields acting the ESW process, considered in the paper, has its advantages and disadvantages and relevance of application of that or another scheme should be considered separately for each specific case. Movable electromagnetic devices traveling along the weld together with forming sliders is good to use in performance of extended welds. Stationary electromagnets can be used in welding of compact sections.

Since generation of the magnetic field of sufficient induction (0.1–0.2 T) in the welding zone is difficult during ESW, then its application for influence the solidification of weld metal is less efficient than usage of the transverse magnetic fields. At that, application of pulsed fields providing constant (cyclic) rearrangement of structure of pool melt flows or developing its vibration at reduction of mass-and-dimension characteristics of corresponding devices is the most perspective one.

Further investigations in area of electromagnetic control of ESW process should be complex, i.e. by development of efficient schemes of generation of magnetic fields in the welding gap considering structural peculiarities of electromagnetic devices for their generation and designing of power sources for them.

The works are performed with the assistance of the State Fund for Fundamental Researchers of Ukraine (project No.F53.7/027) and Russian Foundation for Basic Research (project Ukr_f_a No.13-08-90444).

1. (1980) *Electroslag welding and surfacing*. Ed. by B.E. Paton. Moscow: Mashinostroenie.
2. Yushchenko, K.A., Lychko, I.I., Sushchuk-Slyusarenko, I.I. (1998) Effective techniques of electroslag welding and prospects for their application in welding production. In: *Welding and Surf. Rev.*, Vol. 12, Pt 2. Amsterdam: Harwood Acad. Publ.
3. Paton, B.E., Dudko, D.A., Palti, A.M. et al. (1999) Electroslag welding (prospects of development). *Avtomatich. Svarka*, **9**, 4–6.
4. Kompan, Ya.Yu., Shcherbinin, E.V. (1989) *Electroslag welding and melting with controllable MHD-processes*. Moscow: Mashinostroenie.
5. Kuznetsov, V.D., Kozakov, N.K., Shalda, L.M. (1987) *Magnetic control of electroslag process*. Kiev: Vyshcha Shkola.
6. Dudko, D.A., Rublevsky, I.N. (1960) Electromagnetic stirring of slag and metal pools in electroslag process. *Avtomatich. Svarka*, **9**, 12–16.
7. Trochun, I.P., Chernysh, V.P. (1965) Magnetic control of solidification in ESR. *Svarochn. Proizvodstvo*, **11**, 3–5.
8. Protokovilov, I.V., Porokhonko, V.B. (2012) Control of formation of welded joints in ESW (Review). *The Paton Welding J.*, **10**, 49–54.
9. Kompan, Ya.Yu., Petrov, A.N., Sharamkin, V.I. (1978) Some peculiarities of electroslag welding in longitudinal-radial magnetic fields. *Avtomatich. Svarka*, **9**, 39–43.
10. Porokhonko, V.B., Protokovilov, I.V., Petrov, D.A. (2012) Specifics of electroslag welding of titanium using electromagnetic methods effects. *Visnyk Adm. Makarov NUK*, **5**, 170–176. *http://* ev.nuos.edu.ua/ua
11. Volkov, G.G. (1975) Electroslag welding with application of alternative electromagnetic field. *Montazh i Spets. Raboty v Stroitelstve*, **8**, 14–15.
12. Kazakov, N.K., Kuznetsov, V.D., Korab, N.G. (1981) Selection of magnetic field input method during electroslag welding. *Vestnik KPI*. Series Machine Building, Issue 18, 76–78.
13. Ryzhov, R.N., Kuznetsov, V.D. (2006) External electromagnetic effects in the processes of arc welding and surfacing (Review). *The Paton Welding J.*, **10**, 29–35.
14. Razmyshlyaev, A.D., Mironova, M.V., Yarmonov, S.V. (2013) Transverse magnetic field input devices for arc welding and surfacing processes (Review). *Ibid.*, **1**, 39–43.
15. Kompan, Ya.Yu., Nazarchuk, A.T., Protokovilov, I.V. et al. (2012) Possibilities of application of pulse electromagnetic effects in electroslag processes. *Sovr. Elektrometallurgiya*, **2**, 8–13.

Received 15.08.2013

INFLUENCE OF DESIGN FEATURES OF RELOADER WELDED ASSEMBLIES ON ITS PERFORMANCE

P.A. GAVRISH and **V.P. SHEPOTKO**
Donbass State Mechanical Engineering Academy
72 Shkadinov Str., 84313, Kramatorsk, Ukraine. E-mail: nauka_breda@mail.ru

Improvement of reliability and safety of structures of machines and mechanisms in long-term operation under cyclic loading is becoming ever more urgent. Welded assemblies of a reloader were taken as an example for analysis of design solutions for the above assemblies allowing for their load level. Special attention is given to questions of decreasing structural stress raisers of weldments. An improved design of reloader diaphragm assembly, as well as geometry of electrotrolley edge preparation were proposed, ensuring the high quality of welded joints and, therefore, the required fatigue life. 8 Ref., 1 Table, 8 Figures.

Keywords: *stress raisers, welded assembly, analysis procedure, stress-strain state, welded assembly embodiment*

Ensuring reliable and safe operation of the structures of machines exposed to cyclic loads in service is becoming ever more urgent, as physical wear of machines in enterprises occurs much faster than the tempos of their technical re-equipment. A metal structure, most often welded, is the basis for all the machines and mechanisms, so that their further operation is influenced mainly by reliability and safety of its service. In Ukraine not every enterprise has enough funds for technical re-equipment. Therefore, timely detection of damage and upgrading of metal structures allow counterbalancing the problems of machine ageing and of their reliable and safe service [1]. Analysis of item embodiment is performed after its examination. Assessment of technical condition is one of the routine procedures performed to check the level of reliability (operational safety) and service life of structures, as well as determine their fitness-for-purpose under the conditions envisaged by the project and during specified service life [2].

The objective of special examinations, which are performed usually by specialized organizations, is obtaining factual data on the structure technical condition. The procedure of analysis of metal structure embodiment is applied to develop recommendations on their further operation. The scope and degree of examination detailing depend on availability of technical and maintenance documentation, state and degree of structure damage, and eventually, determine the package of reconstruction and repair operations.

Lowering of the level of welded assembly performance is observed with the following structure damage [3]:

- residual deformations of metal structure;
- local element damage;
- failure or reduction of element cross-sectional area due to corrosion;
- failure, buckling of closed section elements or element bulging due to water freezing in them.

Repair and upgrading of welded assemblies of metal structures should be performed so as to eliminate their design shortcomings as much as possible.

Analysis of design deficiencies of embodiment of reloader welded assemblies and examples of their improvement. The case of geometrical features of manufacturing welded assemblies of TAKRAF Company reloader was taken as an example to study their influence on crane service life [4–6].

Mounting longitudinal stiffeners in the reloader inner compartments increases the section moment of inertia and reduces the cyclic load range (Figure 1). Such a design of reloader main beams, however, can lead to negative consequences in lifting construction service, as welding of the lower longitudinal stiffener near the diaphragm creates a structural stress raiser [2].

Figure 2 shows the structure of reloader welded assembly.

Its service life is determined by the following features [5, 6]:

- stress concentration near the angle ends;
- residual welding stresses caused by metal heating by a concentrated heat source;
- weld location at not less than 10–20 mm distance;

Figure 1. Stiffeners in reloader inner compartments

• nonuniformities of geometrical shape, composition, mechanical properties and microstructure;

• increased rigidity of the structure in points of welds coming closer to each other.

Reloader operation under the conditions of cyclic stresses leads to initiation of fatigue and lamellar fractures. Figure 2 shows cracks detected at angle ends. Ultrasonic examination revealed through-thickness cracks of lower girth. Strength analysis performed by finite element method showed the following stress values in reloader girder assemblies (Table).

Girder damage develops in reloader operation under cyclic loading. Analysis of conclusions of expert examinations of reloaders, operating in the Krym Soda Works for 30 years, showed that cracks are localized in under-rail zone of upper girth, points of force flow transfer (rigid or flexible support) of the lower girth, as well as in points of connection of wind brace to lower girth (Figure 3). As a rule, damage accumulates in girders in the rigid and flexible supports, in the span middle part, and for reloaders with a combined system — in point of connection of suspension elements to box girders. Crack initiation is the consequence of insufficient moment of inertia of reloader compartments, deficiencies of welded assembly design, unsound preparation of the edges for welding, and welding technology defects.

Experimental investigations of the level of alternating stresses in reloader operation were performed with application of strain gauges, which were combined into strain gauge rosettes and were mounted in the points of highest calculated stresses.

Processing of experimental investigation data allowed establishing the sites of defect initiation in the upper girth of girders: on flexible support, where tensile stresses vary in the range of (0.2–

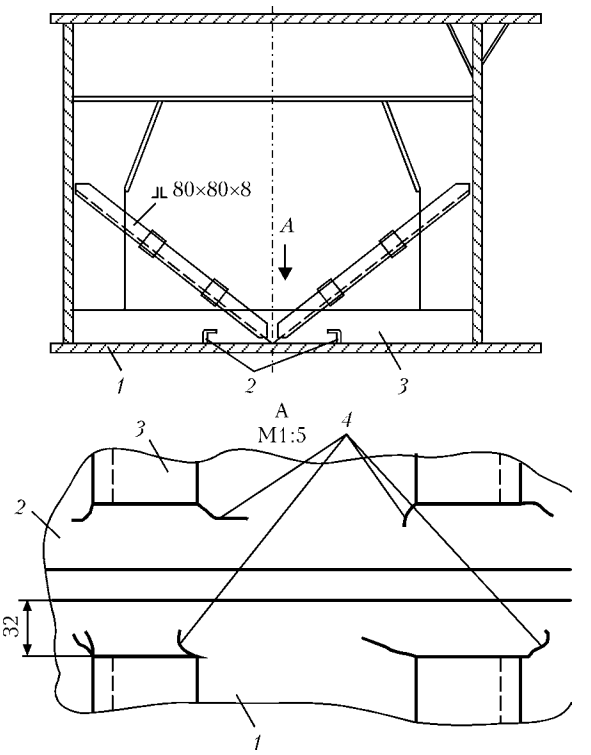

Figure 2. Schematic of lower welded girth of reloader girders: *1* — lower girth of reloader girder; *2* — diaphragm; *3* — angle stiffener; *4* — cracks

0.7)σ_y at location of the loaded trolley in the carriage unloading section (flexible support arm); on rigid support, where tensile stresses vary in the range of (0.1–0.5)σ_y at location of loaded trolley in the section of hopper charging (rigid support arm). It was established that tensile stresses vary in the range of (0.2–0.6)σ_y at movement of loaded trolley in the span middle.

To lower the probability of cracking in the lower girth (diaphragm and angle stiffeners) the design of angle stiffener welded assembly was changed. Stress raisers were eliminated by

Dependence of calculated stresses (MPa) in reloader girder assemblies on load position

Calculated elements of reloader girders	Without load (dead weight)	On the arm on the left	In midspan	On the arm on the right
3-4	127	144	280	133
4-5	160	198	260	155
5-6	250	280	320	250
6-7	170	220	290	190
7-8	170	180	240	180
8-9	190	250	270	200
9-10	130	230	290	142
10-11	250	270	310	260
11-12	190	226	288	210

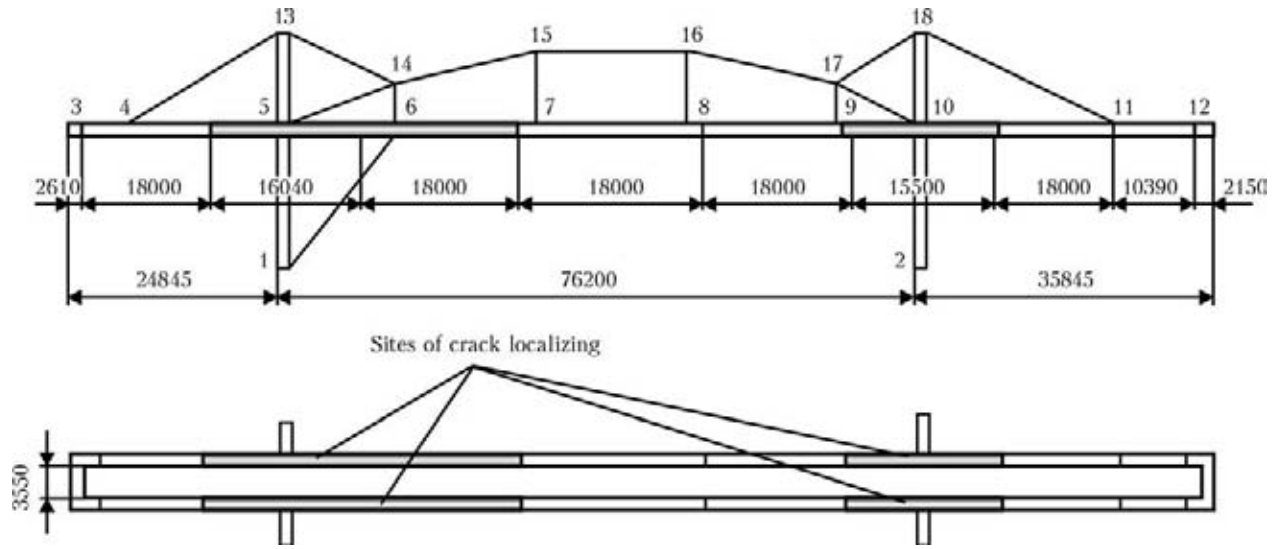

Figure 3. Sites of reloader crack localizing

smooth transition from base metal (lower girth) to the angle proper (Figure 4).

Smooth transition from base metal to angle metal reduced stress concentration. Such a change of the assembly design features eliminated crack initiation at angle ends (during 3 years of service). However, cracks appeared in the fusion zone of diaphragm weld (Figure 5) that is due to the impact of cyclic stresses on lower girth and absence of stiffener near the diaphragm. To eliminate this defect, a variant of welded assembly embodiment with angle stiffener continuation through holes in the diaphragm was selected (Figure 6).

After the welded assembly design has been modified, no cracks developed in the fusion zone of weld diaphragm.

It is shown that in welding and surfacing of reloader electrotrolleys, mounted along the main beam, the strength of copper-to-steel joint is in-

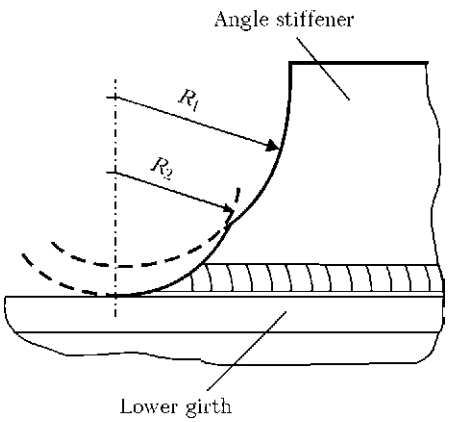

Figure 4. Change of angle stiffener welded assembly design

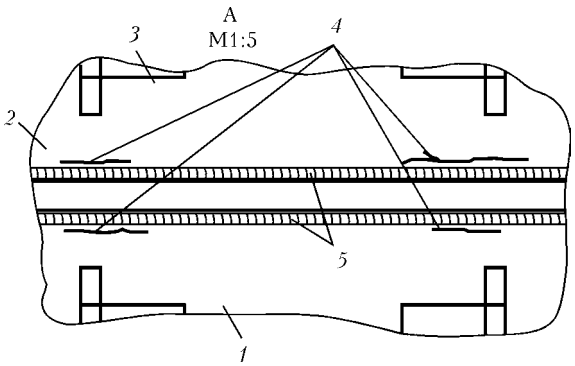

Figure 5. Cracks in the fusion zone of diaphragm weld: *1–4* — see Figure 2; *5* — diaphragm welds

Figure 6. Welded assembly of modified design

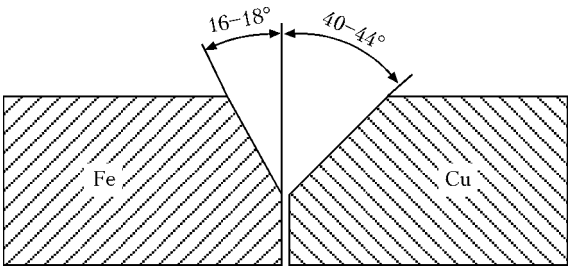

Figure 7. Schematic of edge preparation of reloader electrotrolley parts

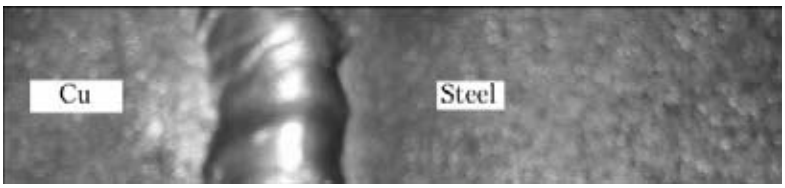

Figure 8. Sound welded joint of copper to steel

sufficient. Frequent failures of electrotrolleys lead to crane outage. Shape of edge preparation in welding copper to steel was symmetrical that did not correspond to different thermophysical properties of copper and steel. Analysis of edge preparation geometry allowing for physicochemical properties of copper and steel showed that edge preparation design should be asymmetrical to ensure equivalent strength of welded joint and sound weld [7, 8]. Figure 7 shows the schematic of edge preparation of electrotrolley parts for welding.

Welding of electrotrolley parts and their operation showed the rationality of application of the proposed geometry of edge preparation. Figure 8 illustrates a sound welded joint of copper to steel.

The proposed design of welded assemblies from dissimilar metals essentially improved welded joint quality and its service life.

Conclusions

1. Calculated and experimental investigation of the locations of damage initiation in reloader girders and their loading conditions showed the need for improvement of welded assembly design.

2. An improved design of diaphragm assembly of reloader main beams was proposed which demonstrated its high performance.

3. A new geometry of edge preparation in dissimilar metal welded assembly of reloader electrotrolleys was proposed which ensures high quality of welded joint and required service life.

1. Grote, K.-G., Postnikov, Yu.E., Makarenko, N.A. et al. (2012) Procedure of analysis of welded metal structure embodiment. In: *Abstr. of Int. Sci.-Techn. Conf. on University Science*. Mariupol: PGTU, Vol. 2, 303.
2. Gavrish, P.A., Shepotko, V.P., Kassov, V.D. (2012) *Damage of crane metal structures. Diagnostics. Repair*: Manual. Kramatorsk: Donbass DMBA.
3. Emelianov, O.A., Shepotko, V.P., Pikhota, Yu.V. et al. (2004) Fatigue damages of welded crane bridges. *The Paton Welding J.*, **5**, 29–35.
4. Shepotko, V.P., Gavrish, P.A. (2012) Analysis of embodiment of welded assemblies in repair of crane metal structures. *Podjomnye Sooruzh. i Spets. Tekhnika*, **4**, 10–11.
5. Shepotko, V.P., Gavrish, P.A. (2012) Adaptability-to-fabrication of repair welding of crane metal structures. *Ibid.*, **5**, 12–13.
6. Grote, K.-G., Postnikov, J., Makarenko, N. et al. (2012) Die Bewertungsmethodik der bauausfuehrung der untergleiszone der haupttrager der verladebrucke. *Visnyk Donbass DMBA*, 28(**3**), 110–113.
7. Gavrish, P.A., Tulupov, V.I. (2010) Preliminary heating at welding of copper with steel. In: *Proc. of 10th Int. Conf. on Research and Development in Mechanical Industry* (Donji Milanovac, Serbia, 16–17 Sept. 2010). Donji Milanovac: RaDMI, 156–158.
8. Gavrish, P.A., Tulupov, V.I. *Method of welding of dissimilar metals*. Pat. 75036 Ukraine. Int. Cl. B 23 K 13/00. Fil. 12.03.2012. Publ. 26.11.2012.

Received 04.07.2013

INDEX OF ARTICLES FOR TPWJ'2013, Nos. 1–12

LIST OF AUTHORS